The host galaxies and possible progenitors of fast radio bursts

By

Lachlan Marnoch

A thesis submitted to Macquarie University
for the degree of Master of Research
Department of Physics & Astronomy
26 December 2019

MACQUARIE
University
SYDNEY·AUSTRALIA

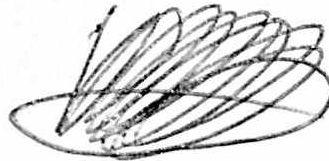Typeset in LaTeX 2_ε.

The content of this thesis is my own work, except where specifically described below.

The VLT observing programs upon which this thesis is based are the result of proposals from other members of the CRAFT collaboration, with Jean-Pierre Macquart (Curtin University) as Principal Investigator. Imaging was obtained primarily in Service Mode by ESO staff, or in Visitor Mode by Stuart Ryder (Macquarie University) and myself, with valuable assistance from Juan Carlos Munoz-Mateos (ESO). I undertook the image reduction, with some assistance from John Pritchard (ESO) with installing the ESO Reflex software.

FRB localisation positions and uncertainty calculations were provided by Adam Deller and Cherie Day (Swinburne University), together with Shivani Bhandari and Emil Lenc (CSIRO) based on ASKAP observations.

Stuart Ryder, Richard McDermid (Macquarie University) and Elaine Sadler (CSIRO) supervised the work undertaken for this thesis, and provided feedback and suggestions throughout the year. The thesis title and basic idea for the project were provided by Stuart Ryder.

Except where acknowledged in the customary manner, the material presented in this thesis is, to the best of my knowledge, original and has not been submitted in whole or part for a degree in any university.

Lachlan Marnoch

Acknowledgements

This thesis would not have been possible without several key people, to whom I would like to extend my heartfelt thanks.

I would firstly like to thank my supervisors: Doctors Stuart Ryder, Elaine Sadler and Richard McDermid. Elaine and Richard made time in their incredibly busy schedules to look over my work, and they never had to be asked twice for their advice, which is worth its weight in neutronium. Stuart was my primary supervisor in all but name, and his constant availability, encouragement, support and apparently bottomless patience ensured that I was never too lost. As well as being an invaluable source of scientific and technical insight (I was frequently astounded at the spouts of obscure instrumental knowledge he is capable of producing at a moment's notice), he has been my guide and advocate in the world of scientific bureaucracy. He made sure I had the best opportunities available to me, and pushed me to follow through on them - including attendance of an observation run at the Very Large Telescope. He has advocated for me throughout this project, ensuring that my name ended up on posters, papers and proposals. He also provides extraordinarily prompt feedback on thesis chapters and other writing, often with a wait time on the order of a day. At the times when I was beginning to think that I could be the slowest and least competent MRes student of all time, he made sure to convince me otherwise. For all of this, I am deeply grateful.

I want to thank CRAFT, again for their patience, and particularly Doctors J. Xavier Prochaska, Jean-Pierre Macquart and Shivani Bhandari for allowing my name to worm its way onto their papers. Special thanks are also owed to Juan Carlos Munoz-Mateos, the VLT/X-shooter Night Astronomer whose determination to do right by our observations, sleep schedule be damned, resulted in some lovely data.

The Macquarie University student magazine, *Grapeshot*, should not go unthanked for its role in my year. Thank you also to Jo Dawson, our MRes coordinator, who is a brilliant person to have on your side. She's been a valuable advocate of my cohort and all of our needs. While I'm on the subject, those other Masters students of the department have been a big psychological help, always responding to news with the appropriate level of congratulations or commiserations.

I also sincerely thank my family, for support both moral and occasionally financial, for attending talks, and for enduring baffling explanations of my project and making the effort to understand them.

And finally, I want to thank Nayoung Lee, for pushing me to get up on time, exercise, and eat the occasional healthy meal - and for nourishing me with all the love and support I could ever need. Without you there, this year would have been *much* harder.

List of Publications

- (1) J. Xavier Prochaska, Jean-Pierre Macquart, Matthew McQuinn, Sunil Simha, Ryan M. Shannon, Cherie K. Day, Lachlan Marnoch, Stuart Ryder, Adam Deller, Keith W. Bannister, Shivani Bhandari, Rongmon Bordoloi, John Bunton, Hyerin Cho, Chris Flynn, Elizabeth K. Mahony, Chris Phillips, Hao Qiu, Nicolas Tejos, *The low density and magnetization of a massive galaxy halo exposed by a fast radio burst*. Science **366**(6462), 231-234 (2019)

  The candidate contributed reduced, co-added images and integrated magnitudes of the galaxies HG 181112 and FG181112_13_5, and a description of the process by which they were obtained (§ 2.2).

- (2) Jean-Pierre Macquart, J. Xavier Prochaska, Matthew McQuinn, Keith W. Bannister, Shivani Bhandari, Cherie K. Day, Adam T. Deller, Ron D. Ekers, Clancy W. James, Lachlan Marnoch, Stefan Osłowski, Chris Phillips, Stuart D. Ryder, Ryan M. Shannon, Nicolas Tejos, *A direct detection of the diffuse missing intergalactic baryons from a set of localised fast radio bursts*. Submitted to Nature on September 27, 2019

  The candidate contributed reduced, co-added images and plots of FRB host galaxies, nuclear offset calculations, and a description of the process by which each was obtained.

- (3) Shivani Bhandari, Elaine M. Sadler, J. Xavier Prochaska, Sunil Simha, Stuart D. Ryder, Lachlan Marnoch, Keith W. Bannister, Jean-Pierre Macquart, Chris Flynn, Ryan M. Shannon, Nicolas Tejos, Felipe Corro-Guerra, Cherie K. Day, Adam T. Deller, Ron Ekers, Sebastian Lopez, Elizabeth K. Mahony, and Chris Phillips *ASKAP FRB host galaxies and their progenitors*. Submitted to Astrophysical Journal on October 8, 2019

  The candidate contributed reduced, co-added images and integrated magnitudes of FRB host galaxies and a description of the process by which they were obtained.

Abstract

Fast radio bursts (FRBs) are millisecond-scale radio pulses from extragalactic sources, the origin of which remains mysterious. This is partially because of the difficulty in localising FRBs to host galaxies, previously achieved only with the repeating source FRB 121102. Now, the Commensal Real-time ASKAP Fast Transients (CRAFT) survey has traced several FRBs to their hosts. These localisations provide the opportunity to study the host galaxies at a range of wavelengths, which will shed light on FRB source environments, and, in the future, the nature of their progenitors.

This work focuses on optical follow-up of CRAFT fast radio bursts using Very Large Telescope imaging. Photometric measurements of five host galaxies are performed, and their nature discussed. Four FRB hosts are examined, using the method of direct subtraction of two epochs, for supernova-like optical counterparts to the FRBs. None are identified. Limits are placed on the brightness of any associated transients, and a Monte Carlo approach is used to estimate the probability of a supernova associated with each FRB going undetected. It is found that Type Ia and IIn supernovae are unlikely to accompany all FRBs. Implications for FRB progenitor models are discussed.

Contents

List of Figures

List of Tables

1

Introduction

Fast radio bursts (FRBs) are bright, millisecond-timescale radio-frequency pulses of mysterious, extragalactic origin (6). With a detectable all-sky rate on the order of a thousand per day (7), these events are clearly common in the universe - and yet we remain in the dark as to what generates them. Precise localisation, long-elusive but slowly emerging, has become central to further progress in this respect (8), and will allow several classes of progenitor model to be tested.

Some hypotheses for fast radio burst generation involve a luminous transient event, such as a supernova (9) or kilonova (10). Thus, multi-wavelength observations of the FRB field may detect a luminous transient, particularly if it resembles a supernova (11). Supernovae are stellar explosions that have been known to outshine their host galaxies (12). With observations in the weeks following the FRBs, optical follow-up can now be performed directly on identified host galaxies in order to search them for supernovae or other optical transients. Such a search is undertaken in this work.

1.1 Fast Radio Bursts

The first fast radio burst (FRB) was discovered in archival Parkes data in 2007 (13), commencing a new sub-field of astronomy. The name wasn't adopted until six years later, when evidence began to mount for the astrophysical reality of the phenomenon (14). Although it now seems quite certain that they are true astronomical transients, their underlying nature remains unclear, despite intensive effort.

When a radio pulse travels through an ionised medium, its arrival time is delayed by an amount inversely proportional to the square of its frequency. Hence, for broadband emissions, the highest-frequency components arrive first, and the burst sweeps downward in frequency, as pictured in Figure 1.1. This is known as dispersion, and is quantified with the dispersion measure (DM - see § 1.1.2).

To qualify as an FRB, a radio pulse must have a greater DM than the ionised medium of the Milky Way can account for (15). Although certain properties are common to most or all events (16), others, such as burst profile shape, temporal width and polarisation properties demonstrate considerable variation (6, 16, 17). The 'fast' in fast radio burst comes from

Copyright material redacted from digital thesis

Figure 1.1: A waterfall plot of FRB 110220, with de-dispersed pulse profile above. Figure from Petroff 2017 (4).

the characteristic brevity of the events, on the order of a millisecond[1]. From this, causality arguments imply that the FRB emission region must be tiny (6); with a timescale of 1 ms, the diameter of the region can only be of order 10^2 to 10^3 km [2], even before accounting for extrinsic broadening. Some FRBs are of much shorter timescales, down to $\sim$ 30 μs (18). For such distant sources FRBs are very bright, with spectral flux densities of 50 mJy to 100 Jy (16). Particularly if the emission is isotropic, and not beamed, this implies that an enormous amount of energy must be involved in their production, restricted to a rather compact environment. The large brightness temperature of the bursts at cosmological distances also exclude thermal emission and favour coherent mechanisms, making the involvement of a strong magnetic field probable (6).

These constraints have not proved especially constraining, resulting in a good deal of progenitor speculation (15, 19). Adding to the FRB enigma is the difficulty in precisely locating them, with only one published source localised to a host galaxy until July 2019 (20).

This first localised source is FRB 121102[3], often called 'The Repeater' - as it was the first of the small subset of FRB sources that are known to repeat (22). The repetition does not have a fixed period and the repetition rate is non-Poissonian (23). A second repeating source (FRB 180814.J0422+73) was announced in 2019, sharing key properties with the first (24). Henceforth they are referred to as R1 for the first and R2 for the second. The Canadian HI Mapping Experiment (CHIME) later reported eight further repeating sources (25), and repeat bursts from an FRB detected with the Australian Square Kilometer Array Pathfinder (ASKAP; 26) FRB have been detected with the Green Bank Telescope (27); none but R1 have been localised to a host galaxy.

The current convention for naming FRBs follows 'FRB YYMMDD', giving the date of detection in Coordinated Universal Time (UTC); for example, FRB 150418 was detected on

---

[1]When de-dispersed, that is; the total length of the detection event is on the order of seconds.

[2]$d = ct = 3 \times 10^8$ m s^{-1} $\times 10^{-3}$ s $= 3 \times 10^5$ m $= 300$ km

[3]FRB 121102 was also the first FRB to be detected by a facility other than the Parkes radio telescope (16, 21).

the 15th of April, 2015 (28).

1.1.1 Progenitors

Although several applications of FRBs don't require any particular knowledge about the progenitor (see § 1.1.2), the nature of FRB generation is an important question, and, naturally, an object of intense speculation.

There is no shortage of suggested answers to this question[4] (15, 19). Hypotheses span the spectrum of physical mechanisms, the most mundane being terrestrial radio-frequency interference[5], and the most exotic involving axion quark nuggets (30) or cosmic string cusp decay (31). FRBs have been invoked as evidence for several flavours of quantum gravity (31–34), dark matter (30, 35, 36), and in one case both (37). Extraterrestrial intelligence has, inevitably, been suggested as a culprit, whether by way of communicative signals (38) or incidental byproducts of intergalactic exploration (39). At least two such papers were written as April Fool's jokes (40, 41), demonstrating the existence of a sense of humour within the FRB community.

Although there are several ways of classifying the models, one of particular relevance is whether they are cataclysmic or non-cataclysmic - ie, produced in single events that irreversibly alter the source object, or by sustained mechanisms (16). Cataclysmic models are incompatible with repeating sources (15), but are still valid for non-repeaters. It is also possible for non-cataclysmic progenitors to be non-repeating. Other predictions that might prove discriminating include volumetric source rates, expected source environment, and multi-wavelength or multi-messenger counterparts (8, 19; see § 1.1.3).

Similarly, the mechanism behind pulsar[6] emission, a thoroughly observed and pinpointed phenomenon, is still not well-understood (15, 16, 44). However, the progenitor objects are universally held to be spinning, magnetised neutron stars[7] (43, 44). With this in mind, perhaps the most we can hope for regarding FRB progenitors - in the near future, at least - is a conclusion on which objects they originate from, rather than the physical mechanism itself. That is, it seems likely that we will know *what* is producing them long before we know *how*. Given that they are well-known (yet not fully-understood) radio emitters, and that they satisfy the necessary compactness and probable magnetisation of an FRB emitter, it is hardly surprising that neutron stars are the focus of current speculation (6, 15, 16).

Current thinking, largely based on the characteristics of repeater R1, favours young magnetars[8] as the origin of FRBs; however, this is only valid insofar as all progenitor environments are similar to that of R1 (46), which is unlikely (47). It has, however, been suggested that all fast radio burst sources could be repeaters of some kind, and that we simply don't detect the repetitions - for reasons of sensitivity, directionality, event rate, or other concerns (17, 48). If this is true - and it may be difficult to rule out entirely - it would eliminate all cataclysmic progenitor models. However, by prolonged observation of the regions in which FRBs were detected, strong upper bounds have been placed on repetition luminosity and frequency for many bursts; if all sources are repeaters, then the majority must have quite different rate statistics to that of R1 (48, 49), to say nothing of their host

---

[4]The FRB Theory Wiki (https://frbtheorycat.org/index.php/Main_Page; 19) provides a useful summary.

[5]Although RFI events known as perytons did indeed imitate key properties of FRBs, they were eventually traced to local microwave ovens and shown to be distinct from true FRBs (29).

[6]Pulsars are variable radio sources with short, and highly regular, periods (42, 43) - also at one time suggested to be alien signals.

[7]Neutron stars are stellar remnants generated by the core collapse of a massive star, on the order of 10 km across and composed of super-dense matter (45).

[8]Neutron stars with extremely powerful magnetic fields

environments. By analogy with gamma ray bursts (GRBs), which are produced by at least four distinct mechanisms (8), it seems likely that there are two or more populations of FRBs, with R1 and R2 (at least) (24) belonging to one distinct from the majority. This can be true even if all FRB sources repeat.

Despite the lack of associated multi-wavelength events (16), several FRB hypotheses call for association with some kind of luminous transient event, such as a supernova (9) or kilonova[9] (10, 51, 52). Indeed, given the phenomenal energy implied by the brightness of the bursts, cataclysmic events such as these are especially appealing. Candidate models include magnetic reconnection due to mergers of white dwarfs (9) or neutron stars (10, 51) and interactions between supernova shocks and neutron stars (53).

Event rates offer some tantalising agreements. Some analyses suggest that the FRB rate is consistent with the merger rate of binary neutron stars, which would produce a kilonova counterpart (16, 51, 54). Another suggests it is consistent with that of binary white dwarfs (9), which could produce a Type Ia SN counterpart (an example light curve is provided in Figure 1.2). With some assumptions about FRB volumetric distribution, the event rate of Type Ib/c SNe is consistent to within an order of magnitude (16, 55, 56), and the rate of core-collapse SNe in general is higher by two orders of magnitude with the same assumptions (16, 57). Depending on the extent to which FRBs are beamed or isotropic, each of these events offers a viable optical FRB counterpart. If one or more FRB populations have luminous transient counterparts, multi-wavelength observations may allow us to associate such an event with an FRB (11).

1.1.2   FRBs as cosmic probes

An FRB carries a memory of its own journey across space. Encoded in the dispersion measure (DM) is information about the density of electrons in the intervening space; and in its rotation measure (RM), information about the magnetic field along the line-of-sight. Measurements of scatter as a function of frequency can also be used as an indicator of turbulence in the propagating medium (6, 58).

The dispersion is measured using (16):

$$t_{\text{low}} - t_{\text{high}} = \text{DM} \times \frac{q_e^2}{2\pi m_e c} \left(v_{\text{low}}^{-2} - v_{\text{high}}^{-2} \right) \tag{1.1}$$

where t_{low} and t_{high} are the arrival times of the respective burst components; q_e is the fundamental charge; m_e is the electron mass; c is the speed of light; and v is the frequency, with v_{low} and v_{high} being the lower and higher frequency limits, respectively. Then, theoretically, DM is given by (16, 59):

$$\text{DM} = \int_0^d \frac{n_e(l)}{1 + z(l)} \, \mathrm{d}l \tag{1.2}$$

where d is the distance to the FRB source; n_e is the electron number density; l is a position along the path of the burst; and z is the redshift at a given position, to correct for cosmological time dilation. For nearby positions l, for example when calculating the Milky Way contribution, the $(1 + z)$ correction may be excluded.

The matching DMs of the R1 bursts ($\sim 560\,\text{pc cm}^{-3}$) were key to initially characterising it as a repeating source rather than a series of mere chance sky alignments (22); the same goes

---

[9]A multi-wavelength (and multi-messenger) transient event caused by compact-object mergers (50).

for R2 ($\sim$ 190 pc cm^{-3}; 24), the subsequent CHIME repeaters (25) and the ASKAP/Green Bank repeater ($\sim$ 460 pc cm^{-3}; 27).

The DM as a measure of electron column density makes it a powerful probe of ionised media. This characteristic has been used with pulsars to measure the interstellar medium (60); the same technique can be applied, using FRBs, on the intergalactic scale (2, 61), and has been extended to probing the halos of foreground galaxies (1). With a cosmological distribution of FRBs becoming apparent, and an emerging relationship between DM and cosmological redshift (2), the DM of an FRB can also be used as a rough distance indicator, albeit dependent on models of host and Milky Way contribution. As a coarse rule of thumb, $z \lesssim \frac{DM}{1000 \text{ pc cm}^{-3}}$ (16, 49).

Complementing the dispersion measure's utility as a probe is the rotation measure, which arises from Faraday rotation. When an FRB passes through a magnetic field in an ionised medium, a change in polarisation angle, proportional to the square of the wavelength, results (16). Thus, FRBs that have encountered a net magnetic field exhibit wavelength-dependent polarisation, proportional to the magnetic field component parallel to the line of sight. This makes them useful probes of astrophysical magnetic fields.

1.1.3 Follow-up at other wavelengths

No non-radio transient counterpart to an FRB has ever been detected (16). This includes R1, despite observations in the optical (62), X-ray (63) and γ-ray bands (64) during which bursts were detected in the radio (and which also failed to detect any associated persistent γ- or X-ray sources; 16). It is entirely possible that no transient counterparts exist; for example, if FRBs are giant neutron star pulses similar to those emitted by the Crab pulsar from time to time (65), no detectable multi-wavelength emission is expected (66).

However, if multi-wavelength FRB counterparts do exist, they would be valuable tools. Again by analogy with gamma ray bursts, it seems that detection of multi-wavelength counterparts is almost as important to the FRB field as localisation, as it will almost certainly provide vital clues as to the bursts' origin (17). In the past, multi-wavelength and -messenger observations have been instrumental in characterising a long list of previously mysterious astrophysical phenomena, including pulsars, supernovae, neutron star mergers, gamma-ray bursts and active galactic nuclei (8, 67, 68). Non-radio counterparts may also help solve the thorny problem of disentangling the DM components contributed at different points of the burst's journey (see § 1.1.2) by providing more information about the source environment (67). Accompanying neutrino or gravitational wave signals are also possible, depending on the progenitor mechanism; gravitational waves are especially relevant if a compact-object merger is involved, as demonstrated by LIGO (67, 68). There have been attempts at calculating the forward-shock afterglow emission of an FRB event, analogous to that seen for GRBs, with assumptions about redshift and total intrinsic energy (69).

The short optical transient space is not well-explored, and may contain undiscovered events, a subclass of which might be FRB counterparts (70). There has been suggestion of 'fast optical bursts', hypothetical optical counterparts occurring at the same timescale as the radio burst (8); it has even been suggested that they could be briefly visible to the naked eye (66). However, a more sophisticated analysis finds that such a phenomenon, if it occurs, is unlikely to be detectable with current sensitivity (71).

Searches for faint optical transients at minute timescales have been undertaken by the *Deeper, Wider, Faster* programme, with the primary goal of finding FRB counterparts (70). The programme also undertook simultaneous observation in γ-ray and radio observation (70). The survey has so far found four events which might belong to a new class of transient;

Copyright material redacted from digital thesis

Figure 1.2: A typical Type Ia supernova light curve. Figure from Maguire 2016 (5).

however, simultaneous radio observation at Parkes and Molonglo radio telescopes found no FRB counterpart, and the events are considered most likely to be stellar flares (70).

Perhaps more promising, in terms of detectability, are slow optical transients such as supernovae (SNe). As mentioned in § 1.1.1, some FRB progenitor models do predict an association, and some event rates are consistent. A study of the field containing FRB 151230 was undertaken with the goal of locating optical transient counterpart candidates (11). Lacking a localised host galaxy, it found no less than 8 candidates, which Tominaga et al concede may all be unrelated to the burst (11). However, one of the most likely candidates was consistent - albeit with a somewhat poorly-constrained fit - with a supernova that could have occurred at the same time as the FRB (11). The study also ruled out association of that particular FRB with a Type Ia supernova to $z \leq 0.6$, although the high dispersion measure of $960.4 \pm$ pc cm^{-3} makes a host redshift closer to $z \sim 0.8$ more likely (11).

The field of FRB 140514 was checked thoroughly for transients in X-ray, near-infrared, optical and radio bands, ruling out an accompanying supernova or long GRB out to redshift 0.3 (72). The observations took place from 8.5 hours out to 55 days after the burst (72). This does not, however, rule out a supernova at greater distances, and the DM of this burst (562 pc cm^{-3}) is consistent with a redshift as high as 0.5 (72).

These searches have in common that they lacked a verified host galaxy, which would make a direct comparative search considerably more achievable.

1.2 Localisation of Fast Radio Bursts

Much like gamma ray burst science, precise localisation has become pivotal to the rate of progress in the FRB field (8, 73). Localisation is the first step in culling the array of progenitor

theories (8) - knowledge of the position of an FRB within a host galaxy can invalidate or reinforce a hypothesis (see § 1.1.1). Precise localisation is also necessary in order to fulfil the potential of FRBs as cosmic probes (see § 1.1.2) - a reliable measure of distance, via redshift, is necessary to measure the baryon density along an FRB's path (6, 73).

As CHIME has demonstrated, increases in radio sensitivity are on the threshold of providing us with a large sample of FRBs at a range of DMs (6, 74). What is not yet a reality is a large sample of well-localised ones. For some time, the size of the published sample sat squarely at one - R1, which was localised to sub-arcsecond precision in 2017 (20). This was made possible through observations of the source's repetitions (16, 46). No localisation of a single burst to a host galaxy was published until July 2019 (73), although attempts were made.

A host galaxy candidate for non-repeating burst FRB 150418 was found by association with a declining radio source, which the authors took to be a fading transient and likely afterglow of a progenitor event (28). However, there was still a variable radio source, consistent with scintillating emission from an AGN, present at the position a year later, casting doubt on this association (75–77).

A search for the host galaxy of FRB 171020 was conducted; as it had a low DM of 114 pc cm^{-3}, its location was confined to a small search volume with 16 candidate galaxies, with the single most likely selected for analysis (47). As an indirect localisation, this was not definitive; however, it did show that there was no R1-like persistent radio source in the search volume (47).

1.2.1 The era of localisation

The CRAFT survey (78) was the first to achieve a host galaxy localisation for a single burst, using ASKAP (26, 73). FRB 180924 was localised to sub-arcsecond precision, which enabled not only association with a host galaxy, and subsequent characterisation of redshift and other galactic properties, but also placement within the structure of the galaxy itself (73).

CRAFT has now localised several FRBs, including FRB 181112 (1), FRB 190102 (2, 3), FRB 190608 (2, 3) and FRB 191001. Although made to varying degrees of precision, each of these localisations resulted in the identification of a host galaxy. Limits have also been placed on repetition from the CRAFT sample. FRB 180924 in particular, with follow-up observations taken of its host galaxy, was not found to repeat - the conclusion being that if any repetition occurs it is different in nature to R1 (73). In addition to the CRAFT bursts, FRB 190523 has been localised to a region of 3 by 8 arcseconds by DSA-10, and a galaxy inside that region is identified as the host of the burst (79).

The newfound ability to localise FRBs is a substantial breakthrough, and provides a wealth of scientific opportunity. Besides the potential to weigh the intergalactic medium (61) and characterise the 'typical' FRB host environment, we can now begin searching more precisely for the multi-wavelength signatures predicted, by some theories, to accompany the bursts (15, 67).

CRAFT host galaxies are named following HG YYMMDD, corresponding to the name of the FRB itself. This project focuses on the host galaxies of five CRAFT-localised FRBs: HG 180924, HG 181112, HG 190102, HG 190608 and HG 191001. The host galaxies of these and other localised FRBs will be discussed in the main body of this work. Details of the FRBs traced to these galaxies are provided in Table A.1.

1.2.2   Localising an FRB

Technical limitations make FRB localisation difficult. For single-dish telescopes, the localisation uncertainty is the same as the half power beam width, $\theta_{\text{HPBW}} \approx 1.22\frac{\lambda}{D}$ (in which λ is the wavelength and D is the dish diameter; 16). For a typical FRB frequency of 1400 MHz, and the Parkes dish diameter of 64 m, this results in uncertainties on the order of[10] $0.2°$. Interferometric radio telescopes improve on this, giving a D roughly equivalent to the longest baseline (16). With use of a phased-array feed and digital beam-forming this can be reduced even further (78). The process is, however, computationally complex, requiring a good deal of processing power - especially when attempted in real-time (16). Compounding the localisation difficulty is the fact that, because of the trade-off between field-of-view and spatial precision, a higher rate of FRB detection usually means less-precise localisation (80). Neatly demonstrating this is CHIME, which has proven extraordinarily effective at detecting large numbers of FRBs but can only locate them down to a few arcminutes at best (24, 74); and CRAFT, which can localise FRBs to an arcsecond or less but has done so on the order of ten times.

ASKAP has 36 twelve-metre antennae, each equipped with a phased-array feed, and a 6 km maximum baseline. It is thus able to achieve an angular resolution of ~ 10 arcseconds at 1320 MHz, and can pinpoint positions to a statistical uncertainty of ≈ 10 arcsec / (2×S/N), where S/N is the signal-to-noise ratio of the source (73). The CRAFT localisations were achieved on ASKAP with a real-time mode designed for the specific purpose of localising FRBs (73). The refined burst data of FRB 180924 had S/N of 194, which enabled statistical uncertainty down to 0.04 arcseconds (73). The ASKAP interferometric image was bootstrapped to a deeper Australia Telescope Compact Array (ATCA) observation, which contained a well-localised continuum radio source that also happened to have an optical counterpart in the Dark Energy Survey (73, 81). Thus the FRB was located within an optical frame and pinpointed to a host galaxy, which also appeared in the Dark Energy Survey (73). The final uncertainty, a combination of systematic and statistical, rests at 0.12 arcseconds (73).

1.3   Luminous transients

As mentioned in previous sections (§ 1.1.1, § 1.1.3), there are a number of candidate FRB mechanisms which predict association with a supernova, kilonova or other luminous optical transient. Supernovae are enormously bright explosions that mark the endpoints of certain stars (12). They are understood to occur through two primary mechanisms - core collapse of massive stars and runaway fusion in white dwarfs. These mechanisms are not, however, the primary basis for their classification - rather, they are classified observationally, based on their spectral lines and light curves. Type II supernovae exhibit strong hydrogen lines, while Type I do not (82). There are then several subclasses, the primary of which are summarised below (82):

Type Ia: Prominent Si II absorption line; believed to be generated by white dwarfs undergoing runaway nuclear fusion, either from a merger of two white dwarfs or accretion from a companion, with light curves like that shown in Figure 1.2 (5).

Type Ib: No silicon absorption line; strong He I absorption line; believed to be core-collapse events in which a massive star's outer envelope has been lost (83).

Type Ic: No silicon absorption line; weak to no He features; also a product of stripped-envelope core collapse, but where both hydrogen and helium have been lost (83).

---

[10] $\theta_{\text{HPBW}} = 1.22\frac{c}{fD} = \dfrac{3 \times 10^8 \text{ m s}^{-1}}{1400 \times 10^6 \text{ Hz} \times 64 \text{ m}} = 0.0041 \text{ rad} = 0.235°$)

Type IIb: Initially display hydrogen features but evolve to become more like Type Ib events; also likely to involve a depleted envelope (83).

Type IIn: Demonstrate narrow emission lines, thought to result from interactions between supernova ejecta and a dense circumstellar medium (82, 84)

Type II-L: The light curve (plot of magnitude versus time) declines linearly following peak (85).

Type II-P: After peak, the light curve enters a plateau phase before sinking again, which is understood to result from a shift in opacity of the star's outer layer (85).

Within these subclasses are a number of peculiar sub-subclasses; as the distinctions between them are chiefly spectroscopic, and the focus of this work is on their photometric properties, these peculiar types will not be explored here (82). However, because of their possible association with magnetars - objects which are of special interest to FRB science because of their potential as progenitors - superluminous supernovae (SLSNe) are worth mentioning (86). SLSNe demonstrate a set of spectroscopic characteristics as diverse as their regular kin, and are classified similarly; but with the unifying characteristic of peak luminosities well in excess of the regular population (86).

Kilonovae[11] are the electromagnetic signatures of compact-object mergers, particularly those between binary neutron stars (87). Although the optical components of kilonovae are fainter than those of supernovae, they are observable at least at low redshifts, as demonstrated by observations of AT 2017gfo (the optical counterpart of GW170817; 68). Detecting them optically out to redshift 0.5 will likely be substantially more challenging. It has been suggested that distant kilonovae might be observed through the shock afterglow of the associated gamma-ray burst (89).

Aside from these two classes of slow luminous transient, it could also be that FRBs are associated with a yet-unknown optical counterpart, which might be detected by similar methods to supernovae.

---

[11]So-named because they are approximately 1000 times more luminous than a regular nova (87); they are still, however, two to three orders of magnitude less luminous than supernovae (88)

<div style="text-align: right; font-size: 4em; color: #ccc;">2</div>

Imaging & photometry

The first stage of this project was to undertake a basic photometric analysis of the FRB host galaxies. Using these data and other information on the hosts, we can draw some inferences on the nature of a single-burst host galaxy.

2.1 Data

The primary imaging data for this project were taken on the **Fo**cal **R**educer and low dispersion **S**pectrograph **2** (FORS2; 90), an instrument mounted on Unit Telescope 1 (UT1) of the Very Large Telescope (VLT). Secondary data was also taken using X-shooter (91) on UT2, in imaging mode[1].

FORS2 has two CCD chips. As a result, two FITS (93) files are output from FORS2 for each exposure, one for each chip. The target coordinates fall on Chip 1. Since part of the CCD is masked by the filter frame, there is a blank border around the edges of the science images, resulting in a field-of-view of 6.8 by 6.8 arcminutes, and a pixel scale, with the 2×2 binning used here, of ~ 0.25 arcseconds per pixel. The X-shooter pixel scale is 0.17 arcseconds per pixel, with a single CCD chip and a field-of-view of 1.5 by 1.5 arcminutes. The throughput curves for the FORS2 filter set are available for reference in Figure A.1.

The host galaxies of three well-localised FRBs (FRB 180924, FRB 181112, and FRB 190102) were each observed using FORS2 and X-shooter, while HG 190608 was observed only on X-shooter and HG 191001 was observed only on FORS2. A summary of the VLT observations is given in Table 2.1. Each observation consists of several dithered (at slightly different pointings) exposures. Although observations of the three main host galaxies were taken relatively soon after the burst, the repeat observations necessary to undertake a subtraction (described in § 3.1) were delayed for quite some time in order to allow time for any supernova-like counterpart to fade. For the case in which the required images were not acquired on FORS2 in time for this project, backup observations were taken using X-shooter's imaging mode, during CRAFT's Visitor Mode night on 2019-08-21. However, satisfactory repeat observations on FORS2 of all three galaxies, in the *g* and *I*-bands, were finally taken on 2019-08-23.

---

[1]Although primarily a spectrograph, X-shooter does now offer an imaging mode using the acquisition camera (92).

FRB	Date (UTC)	Instrument	Filter	t_{exp} (s)	FWHM (arcsec)
180924	2018-11-09	FORS2	g_HIGH	5×500	1.29
			I_BESS	5×90	1.34
	2019-08-21	X-shooter	g_prime	9×300	0.80
			I	9×120	0.77
	2019-08-23	FORS2	g_HIGH	5×500	1.11
			I_BESS	5×90	1.40
181112	2018-12-03	FORS2	g_HIGH	5×500	1.02
			I_BESS	5×90	1.00
	2019-08-21	X-shooter	g_prime	9×300	1.03
			I	9×120	0.72
	2019-08-23	FORS2	g_HIGH	5×500	1.14
			I_BESS	5×90	1.20
190102	2019-01-12	FORS2	g_HIGH	3×500	1.57
			I_BESS	5×90	1.42
	2019-06-17	FORS2	u_HIGH	5×660	1.79
			z_GUNN	5×30	1.18
	2019-08-21	X-shooter	g_prime	9×300	1.00
			I	9×120	0.71
	2019-08-23	FORS2	g_HIGH	5×500	1.13
			I_BESS	5×90	1.11
190608	2019-08-21	X-shooter	g_prime	8×300	0.74
			I	8×120	0.70
191001	2019-10-05	FORS2	g_HIGH	10×500	1.11
			I_BESS	10×90	0.99

Table 2.1: VLT imaging runs for each FRB host galaxy. The full width at half-maximum of the delivered point-spread function was measured using PSFEx; it is the combined result of atmospheric seeing, instrumental response and coaddition (which could potentially modify the point-spread function).

We were thus able to use both datasets, especially in Chapter 4.

2.2   Image Processing

A set of pipelines was written, using bash, Python (particularly the module ASTROPY (94, 95) and other modules where noted), and a handful of external packages, for automating the processing of the images to the state required by this project and the CRAFT group. The procedures for these pipelines are outlined below. All code written for this project, including these pipelines, is available in the GitHub repository located at https://github.com/Lachimax/craft-optical-followup. The final products of the processes below are shown in Figure 2.5 and Figure 2.6.

2.2.1   FORS2

1. The science images and raw calibration data are downloaded from the ESO Raw Data Archive[2] using a script retrieved from the archive.
2. Raw frames are reduced with the ESO Reflex FORS2 pipeline 2.9.1 (§ 2.2.3).

---

[2]https://archive.eso.org/eso/eso_archive_main.html

Survey	180924	181112	190102	190608	191001
Dark Energy Survey	Yes	Yes	No	No	Yes
SDSS	No	No	No	Yes	No
SkyMapper	Yes	Yes	Yes	Yes	Yes

Table 2.2: Survey coverage of CRAFT-localised FRB fields.

3. Reduced frames are trimmed to remove the noise border (§ 2.2.4).
4. FITS files are each converted to ADU (analogue-to-digital units) per second (§ 2.2.4).
5. The individual frames are co-added using Montage (§ 2.2.5).
6. The co-added image is trimmed again in Python.
7. The co-added image is uploaded to Astrometry.net to improve the World Coordinate System (WCS) solution; if necessary this is tweaked using a survey catalogue (§ 2.2.6).
8. Photometric calibration is undertaken using SExtractor and Python by comparison with an external catalogue (§ 2.3). This is performed either:
    (a) Directly on the science field; OR:
    (b) On the standard-field images provided as calibration data.
9. Integrated magnitudes of the objects of interest are taken using SExtractor (§ 2.4).

2.2.2 X-shooter

1. The science images and raw calibration data are downloaded as above.
2. De-biasing and flat-fielding is performed using CCDPROC in Python (§ 2.2.3).
3. A fringe map of the CCD is constructed and used to subtract fringe patterns (§ 2.2.3).
4. Science images are co-added with Montage (§ 2.2.5).
5. Astrometry is tweaked using a survey catalogue (§ 2.2.6).
6. Photometric calibration is undertaken as above.
7. Photometry is extracted with SExtractor (§ 2.4).

2.2.3 Reduction

For FORS2, initial reduction is undertaken with ESO Reflex[3] 2.9.1 (96), using FORS pipeline 5.4.3. ESO Reflex takes care of flat-fielding and de-biasing, using the raw calibration data downloaded from the ESO portal.

For the X-shooter images, for which a pipeline is not provided, these tasks were accomplished using a custom Python script that makes use of the package CCDPROC[4] (97). The bias frames are median-stacked to produce a master bias, which is then subtracted from the science and sky flat-field images. The flat-field images are also median-stacked, this master flat is normalised to 1, and the science images are divided by the master flat.

X-shooter's imaging mode, utilising a thinner CCD than FORS2, falls prey to significant fringe patterns - a phenomenon caused by thin-film interference effects in the chip itself. These are worse at longer wavelengths, being imperceptible in our g images but quite prominent in our I images. These are dealt with here by constructing a fringe map by median-stacking the images, scaling it to each individual frame, and subtracting it, based on the steps suggested on the EFOSC2 website[5].

---

[3]https://www.eso.org/sci/software/esoreflex/
[4]https://ccdproc.readthedocs.io/en/latest/
[5]https://www.eso.org/sci/facilities/lasilla/instruments/efosc/inst/fringing.html

2.2.4 Further processing

During the course of reduction, a good deal of noise is introduced to the previously blank border of the images, which exceeds the sky background and is frequently brighter than typical sources in the field. This 'noise border' is cropped here to avoid problems with Montage and SExtractor later on, and the image WCS corrected to compensate for the shift in reference pixel. The pixel values of the files are then divided by the image exposure time, which converts the image units to ADU per second.

2.2.5 Montage

The co-addition of our images required a separate code. SWarp[6] (98) was tested and discarded due to lack of compatibility and support. Other options, such as AstroImageJ and IRAF, were also considered, but Montage was selected for its ease of use and compatibility.

Montage is a package designed for mosaicing astronomical images (99). It applies robust techniques to dealing with overlapping regions, which also makes it useful for co-adding multiple exposures of the same field. The software is broken up into a series of modules which can function independently; the procedure used here loosely follows the one given in the tutorial at http://montage.ipac.caltech.edu/docs/first_mosaic_tutorial.html. Detailed explanations of the algorithms used can be found in the Montage documentation[7].

Montage first examines the input images and the WCS properties listed in their headers. It then re-projects the pixels of each image into a common pixel grid, by first mapping the pixels from the input pixel space to sky coordinates and then from sky coordinates to the output pixel space. Care is taken to conserve flux. Now that the images are mapped to the same pixel space, the software analyses the overlaps between them. For each pair of overlapping images, a difference image is produced, subtracting one from the other in the overlapping region. To model the sky background, a simple plane is fitted to the pixel values of the difference image, rejecting outliers. The full set of overlap brightness planes is then used to determine which corrections to apply to each image, generating a plane to be subtracted from each image, in order to globally minimise difference in sky background between images. Once these corrections are applied, the re-projected, background-corrected images are co-added. We use a median co-add - thus, for each pixel, the median value is selected from the stack of re-projected pixel values. This eliminates cosmic rays, reduces instrumental effects, and somewhat flattens the background noise.

Outside of Montage, the co-added image is trimmed again in Python, using the area files produced by Montage, to exclude the regions with least overlap. This is done because SExtractor had difficulty with the edges of the overlap region, which do produce a discontinuity in the background noise.

2.2.6 Astrometry

The values of the WCS keywords provided by the instruments used in this project are not perfectly accurate, and correction to a well-understood reference frame is necessary - especially given the importance of astrometry to the CRAFT project in general. For the bulk of this project, this was achieved by uploading the co-added image to Astrometry.net (100). This is an online service which is able to ascertain the WCS information - that is, the pointing, orientation and image scale - from the pixel values alone.

However, the solution generated by Astrometry.net, although better than the default

---

[6]https://www.astromatic.net/software/swarp
[7]http://montage.ipac.caltech.edu/docs/index.html

FORS2 output, is also imperfect. A definite offset from Dark Energy Survey (DES; 81) positions of 0.25 to 0.5 arcseconds is apparent in the images processed by Astrometry.net. The tool has not yet been updated with *Gaia* (101) positions, which have become the gold standard of astrometry. Rather, it is based on catalogues such as USNO-B, 2MASS and SDSS, which, in terms of astrometry, are becoming less valid for current epochs. It also does not work with X-shooter images because of the small field-of-view.

When it is required that the astrometry line up with a survey frame (usually DES or *Gaia*), this is resolved by directly bootstrapping from that catalogue. SExtractor (see § 2.2.7) is first used to produce a catalogue directly from the image; the image sources are matched to the external catalogue, the offsets (in RA and DEC) of the two sets of positions are calculated, and the median of these is simply subtracted from the reference values (CRVAL1 & CRVAL2) in the FITS header. If this automated result is still insufficient, an offset can be specified manually after examining the images and over-plotted positions.

2.2.7   Source Extraction

To extract useful photometry information from the images, another intermediate code was necessary. PHOTUTILS[8] (102), SExtractor (103) and DOLPHOT[9] (104) were each tested for this purpose. DOLPHOT was considered but was found to be unsuited to our data.

Although a substantial amount of initial work was done with PHOTUTILS, and it proved very useful as a low-level toolset for photometry, SExtractor was eventually selected. After some initial hurdles, SExtractor proved easiest to work with, and is also quite feature-rich and well-documented[10] compared to PHOTUTILS - which has not yet implemented some of SExtractor's more useful second-order features. Among these is the parameter CLASS_STAR, which uses a neural network to provide an estimate of the probability that a given object is a star, as opposed to an extended object. Values approaching 1 are star-like, and values closer to zero are galaxy-like. Although it is far from infallible (sometimes varying significantly between filters; 70), it is useful as a general indicator of how point-like an object is. This quantity has previously been used by Andreoni et al (70) for assessing the classification of stars. The CLASS_STAR feature became particularly useful for calibration (§ 2.3), which is more straightforward when the objects considered are limited to point sources.

A superior output called SPREAD_MODEL exists in newer versions of SExtractor, which functions similarly; the SExtractor documentation[11] recommends it over CLASS_STAR. However, it is an order of magnitude slower. SPREAD_MODEL was tested here instead of CLASS_STAR for use in zeropoint calculation (see § 2.3.1), but results were nearly identical. The trade-off in speed was considered too great, so CLASS_STAR was adopted instead.

SExtractor does not make use of an annulus for background subtraction, instead calculating a map of the background across the entire image. This process is explained thoroughly in the SExtractor documentation[12].

SExtractor is fairly widely-used (7, 79, 92, 100, 106–109). It comes packaged with the ESO Reflex pipeline and is used there for source detection (110, 111). It was also, importantly, used in the generation of the Dark Energy Survey (DES) catalogue (81), which the following sections make use of.

---

[8]https://github.com/astropy/photutils (102).

[9]http://americano.dolphinsim.com/dolphot/

[10]Liberal use was made here of Source Extractor for Dummies (105).

[11]https://sextractor.readthedocs.io/en/latest/Model.html#model-based-star-galaxy-separation-spread-model

[12]https://sextractor.readthedocs.io/en/latest/Background.html

2.3   Photometric calibration

2.3.1   Zeropoint determination

The instrumental magnitude of an astronomical object is given by:

$$m_{ins} = -2.5 \log_{10} \left(\frac{F}{t_{exp}} \right) \tag{2.1}$$

in which F is the total flux from the object as counted by the instrument over the exposure time, in ADU; and t_{exp} is the exposure time in seconds. Then, the true apparent magnitude of the object m_0, as though observed from above the atmosphere, is given by:

$$m_0 = m_{ins} + m_{zp} - kX + cC \tag{2.2}$$

where m_{ins} is the instrumental magnitude of the object; m_{zp} is the instrumental zeropoint; k is the extinction coefficient; X is the airmass, usually approximated as $\sec(z)$, where z is the angle from vertical; c is the colour term; and C is the colour of the object.

The instrumental zeropoint is the brightness of an object, in magnitudes, required to generate one ADU per second in the given CCD and filter. Clearly this value is necessary in order to perform accurate absolute photometry; however, it is not provided for all filters on FORS2. ESO Quality Control[13] does provide zeropoints and other calibration parameters for the filters b_HIGH, v_HIGH, R_SPECIAL and I_BESS, each calculated for every night in which the relevant filter is used. It does not provide zeropoints for g_HIGH, u_HIGH or z_GUNN (or, indeed, any photometric calibration quantities for these filters). Thus, it was necessary to calculate these quantities for the photometric measurements of our host galaxies.

If we take the colour term as negligible, we can reduce Equation 2.2 as follows:

$$
\begin{aligned}
m_0 &= m_{ins} + m_{zp} - kX \\
m_{ins} &= m_0 - (m_{zp} - kX)
\end{aligned}
\tag{2.3}
$$

As both m_{zp} and kX are approximately constant over a single exposure, this gives us an equation of the form $y = mx + b$. The y-intercept is $b = -(m_{zp} - kX)$, while the slope is simply $m = 1$. So, when the instrumental magnitudes of the stars in an image are plotted against their magnitudes in a reliable catalogue, we can retrieve the calibration information $m_{zp} - kX$.

This was implemented by fixing the slope to 1. Only point-sources, as the most reliably measurable, are used. Whether a source qualified as point-like was decided using CLASS_STAR, generally with a threshold of 0.9 to 0.95. A value of 0.95 was adopted for FRB 181112 and 0.9 for FRB 180924. The threshold was chosen to exclude unsuitable sources while also considering enough stars for a reasonable uncertainty estimate. In case the slightly differing sensitivities and photometric properties of the two CCD chips have an effect (ESO provides two sets of calibration quantities, one for Chip 1 and one for Chip 2), only objects on Chip 1 are used.

Those objects that are bright enough to deviate from linear behaviour are cut from the appraisal; faint magnitudes are also excluded, as their lower signal-to-noise ratio results in greater scatter. These cuts were set on a case-by-case basis, by inspection of the resulting plots. An example of the fit is shown in Figure 2.1.

---

[13]http://archive.eso.org/bin/qc1_cgi?action=qc1_browse_table&table=fors2_photometry
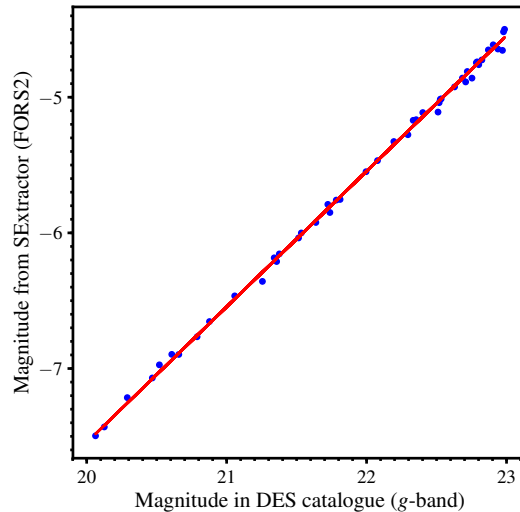
Figure 2.1: An example of the zeropoint determination method used, here operating on the co-added FORS2 image of the field of FRB 180924. Each of the blue points is a point-source, and the red line is the line of best fit with the slope fixed to 1. The resulting $m_{zp} - kX$ is 27.55 ± 0.04 magnitudes.

After one fit iteration, objects offset from the line by more than 0.1 magnitudes are also removed - except with X-shooter, which required a greater tolerance of 0.5. Sources with a greater difference are likely to be bad matches, i.e. were matched erroneously to a survey counterpart. The remainder are fit to an $m = 1$ line once again, and the negative of this line's y-intercept is taken as $m_{zp} - kX$. Uncertainty in $m_{zp} - kX$ was calculated as the root-mean square of the scatter of magnitudes from the linear model.

The coverage of our host galaxies in relevant survey catalogues is given in Table 2.2. The catalogue used for the science-field calibration is the Dark Energy Survey DR1 (81). SDSS is too northerly for our science fields and only useful for the equatorial standard fields. SkyMapper does have coverage of all of our fields, and was also tested for science-field determination. However, the catalogue does not go as deep as DES, and any stars bright enough to appear in the SkyMapper catalogue are also bright enough to saturate the FORS2 detector for the exposure times used here, making them unusable for science-field calibration.

When applying this method directly to the field of the target, we do not need to explicitly calculate the extinction coefficients, as the technique results in a "built-in" extinction correction (see Equation 2.3). Two of the three calibrations (181112 and 180924) could be performed directly on the science images, as the fields lie within the DES DR1 footprint. FRB 190102 does not, nor in any other suitable survey footprint, and it was necessary to refer to the nightly observations of standard star fields, performed by ESO in the relevant filters for each, in order to derive a zeropoint. As $m_{zp} - kX_{std}$ is what we actually measure directly from the field, this does require an additional extinction correction when calculating the final magnitude, which takes the form:

$$
\begin{aligned}
m_0 &= m_{ins} + m_{zp} - kX_{sci} \\
&= m_{ins} + (m_{zp} - kX_{std}) - kX_{sci} + kX_{std} \\
&= m_{ins} + (m_{zp} - kX_{std}) - k(X_{sci} - X_{std})
\end{aligned}
\tag{2.4}
$$

where X_{sci} is the airmass of the science observations and X_{std} the airmass of the standard-star

Field	Band	Field	Airmass	Survey	Quantity	Value
180924	g	Science	1.18(5)	DES	$m_{zp} - kX$	**27.55(4)**
					m_{zp}	27.81(5)
		Landolt SA95	1.3515	DES	$m_{zp} - kX$	27.46(3)
					m_{zp}	27.77(3)
	I	Provided	0	-	m_{zp}	**27.658(2)**
181112	g	Science	1.7(2)	DES	$m_{zp} - kX$	**27.63(3)**
					m_{zp}	27.94(7)
	I	Provided	0	-	m_{zp}	**27.612(2)**
190102	g	Landolt SA95	1.3515	SDSS	$m_{zp} - kX$	**27.82(5)**
					m_{zp}	28.07(7)
	g	Stetson L98	1.259	DES	$m_{zp} - kX$	27.83(5)
					m_{zp}	28.07(6)
	I	Provided	0	-	m_{zp}	**27.619(4)**
	u	Stetson MarkA	1.0615	SkyMapper	$m_{zp} - kX$	**24.80(4)**
					m_{zp}	25.15(5)
	z	Stetson MarkA	1.063	SkyMapper	$m_{zp} - kX$	**27.00(3)**
					m_{zp}	27.03(5)
190608 (X-Shooter)	g	Science	1.046(2)	DES	$m_{zp} - kX$	**27.3(3)**
	I	Science	1.054(5)	DES	$m_{zp} - kX$	**26.9(2)**
191001	g	Science	1.18(2)	DES	$m_{zp} - kX$	**27.52(5)**
					m_{zp}	**27.32(6)**
	I	Provided	0	-	m_{zp}	**27.548(4)**

Table 2.3: Zeropoints and $m_{zp} - kX$, derived as per § 2.3.1; those with field labelled 'Provided' are obtained from the ESO QC1 Archive. For those values, uncertainty is also as reported by the archive tool. Names in the 'Field' column other than Science and Provided are the names of standard-star fields observed by ESO, listed at https://www.eso.org/sci/facilities/paranal/instruments/fors/tools/FORS_Std.html. All quantities are in magnitudes, and the quantities adopted in further calculations are in bold.

observation. For information on how k was estimated, see § 2.3.2.

DES, Sloan Digital Sky Survey (SDSS) DR15 (112) or SkyMapper DR2 (109) were used for calibrations on the standard fields, depending on which survey's coverage the field falls into. DES was preferred over SDSS, and SDSS over SkyMapper, because of the differences in filter throughputs (see Figure A.2).

PSF-fitting is used to derive the magnitudes of calibration sources. Although unsuited for deriving photometry for extended objects, PSF-fitting is ideal for measuring unresolved stars, which are the best candidates for calculating a zeropoint. DES, SDSS and SkyMapper all provide PSF-fitted magnitudes. Hence, the PSF-fit flux option, offered by the combination of PSFEx (113) and SExtractor, was used. SExtractor is first used to extract sources from the image, while also including a 35 by 35 pixel 'vignette' cutout image[14] of each source in the output catalogue. This catalogue is fed to PSFEx, which constructs a model of the point-spread function using appropriate point sources. This model is then fed back to SExtractor, which uses it to produce the quantities FLUX_PSF and MAG_PSF. These quantities should not be used for extended sources (81), as the program fits the model and derives the flux

---

[14]Larger vignette sizes were tried, in case they better captured the PSF, but they did not impact any measurements.

with the assumption that the object is point-like. Further information can be found in the PSFEx documentation[15]. This method cuts the necessity of selecting an aperture size and also negates the danger of selecting an aperture too narrow for the PSF of a given observation (which would result in lost flux and incorrect magnitudes).

As two standard fields were observed in g on the night of the FRB 190102 observations, $m_{\rm zp} - kX$ was measured on both. The two measurements are consistent, yielding (after correcting for atmospheric extinction - see § 2.3.2) $m_{\rm zp} = 28.07 \pm 0.07$ magnitudes and $m_{\rm zp} = 28.07 \pm 0.06$ magnitudes. Although strictly necessary only for FRB 190102, this method was also applied to FRB 180924, as a check of both science-field and standard-field methods. After extinction correction, the results are again consistent, with $m_{\rm zp} = 27.81 \pm 0.05$ mag for the science field and $m_{\rm zp} = 27.77 \pm 0.03$ mag for the standard field. The full set of zeropoints used in this project are given in Table 2.3.

2.3.2 Atmospheric extinction

The Earth's atmosphere acts to reduce the brightness of astronomical sources, particularly in bluer bandpasses. For the cases in which $m_{\rm zp} - kX$ is determined directly from the science field, an extinction correction is not necessary. However, it is required for calculations involving a zeropoint derived from a standard field, i.e. for HG 190102. As with the zeropoint, the ESO QC1 archive does not provide extinction coefficients for g_HIGH, u_HIGH or z_GUNN. They were instead estimated by assuming that extinction is purely a function of the filter's effective wavelength $\lambda_{\rm eff}$. An estimate is derived by fitting an exponential curve using scipy.optimize.curve_fit(), with the four available coefficients (b_HIGH, v_HIGH, R_SPECIAL and I_BESS) as the y-values and effective wavelength $\lambda_{\rm eff}$ as the x. The mean airmass of the individual frames is used for the co-added images.

2.3.3 Galactic extinction

The magnitudes calculated using the methods below (§ 2.4) represent the brightness of the galaxies as seen from above the Earth's atmosphere. However, if one was to view them from outside the Milky Way Galaxy, one would see something different again. The dust grains in the interstellar medium cause extinction similar in principle to that of the atmosphere, with shorter wavelengths dimmed by a greater amount than longer wavelengths. The result is Galactic reddening (114). For a measurement of an object's true colour, a correction for the Galactic extinction in each band is required. This correction is found in the quantity A_λ, the total extinction along a particular line-of-sight at a given wavelength λ.

The values A_λ for each filter used, and $E(B - V)$ along the line of sight, were found using the IRSA Dust tool[16]. This tool provides $E(B - V)$ and A_λ values for both S&F (Schlafly & Finkbeiner; 115) and SFD (Schlegel, Finkbeiner & Davis; 116) reddening maps; S&F, which applies the Fitzpatrick 1999 (F99; 117) extinction law, was selected as the most up-to-date. A range of extinction values A_λ are provided by IRSA for various common bandpasses. The specific filters used here are not among them, so the values along each line-of-sight were interpolated using the function numpy.interp(), with the assumption that the Galactic extinction is a pure function of effective wavelength. The adopted values are provided in Table 2.4. This interpolated A_λ is then subtracted from the galaxy magnitude. Uncertainty in the quantity A_λ is not provided by the IRSA Dust Tool, and is difficult to estimate, particularly for these interpolated values. It is hence not included here; corrected values are given as estimates only.

---

[15]https://psfex.readthedocs.io/en/latest/
[16]https://irsa.ipac.caltech.edu/applications/DUST/

Quantity	FRB 180924	FRB 181112	FRB 190102	FRB 190608	FRB 191001
Kron factor	1.4	1.6	2.5	2.5	2.2
$E(B-V)_{\mathrm{MW}}$	0.0165	0.0174	0.1994	0.0399	0.0249
A_u (mag)	0.08	0.09	1.0	0.2	0.12
A_g (mag)	0.06	0.07	0.8	0.15	0.1
A_I (mag)	0.04	0.03	0.4	0.08	0.05
A_z (mag)	0.03	0.03	0.3	0.06	0.04

Table 2.4: Miscellaneous calibration parameters used in photometric measurement.

2.4 Integrated Magnitudes

2.4.1 SExtraction

The goal of the calibrations here was to measure the integrated photometric magnitudes of the galaxies of interest. This was done with SExtractor, making use of functions known as MAG_AUTO and FLUX_AUTO. This was partly for parity with the Dark Energy Survey, which used the very same functionality in generating its DR1 catalogue (81). This includes the photometry quoted in CRAFT's papers (1, 73).

The AUTO quantities from SExtractor essentially apply aperture photometry, in which all of the flux within an aperture around a source is summed, but with an elliptical aperture that is automatically scaled by the size and elongation of each individual source. This is performed using an adapted form of Kron's first moment algorithm (118). Once the first moment r_1 is calculated for an individual galaxy, it is scaled by the Kron factor k, which is 2.5 by default but can be specified by the user. The value kr_1 is the Kron radius. In SExtractor output, the Kron radius is given as a number by which a and b, the galactic ellipse semi-major and semi-minor axes as fitted isophotally, are multiplied, to give the semi-major and semi-minor axes of the Kron aperture. More detailed descriptions can be found in the SExtractor documentation[17].

One problem with this automated approach is that the apertures can include light from neighbouring galaxies, especially in the cases of HG 180924 and HG 181112, both of which have galaxies nearby them in the sky. It seemed best to deal with this by reducing the aperture size using the Kron factor k. This was fine-tuned for the 'crowded' galaxies to minimise overlap while including as much flux from the galaxy as possible. The resulting apertures are seen in Figure 2.2, with the specific factors used given in Table 2.4.

SExtractor's 'dual-image mode' is used here in images of the same field taken on the same night, but in different bands. Source detection and aperture determination is performed by SExtractor using the deepest image, and the same apertures are used in the other image. This is done to ensure flux is measured over the same area in the sky. Before the source extraction, the images are trimmed to ensure that they each lie on the same pixel grid.

Once SExtractor has been used to construct a catalogue of image sources, the instrumental magnitude is calculated from FLUX_AUTO using Equation 2.1; the apparent magnitude m_0 is then calculated using Equation 2.3. For the final set of integrated magnitudes, see Table 2.6. As the first FORS2 epoch of each field was taken under photometric conditions, these epochs are assumed to be the more reliable and are used in the calculations.

2.4.2 Uncertainties and the propagation thereof

SExtractor calculates the uncertainty in an aperture flux as:

---

[17]https://sextractor.readthedocs.io/en/latest/Photom.html#automatic-aperture-flux-flux-auto
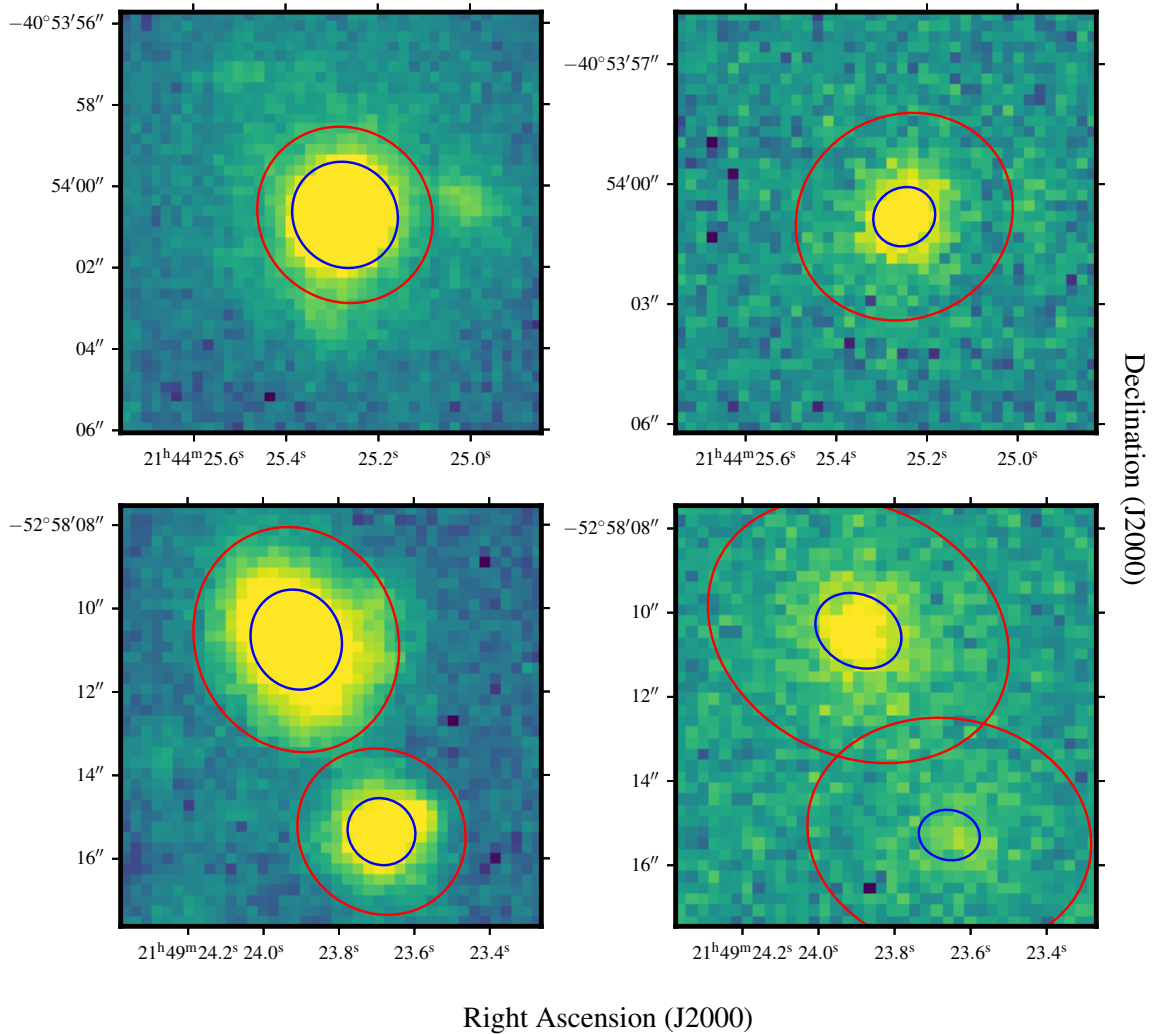
Figure 2.2: A demonstration of the AUTO aperture. Blue ellipses are the fit (a, b and θ) to the galaxy shape by SExtractor, while red ellipses are the Kron apertures used to calculate FLUX_AUTO and MAG_AUTO. Top is HG 180924, and bottom HG 181112 with the foreground galaxy FG181112_13_5. Left are the processed g_HIGH FORS2 images, with ellipses from the generated SExtractor catalogue; right are the g DES cutout images, with ellipses from the DES catalogue.

$$\Delta F = \sqrt{\sum_{i \in A} \left(\sigma^2 + \frac{p_i}{g_i} \right)} \tag{2.5}$$

where A is the set of pixels contained in the aperture, σ is the standard deviation of the local background noise, p_i is the value of the pixel i, and g_i is the effective gain of that pixel. A gain map can be provided to SExtractor, but as the pixels we are concerned with all have the same effective gain, only a single value was provided for each image, $g_i = g_{\mathrm{eff}}$. This was calculated for our co-added images using (105):

$$g_{\mathrm{eff}} = \frac{2 \times N \times g_{\mathrm{ind}}}{3} \tag{2.6}$$

where N is the number of images included in the median stack and g_{ind} is the gain for an individual frame. As the individual images had also been converted to counts per second,

FRB	180924	181112	190102	190608	191001
Angular distance from nucleus (arcsec)	0.7 ± 0.2	$0.5^{+2.7}_{-0.5}$	$0.3^{+0.8}_{-0.3}$	3.2 ± 0.6	2.0 ± 0.2
Angular size distance (Mpc)	971.7	1238.0	908.0	442.1	764.0
Projected offset from nucleus (kpc)	3.5 ± 0.9	$3.1^{+15.7}_{-3.1}$	$1.5^{+3.4}_{-1.5}$	17.2 ± 4.9	7.5 ± 0.6

Table 2.5: Offsets of the FRBs from their host galaxy nuclei, with angular size distances used in the calculation.

this was also converted using $g_{\text{ind}} = t_{\text{exp}} \times g_{\text{original}}$. For FORS2 images, g_{original} is given as 0.8 electrons per ADU.

The flux uncertainty is converted to magnitudes by taking:

$$\Delta m_{\text{ins}} = \max \begin{cases} \left| 2.5(\log_{10}(F) - \log_{10}(F - \Delta F)) \right| \\ \left| 2.5(\log_{10}(F) - \log_{10}(F + \Delta F)) \right| \end{cases} \tag{2.7}$$

The full uncertainty equation for the corrected integrated magnitudes is:

$$\Delta m_0 = \Delta m_{\text{ins}} + \Delta m_{\text{zp}} + kX \left(\frac{\Delta k}{k} + \frac{\Delta X}{X} \right) \tag{2.8}$$

where Δk and Δm_{zp} are the uncertainties in their respective quantities, calculated as per § 2.3.1 and § 2.3.2. In the co-added images, ΔX is the greatest difference between the airmass of an individual frame and the mean value used in calculations, used to account for the variation over the length of the observation.

2.4.3   Other calculations

The angular separation of each FRB from the nucleus of its host galaxy was measured using the host galaxy position provided by SExtractor in the tweaked-astrometry images. The uncertainty in those measurements is the sum of the (quadrature) uncertainty in FRB position ($\sqrt{\Delta x^2 + \Delta y^2}$, all coordinates in arcsecs) with the uncertainty in centroid position (converted from a variance σ^2, as given by SExtractor, to a 2σ uncertainty, and again added with $\sqrt{\Delta x^2 + \Delta y^2}$).

This angular separation is converted to a projected distance using an angular size distance, calculated from the host redshift using Ned Wright's Javascript Cosmology Calculator[18] (119) with default input values ($H_0 = 69.6\,\text{km s}^{-1}\,\text{Mpc}^{-1}$, $\Omega_M = 0.286$, $\Omega_{\text{vac}} = 0.714$). See Table 2.5 for the results of the calculations.

2.5   Results & Discussion

The final results of the photometry measurements are given in Table 2.6. Because the u-band observation of HG 190102 was made during the full moon, resulting in a non-detection, only an upper bound could be placed on its brightness. The photometry for HG 190608 is significantly less precise due to the extra difficulty of calibrating the narrower field-of-view X-shooter data. The magnitudes measured here for g from those catalogued in DES by more than the quoted uncertainties. For I-band, the two are, in all cases, consistent to within uncertainty, despite the differences between the Bessell filter used in this work and the DES

---

[18]http://www.astro.ucla.edu/~wright/CosmoCalc.html

Property	HG 180924	HG 181112	*FG 181112*	HG 190102	HG 190608	HG 191001
VLT						
u (mag)	-	-	-	> 24	-	-
	-	-	-	> 23	-	-
g (mag)	21.38(4)	22.57(4)	21.34(4)	22.6(1)	17.9(3)	19.00(5)
	21.32	22.50	21.27	21.8	17.75	18.90
I (mag)	20.10(2)	21.51(4)	19.27(2)	21.10(5)	17.2(2)	17.886(8)
	20.06	21.48	19.24	20.72	17.12	17.836
z (mag)	-	-	-	20.8(2)	-	-
	-	-	-	20.5	-	-
$g - I$ (mag)	1.28(5)	1.06(8)	2.07(5)	1.54(2)	0.7(5)	1.12(6)
	1.26	1.02	2.03	1.1	0.63	1.06
a (arcsec)	1.34(1)	0.84(2)	1.216(8)	0.93(2)	1.711(4)	1.433(3)
b (arcsec)	1.262(9)	0.78(1)	1.079(7)	0.67(2)	1.590(4)	1.047(3)
θ (degrees)	47.34	40.37	69.44	-88.24	-50.2	-51.27
Kron radius	1.66	2.48	2.25	3.13	3.5	2.8
DES						
g (mag)	21.62(3)	22.71(9)	21.42(3)	-	-	19.225(4)
i (mag)	20.14(2)	21.49(6)	19.34(1)	-	-	17.960(3)
a (arcsec)	0.793(9)	0.73(2)	1.065(8)	-	-	0.7581(5)
b (arcsec)	0.722(8)	0.59(2)	0.847(5)	-	-	0.7432(5)
θ (degrees)	-30.91	10.97	27.77	-	-	10.95
Kron radius	3.5	4.65	3.5	-	-	3.5

Table 2.6: Photometric properties of FRB host galaxies, plus FG181112_13_5, the galaxy in the foreground of HG 181112. For each quantity, the second row (*A*-corrected) has been corrected for Galactic extinction as per § 2.3.3. *a* and *b* are the semi-major and semi-minor axes of SExtractor's isophotal fit to the galaxy, while the Kron radius (in multiples of *a* and *b*) is the radius of the aperture used for the derived AUTO parameters. θ is the angle of the semi-major axis from E toward W. DES (81) catalogue values have been provided for comparison; see § 2.5 for discussion.

filter set (see Figure A.3).

For g, the differences are also most likely due to the differences between the two g-band filters (see Figure A.2), with the FORS2 bandpass having significant additional throughput below 4000 angstrom compared to DES. The differing depth of the images, as made obvious in Figure 2.2, may also contribute - even though their AUTO apertures are larger, the DES source extraction likely misses a significant amount of flux from the hosts to the background.

2.5.1 Host galaxy properties

Further host galaxy properties from CRAFT publications are given in Table A.1. Using the photometry in Table 2.6, our hosts can be placed on the galaxy colour-magnitude diagram in Figure 2.3. Considered alongside CRAFT's published radio and spectroscopic observations (1–3, 73), this sheds some light on the properties of the hosts. They are of particular note when compared (or rather, contrasted) with the host of FRB 121102 (R1).

R1 belongs to a low-mass, low-metallicity dwarf galaxy (80), and is coincident with a region of intense star formation (122). As it was, for quite some time, the single known FRB host galaxy, it has been the focus of a great deal of study and speculation, occasionally inviting extrapolation of its properties to all FRBs (80, 122). In particular, as the host is
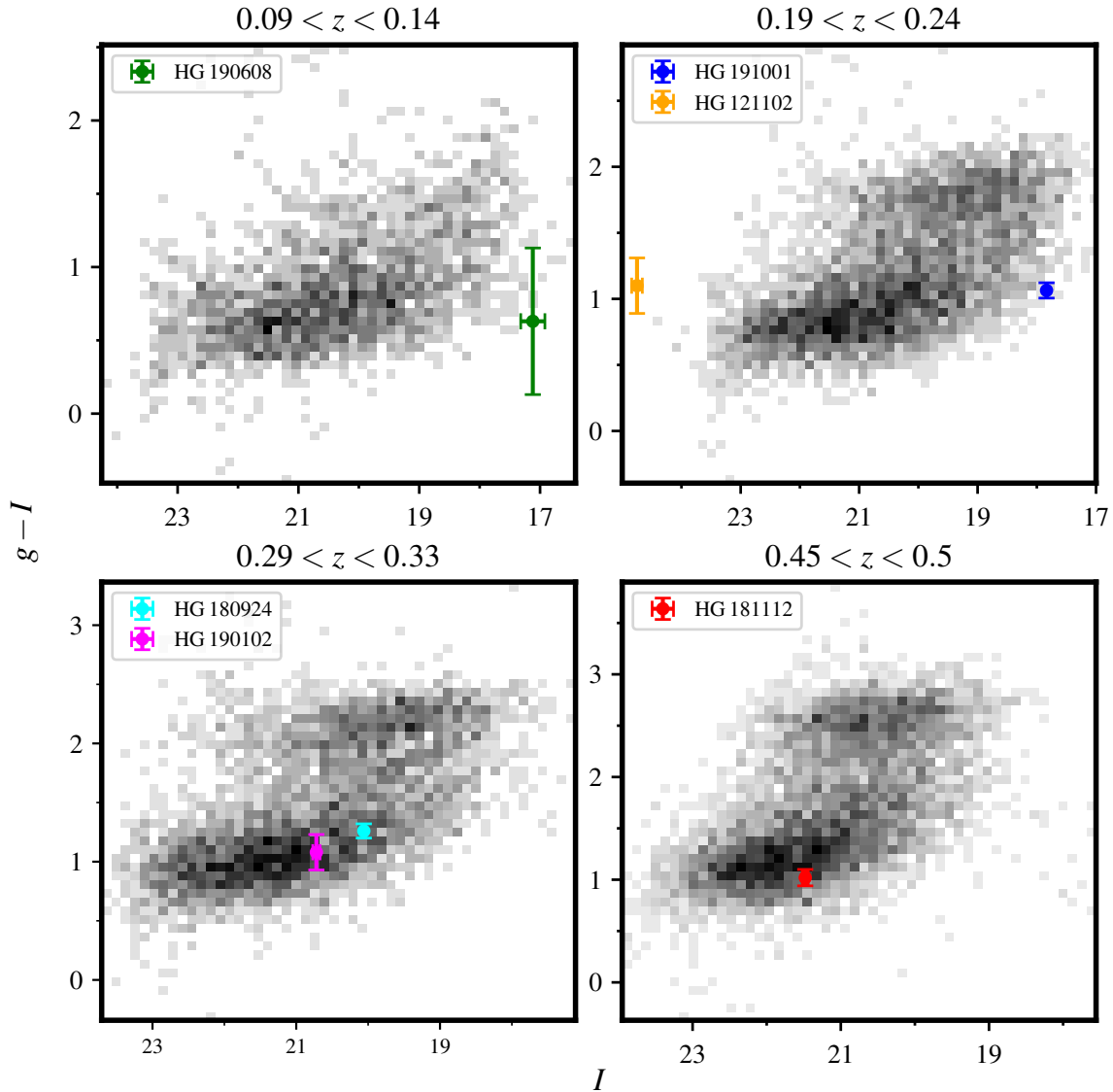
Figure 2.3: Colour-magnitude diagrams using PRIMUS (120, 121) galaxy synthesised observer-frame apparent magnitudes (SDSS bandpass for g, Bessell bandpass for I) in the specified redshift ranges, with FRB host galaxies overlaid using the Galactic extinction-corrected values in Table 2.6. Uncertainties are taken from the non-corrected values. For HG 121102, integrated magnitudes are in g' and i', from Bassa et al 2017 (122), corrected for . Samples are limited to z-quality = 4, the highest quality flag in PRIMUS.

similar to typical hosts of superluminous supernovae and long gamma ray bursts (80), and these are thought to be linked to the formation of magnetars (86), this host association has contributed much to that particular line of progenitor reasoning. Although certainly of relevance to repeaters, extrapolating such properties to FRBs in general is likely to be misleading. Repeaters, and R1 in particular, seem to be exceptional in the FRB population (49, 70). On a BPT diagram[19], such as Figure 2.4, the host galaxy lies firmly in the star-forming locus (80), and R1 itself in an intensely star-forming region (122). R1 is also coincident with a faint, persistent radio source within the host (20).

---

[19]A BPT (Baldwin, Phillips & Terlevich; 123) diagram plots the flux of the [O III]/Hβ emission line of a galaxy against the flux of its [N II]/Hα emission line, and can hence be used to classify LINER, star-forming and Seyfert galaxies based on the dominant source of their emission lines.
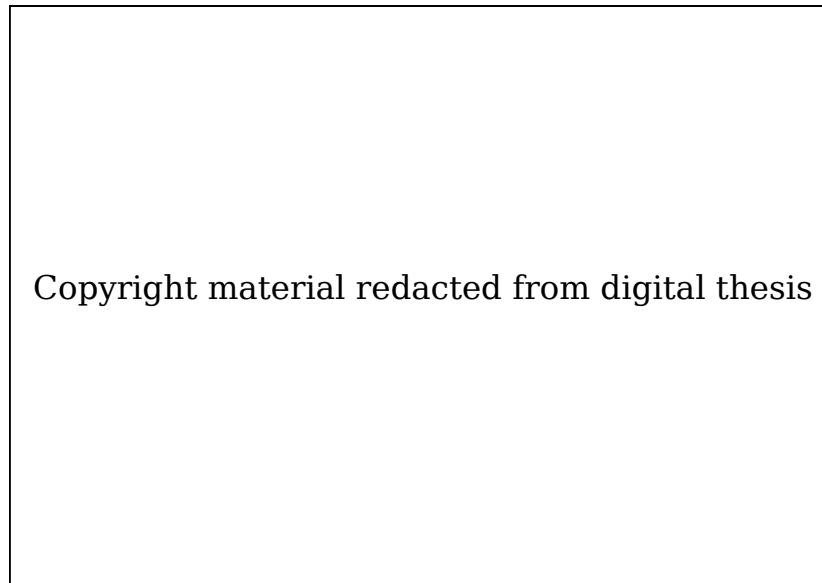
Copyright material redacted from digital thesis

Figure 2.4: A BPT diagram of SDSS galaxies in $0.02 < z < 0.4$ and S/N > 5, with FRB host galaxies added. The solid line denotes the region in which galaxy emission lines are dominated by star-formation, while sources right of the dashed line are dominated by hard spectra. The dotted line separates the AGN-dominated galaxies into LINER and Seyfert galaxies. Figure from Bhandari et al, 2019 (3).

According to the analysis of Bannister et al (73), the host galaxy of FRB 180924 is most consistent in emission characteristics with the LINER (low-ionization nuclear emission region) galaxies, residing within the appropriate region of the BPT diagram. It is also a much brighter, more massive galaxy than the R1 host, but with a star formation rate of less than 2.0 $M_\odot$ per year (73). This is consistent with Figure 2.3; HG 180924 appears on the fringe of the 'green valley', which may indicate that it is transitioning from star-forming towards quiescence (124). The LINER classification of HG 180924 implies the presence of a faint, obscured AGN for HG 180924, but, as FRB 180924 is itself at least 2.5 kpc from the galaxy's nucleus, it is unlikely that there is a relationship between the two (73). HG 180924 also does not appear to contain a persistent radio source, unlike the R1 host; if it does, it must be much fainter (73).

A persistent radio source is also missing from HG 181112, in an analysis from Prochaska et al (1). Also similar to HG 180924, and dissimilar to R1, it appears to have a low star-formation rate; however, it does lie in the star-forming locus of the BPT diagram (1), and, along with HG 190102, firmly in the 'blue cloud' of Figure 2.3. In the work of Bhandari et al, HG 190102 lies between the Seyfert and star-forming regions of the BPT diagram (3). This indicates that the HGs 181112 and 190102 are likely to be spiral galaxies with some star formation (125, 126). The uncertainty ellipses of these two bursts make it impossible to completely rule out an association with AGN activity for those bursts.

HG 190608, the nearest and best-resolved FRB host thus far, is a bright spiral galaxy. It contains a Type I AGN (3), although, as with FRB 180924, the burst's displaced position indicates that it is unrelated to the AGN. FRB 191001, too, originates from a star-forming spiral (127). FRBs 190608 and 191001, localised specifically to spiral arms[20], seem to hint at a link between FRBs and star formation, which is consistent with the placement of each galaxy in the blue cloud here - but it is also possible that FRBs simply trace the stellar population and not necessarily the star-forming one.

---

[20]Unique so far among FRB localisations.

The identified host of FRB 190523, the sole non-CRAFT single-burst localisation, is also a massive galaxy with light star formation. As noted by Ravi et al, it also contrasts significantly with the host of R1 (79).

Also worth considering is whether the FRBs here originate from R1-like dwarf galaxies, aligned with the identified hosts but too faint to detect in our imaging. This remains a possibility at this stage, especially considering the large projected offset of FRB 190608 from the nucleus (see Table 2.5). If this is the case, the fact that all of the localisations align with large galaxies implies that said dwarfs would be companions to these galaxies. However, this would raise the question as to why the R1 host is not also bound to a large galaxy.

A hidden dwarf host notwithstanding, the nature of the CRAFT hosts point away from dwarf galaxies as typical FRB hosts, at least for non-repeaters (1, 73); FRB 190523 lends further weight to this analysis (79). Although it may be too early to draw firm conclusions, large stellar mass and light star formation seem, thus far, typical of single-burst hosts. They also seem to appear consistently on or near the blue cloud of a galaxy CMD. This may imply a link between FRBs and star formation.

Figure 2.5: *g*-band imaging of the host galaxies of five CRAFT-localised FRB host galaxies. The images here were produced using the processes described in Chapter 2. The images of HGs 180924, 181112, 190102 and 191001 are from VLT/FORS2; 190608 from VLT/X-shooter. Ellipses represent the FRB localisation uncertainty; solid ellipses represent statistical uncertainty, dashed ellipses are systematic uncertainty, and dotted ellipses are the quadrature addition of statistical and systematic.
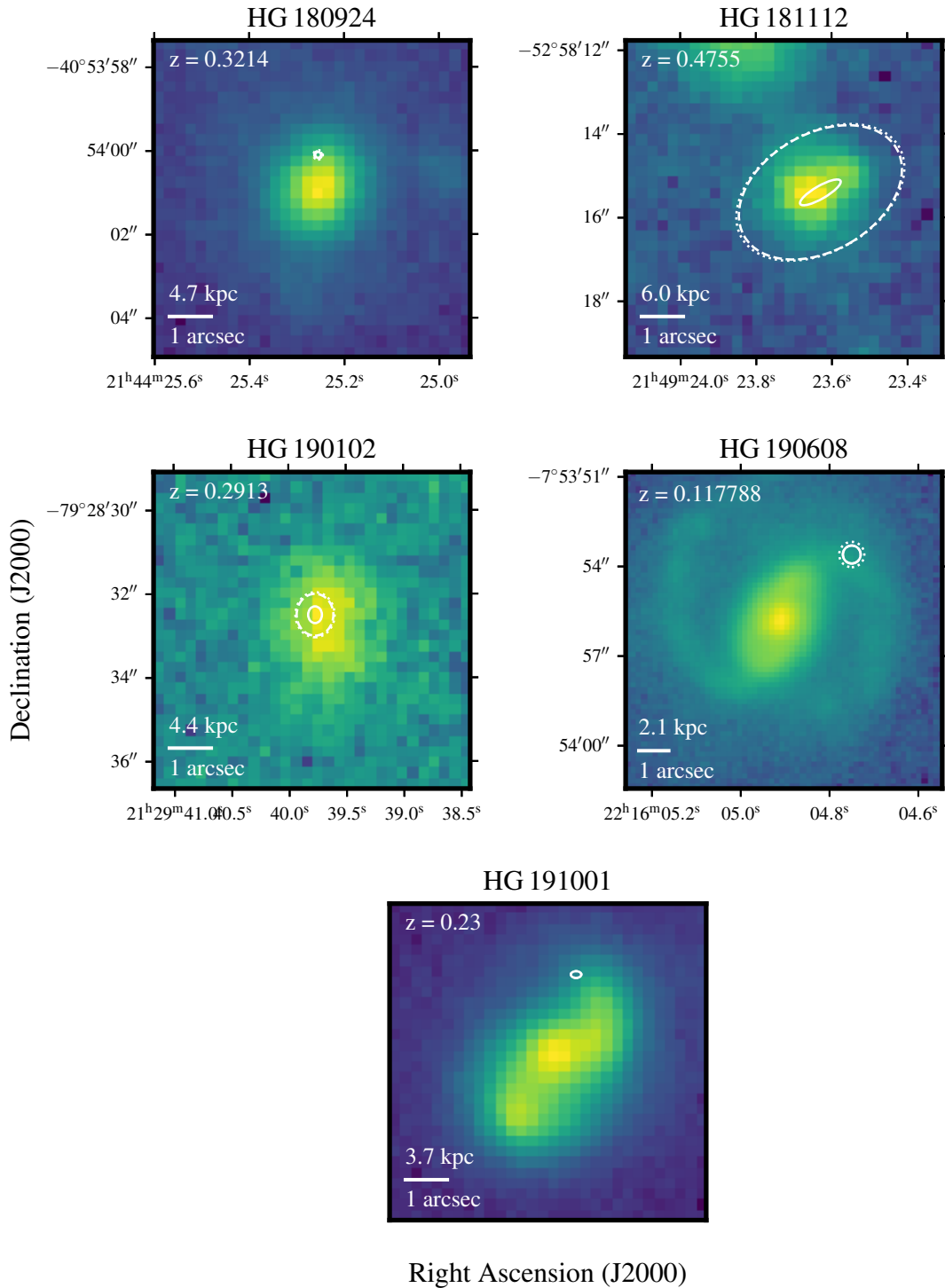
Figure 2.6: *I*-band imaging of the host galaxies of five CRAFT-localised FRB host galaxies. The images here were produced using the processes described in Chapter 2. The images of HGs 180924, 181112, 190102 and 191001 are from VLT/FORS2; 190608 from VLT/X-shooter. Ellipses represent the FRB localisation uncertainty; solid ellipses represent statistical uncertainty, dashed ellipses are systematic uncertainty, and dotted ellipses are the quadrature addition of statistical and systematic.
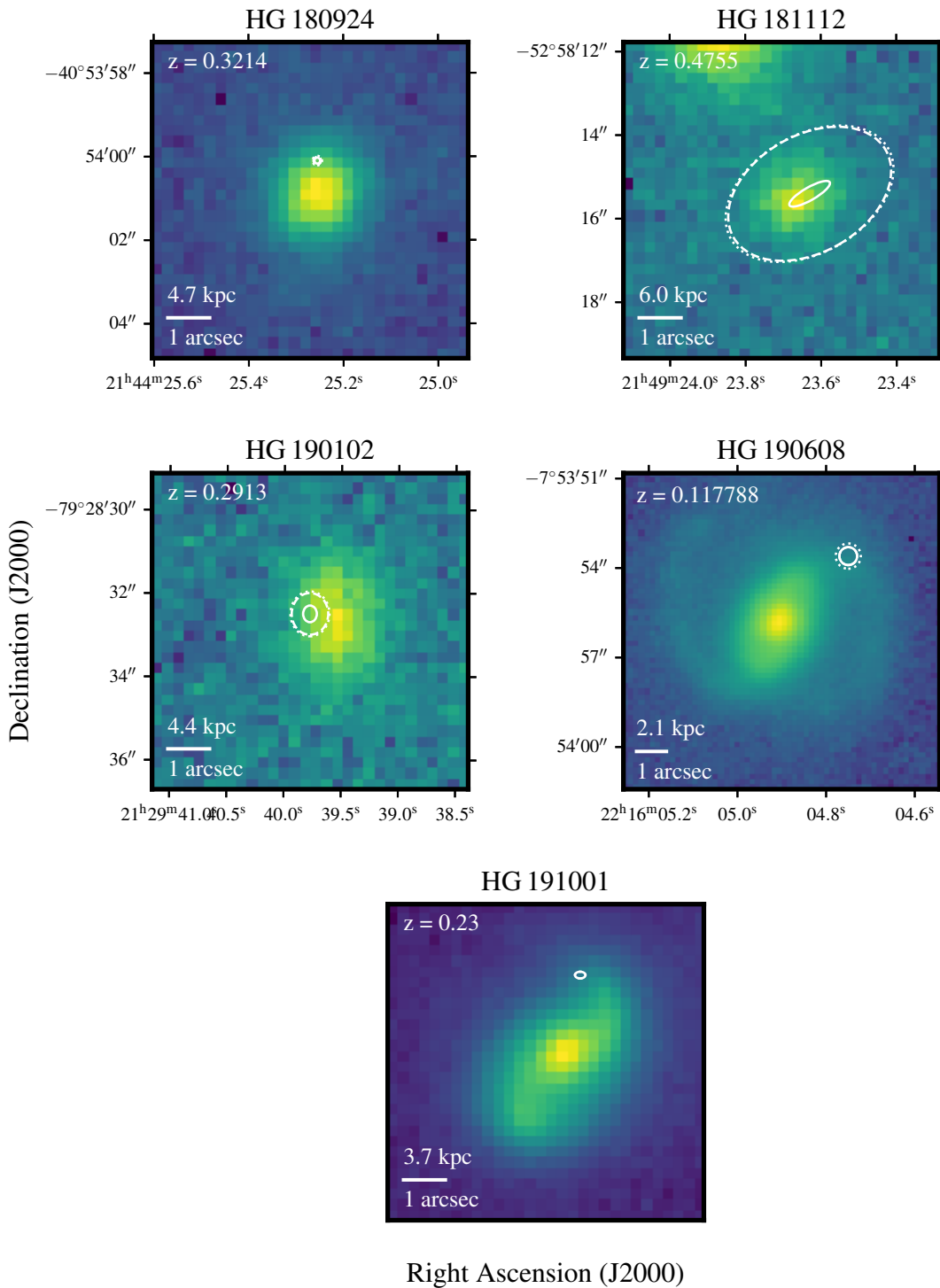
3

Searching for FRB optical counterparts

As discussed in § 1.1.1 and § 1.1.3, it is possible that fast radio bursts are accompanied by transient optical counterparts. With optical imaging of identified FRB host galaxies taken within weeks of the initial burst, it becomes possible to search for them directly. As the original goal of the optical follow-up to CRAFT FRBs was not to search for optical counterparts, the proposals for VLT time were not for Rapid Response Mode or as Targets of Opportunity. As such, the imaging was generally not obtained until some weeks after the burst detection (see Table 3.1). However, for the purposes of searching for counterparts with supernova-like light curves, this delay is actually advantageous.

Searches for optical transients in the fields of FRBs have been undertaken, such as those mentioned in § 1.1.3. However, direct comparative searches for optical counterparts of single bursts, with known host galaxies, have never been performed. This makes the current moment, with a crop of single FRBs localised to their host galaxies and optical imaging available, a unique opportunity to do so.

Simple subtraction of two imaging epochs is the most direct way to search for optical transients. One image is subtracted from another to remove background light (most prominently, the host galaxy) and the residuals are searched for sources, which, if they appear in the difference image, are the result of a source that is brighter in one image than the other (108). Although complicated by subtraction artefacts, differences in point-spread function between images, and non-trivial uncertainty propagation, algorithms for overcoming these problems do exist (128, 129).

A subtraction between a FORS2 image taken soonest after the burst detection (science image) and a suitable template image is undertaken here, with the aim of identifying any sources in the host galaxy that are brighter in the science image than in the template. Templates from three instruments - FORS2, X-shooter and the DES cutouts produced on DECam (81) - are used, in order to assess whether subtractions performed with non-matching instruments can be constraining.

FRB	Burst detection (MJD)	Observation (MJD)	Time after FRB detection (days)	Instrument
180924	58385	56596	-1835	DES (*g*)
		56904	-1572	DES (*i*)
		58431	46	FORS2
		58662	277	FORS2
		58716	331	X-shooter
		58718	333	FORS2
181112	58434	56534	-1900	DES
		58455	20	FORS2
		58716	282	X-shooter
		58718	284	FORS2
190102	58485	**58495**	10	FORS2
		58636	166	FORS2
		58651	151	FORS2
		58716	231	X-shooter
		58718	233	FORS2
190608	58642	58716	74	X-shooter

Table 3.1: CRAFT-localised FRB detection and subsequent optical observation dates. Bold dates in the Observation column were used as science images, while italicised dates were used as template images for the main result (although the others were also experimented with as templates). For further information on the individual epochs, see Table 2.1.

3.1 Image Subtraction

This analysis focuses on the host galaxies of the FRBs 180924, 181112, 190102 and 190608 - although HG 190608, lacking a suitable template[1], is searched without subtraction. As discussed previously (§ 2.1), optical imaging of the host galaxies was conducted using VLT/FORS2 and VLT/X-shooter. In all of the subtractions mentioned here, the final co-added, astrometry-corrected images (as per Chapter 2) were used. Images from the Dark Energy Survey (81) were available for the fields of FRBs 180924 and 181112, and were also used for subtraction, for comparison. See Table 3.1 for a summary of the observations in relation to the burst detections.

3.1.1 Software

Two implementations of the ZOGY (Zackay, Ofek & Gal-Yam; 128) optimal subtraction algorithm were tested, in Python[2] and in MatLab[3] (130). However, HOTPANTS (**H**igh **O**rder **T**ransform of **P**SF **An**d **T**emplate **S**ubtraction; 131) was found to be better-suited to our data, and was integrated into the pipeline. HOTPANTS implements the algorithm for image subtraction set forth by Alard in 2000 (132), which is an iteration on the Alard & Lupton (A&L) 1998 algorithm (133).

To achieve an adequate subtraction, the point-spread functions of the two images must match. This is unlikely to occur by coincidence, even when using the same instrument,

---

[1]SDSS imaging of the galaxy is available, but is not of sufficient depth.

[2]https://github.com/pmvreeswijk/ZOGY

[3]https://webhome.weizmann.ac.il/home/eofek/matlab/doc/subtract_proper.html

so the images must be modified. In A&L, one image is convolved with a PSF kernel to match the other. This kernel is modelled as the sum of a set of Gaussians, multiplied by a polynomial, the terms of which are the set of basis functions in which the kernel is expressed. A least-squares fit, using every pixel in both images, is then used to obtain the coefficients of the optimal kernel. The better-seeing of the two images is then convolved with this kernel. The background variation, differing between the two images, is also fit to a polynomial and subtracted. The Alard 2000 iteration on this algorithm allows the kernel to vary with the position on the image.

3.1.2   Procedure

The subtraction process has been automated using Python and bash scripts available in this project's GitHub repository[4]. To subtract the images properly, they must be astrometrically aligned. Although a procedure to obtain an absolute astrometric solution for each image was undertaken in § 2.2.6, it is more important here to ensure that the two images align with each other than with an absolute reference frame, with particular focus on the FRB host galaxy. This is achieved by selecting a single star relatively close to the host galaxy. The star's centroid position is measured in both images using SExtractor's PSF-fitting, and the offset of the position in the science image from the position in the template calculated. This offset, in right ascension and declination, is subtracted from the reference values in the FITS header of the science image.

Now aligned astrometrically, the images must also be aligned to the same pixel grid, which HOTPANTS does not perform itself. When subtracting two epochs taken on the same instrument, this is straightforward and requires only that the correct number of pixels be trimmed from the edges of each image. However, when comparing images with different pixel scales, one has to be re-sampled to match the other. If the images have different orientations, however slight, this also has to be corrected.

Both tasks are achieved here using the REPROJECT package[5] in Python, which takes one image and re-projects it into the pixel space of another. The function used here is `reproject_exact()`, which is specifically designed to conserve flux. The image with the smaller pixel scale is downsampled to the scale of the other - that is, its output pixels are increased in size, rather than the larger pixels reduced, which would require pixel interpolation. The header of the re-projected image is modified to reflect the changes made by copying the WCS entries from the other image.

With images aligned, the image subtraction can be performed. The PSF FWHM (measured with PSFEx) for each image is converted to σ, for use in HOTPANTS, with the conversion:

$$\text{FWHM} = \sigma\sqrt{8\ln 2}$$
$$\sigma = \frac{\text{FWHM}}{\sqrt{8\ln 2}} \approx \frac{\text{FWHM}}{2.355} \tag{3.1}$$

HOTPANTS convolves one image with a kernel optimised to match its PSF to that of the other image. It is better to downgrade the PSF of the higher-quality image, in order to avoid excess residuals in the difference image. Thus, if σ_{science} is smaller than σ_{template}, we force HOTPANTS to convolve the science image. If the reverse is true, we do as recommended

---

[4]https://github.com/Lachimax/craft-optical-followup
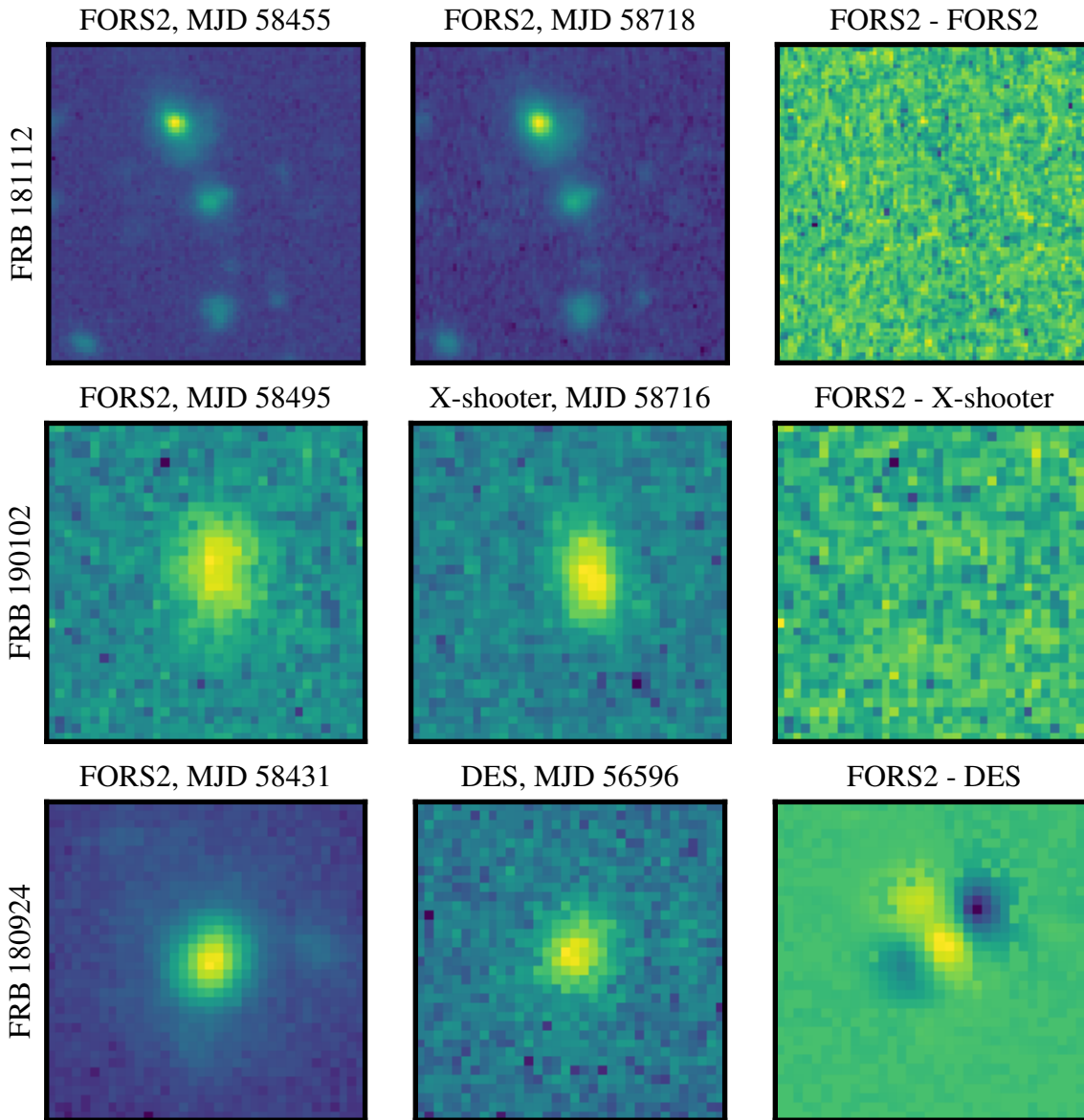[5]https://reproject.readthedocs.io/en/stable/

Figure 3.1: An example of a subtraction for each host galaxy and with a template from each instrument. Each of these subtractions are in *g*-band. For the full set, including *I*-band, see Figures A.5 to A.8.

in the HOTPANTS documentation[6] and set a kernel basis as follows. With an assumption of Gaussian PSFs (roughly true), the Gaussian that matches the PSFs of the two images has $\sigma_{\text{match}} = \sqrt{\sigma_{\text{science}}^2 - \sigma_{\text{template}}^2}$. This is set as the central Gaussian of the kernel basis. The smallest Gaussian of the basis is set to $\frac{\sigma_{\text{match}}}{2}$, and the largest to $2\sigma_{\text{match}}$; HOTPANTS takes care of the rest, and the subtraction is performed. The difference image is normalised to the photometric system of the science image, for ease of extracting transient sources (genuine or synthetic).

The difference images are then passed to SExtractor to search for sources, with a detection threshold set to 1.5 times the background RMS. Values as low as 0.5 were experimented with, but resulted in numerous false-positive residual 'sources'.

The science image of HG 190608 was examined for point sources with SExtractor without

---

[6]https://github.com/acbecker/hotpants

subtraction, with a much-reduced background mesh (specified with the input BACK_SIZE) of 5 pixels (32 pixels for all other purposes). This, as also used in Chapter 4, would make it better-able to find point sources embedded in the spiral arms by essentially perceiving the arms as background.

3.2   Results and Discussion

The saturated point sources in the field are not subtracted cleanly, as one might expect; however, the extended sources surrounding our galaxies are subtracted quite well, as demonstrated in the FRB 181112 subtraction of Figure 3.1. Although residual sources do appear in the host galaxies in several of the difference images, they are generally not point-like and are likely to be artefacts of the subtraction, especially when accompanied by corresponding negative sources. This occurs when the alignment is imperfect. In the case of the DES templates, the kernel-matching has clearly not succeeded, leaving all sources in the image with substantial, similarly-patterned residuals (see Figure 3.1). These are certainly subtraction artefacts, and there is little chance of recovering any true astrophysical transients from the FORS2-DES difference images.

In the case of HG 180924 g-band FORS2 - FORS2 difference, SExtractor detects a magnitude 27 residual source east of the host centroid. However, as seen in Figure A.6, there is a negative source coincident with the centroid. The positive residual source is also not reflected in the I-band difference or in either X-shooter difference. It is also slightly fainter than the median of residual sources found in the image - the vast majority of which are likely to be subtraction artefacts.

SExtractor does not detect any residuals in the vicinity of HG 181112 in either FORS2 - FORS2 difference. There is a positive residual in the FORS2 - X-shooter I difference with a measured magnitude ~ 26, coincident with the galaxy centroid, but it is not reflected in g; there are several similar residuals in the surrounding region, and the median residual source is also ~26th magnitude, so it is most likely an artefact. No residual sources are detected by SExtractor in or near HG 190102 in any of its difference images. No point-sources are found in the spiral arms of HG 190608's science images.

This work can make no positive detection of a transient source in the four FRB host galaxies considered here. Any residuals found in the difference imaging are most likely the result of noise, misalignment or other artefacts of the subtraction. The next step, then, is to estimate how likely this procedure is to have missed such a transient.

4

Placing limits on FRB optical counterparts

Since no transient sources are found in the difference residuals, we would like to put an upper limit on the brightness of any such source that may have been missed (or, at least, on the difference in brightness between template and science image). Here, we aim to do so for any optical transient that has occurred at the position of the FRB. Models of specific transients, specifically supernovae, are used to predict what the brightness of these transients would be at the time of the science epoch, with the underlying assumption that the FRB takes place simultaneously with the supernova explosion. A Monte Carlo analysis is undertaken to estimate the probability (for each SN type) that, if a supernova did occur in the host galaxy at the same time as the FRB was emitted, we would identify it in our difference images. This is done in order to estimate the probability that, if these FRBs have an SN-like optical counterpart, it would not have been detected.

4.1 Synthetic insertion

In order to test the sensitivity of our supernova search, we need to be able to insert synthetic sources into our images. Options for doing so included SkyMaker[1] (134), which is under-documented[2] and under-supported. Instead, ASTROPY and PHOTUTILS were used for source insertion within Python.

Using PHOTUTILS' integrated Gaussian model, a narrow point-source with the appropriate flux is generated; this is then convolved with the PSF model of the image generated by PSFEx and added to the science image. The subtraction is carried out as normal. SExtractor's MAG_AUTO is used to measure any residual sources, such as the one demonstrated in Figure 4.1.

For HG 190608, for which no template image is available, no subtraction is carried out. Instead, the science image, with synthetic source inserted, is passed straight to SExtractor. SExtractor is run with the same background mesh as in § 3.1.2, which causes it to consider the spiral arm in which FRB 190608 is embedded to be background and allows it to more easily find the inserted point source.

---

[1]https://www.astromatic.net/software/skymaker

[2]The SkyMaker web page states, under the Documentation heading, "There is no SkyMaker documentation yet."
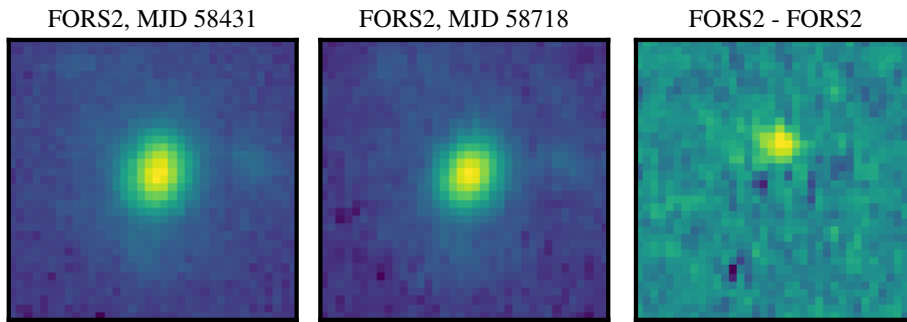
Figure 4.1: Difference imaging of HG 180924, with synthetic point-source of magnitude 24.0 inserted at the FRB position in the science image (left).

4.2   Transient Modelling

In order to model the brightness of SNe at a given epoch, the Python package SNCosmo was used (135). SNCosmo includes a number of built-in spectral supernova models[3]. It allows one to move a supernova model to an arbitrary redshift and to redden it with dust, in both the Milky Way and the host galaxy, using a variety of dust models; and to measure the model's flux with an arbitrary synthetic bandpass. SNCosmo has been used by Pierel et al (136) and Brown et al (137) for supernova light-curve fitting; the latter also used the SALT2 (138) models via SNCosmo, as is done here. Although our data is somewhat under-sampled in the time domain, if a transient had appeared in our data, SNCosmo could also have been used to fit it. Here the reverse is done - a light curve is generated and sampled in order to create an artificial transient.

A source with which to construct the model is chosen from those built into SNCosmo. Parameters such as Galactic reddening $E(B-V)_{\text{MW}}$, host galaxy reddening $E(B-V)_{\text{host}}$ (§ 4.4.1.4), peak rest-frame absolute magnitude M_{peak} (§ 4.4.1.2), and stretch (§ 4.4.1.5) are passed to the model on initialisation. The peak absolute magnitude is set in B-band, and SNCosmo calibrates the light curves in other bands according to its spectral model. The Galactic reddening is set to that given by the IRSA Dust Tool from the S&F reddening map (115), the same used to estimate the host galaxy reddening in § 2.4; the F99 reddening law (117) is then applied with SNCosmo, for consistency with the photometry work done previously. The light curves are generated for the FORS2 `g_HIGH` and `I_BESS` filter bandpasses. To correct coarsely to the selected rest-frame rise-time t_{rise} (§ 4.4.1.3), the light curve is simply shifted in time so that peak luminosity occurs, in the observer frame, at $t_{\text{peak}} = (1 + z) \times t_{\text{rise}}$ (139). This is also done in B-band. Although the SNCosmo models generally do not extend to the epochs at which our templates were taken (> 233 days), it is likely safe to assume that, by then, any supernova would have faded below detectability in the optical.

To insert a transient into an image, the magnitudes for each filter and at the appropriate epoch, are selected from the light curves and passed to the synthetic insertion code as described above.

4.3   First-order brightness limit estimates

In order to estimate the upper limit on the brightness of a transient at the FRB position, we forego any supernova modelling and simply insert point sources at a range of magnitudes from 20.0 to 30.0, in increments of 0.1 mag, at CRAFT's best FRB position. The subtraction

---

[3]Listed here: https://sncosmo.readthedocs.io/en/v2.0.x/source-list.html

is then performed for each insertion. We take the upper brightness limit as the magnitude of the faintest inserted source that SExtractor is able to recover from the difference image, to within 1 magnitude. For HG 190608, this is done directly with the science image.

Where a non-synthetic residual 'source' is present near the host galaxy, the recovered magnitudes tend to drift smoothly from the one-to-one relationship with inserted magnitude, and plateau at about the value of the residual magnitude; that is, beyond a certain faintness, SExtractor stops recovering the inserted source and begins detecting the residual instead. We do not attempt to correct for this, as it represents an upper limit that can be placed on the brightness of any hidden source. It may be that the residual is obscuring a transient, or, indeed, the residual may itself (although unlikely - see § 3.2 for a discussion) be the result of a genuine transient. As it stands, the limits are more conservatively placed at the brightness at which the drift from one-to-one exceeds one magnitude.

For FRB 180924 and FRB 190608, which have very precisely-known locations within their host galaxies, this burst-position limit might suffice. However, it does not for FRB 181112, which, when the full positional uncertainty is considered (see Figure 2.5), might have been emitted from almost any point in the host galaxy. We thus need a more robust estimate of the probability of detecting a transient occurring anywhere within the host galaxy.

4.4 Monte Carlo analysis

With the pieces described above, a Monte Carlo analysis was conducted to estimate the probability of detecting a supernova, had it occurred at the same time as the FRB emission, in the difference imaging. For each supernova type, the parameters of the event (peak rest-frame absolute magnitude, rest-frame rise time, host galaxy reddening, position within the galaxy) are selected from a distribution, modelled with SNCosmo, and inserted in the science image. The subtraction is carried out as per normal, and SExtractor is unleashed blindly on the difference image. If SExtractor is able to recover the coordinates (to within 1 arcsecond) of the inserted synthetic source from the difference image, the trial is counted as a success. In addition to non-detections, any recovered sources that clump around a single image position and magnitude are counted as failures. This is to deal with the same residual problem as described in § 4.3, in which SExtractor detects not the inserted source but a subtraction artefact. The same procedure is undertaken for HG 190608, but without subtraction, and with the smaller background mesh in SExtractor.

100 trials are performed for each SN type, and for each host galaxy. The percentage of successes is taken as the probability of detection for that type. Conversely, the percentage of failures is reported (Table 4.1) as the probability that, if an SN of the given type had occurred in our image, we would have missed it. The distributions from which the parameters are drawn are plotted in Figure 4.2. A sample of the light curves generated by the Monte Carlo analysis after all applicable parameters have been input is in Figure 4.3.

4.4.1 Parameters and distributions

4.4.1.1 Light curve profile

For core-collapse supernovae, in order to somewhat capture the breathtaking variability of observed light curve profiles, the particular SNCosmo source (and hence the particular light-curve shape) is selected at random from those available for the given type. As Type Ia profiles are somewhat more uniform, the built-in implementation of the SALT2 model (138) is used for all Type Ia insertions. SALT2 has been widely used in other results (106, 136, 140–143).
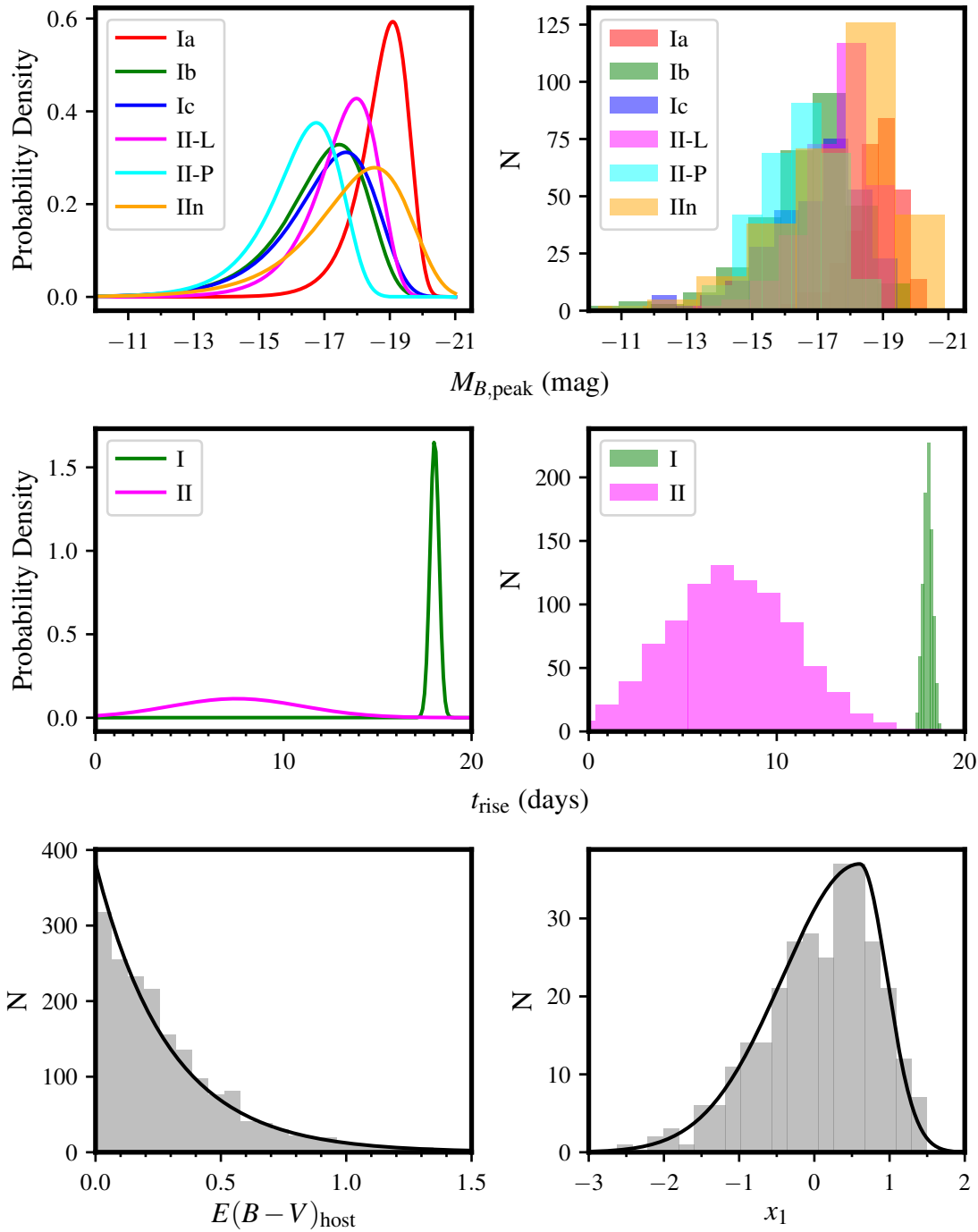
Figure 4.2: The distributions used for Monte Carlo analysis (§ 4.4.1). Curves give the distributions from which the parameters were drawn. Histograms are plotted using the parameters of the final sample, the same used for the results in Table 4.1

4.4.1.2   Peak absolute magnitude

For peak absolute magnitude $M_{B,\mathrm{peak}}$, a right-handed Gumbel distribution[4] is used instead of a normal one, in an attempt to capture the empirical subluminous tail of peak magnitude distributions (144, 145). The Type Ia distribution is based on that found by Ashall et al, 2016 (144), with $\mu(M_B) = -19.09$ and $\sigma = 0.62$. Other values come from the bias-corrected

---

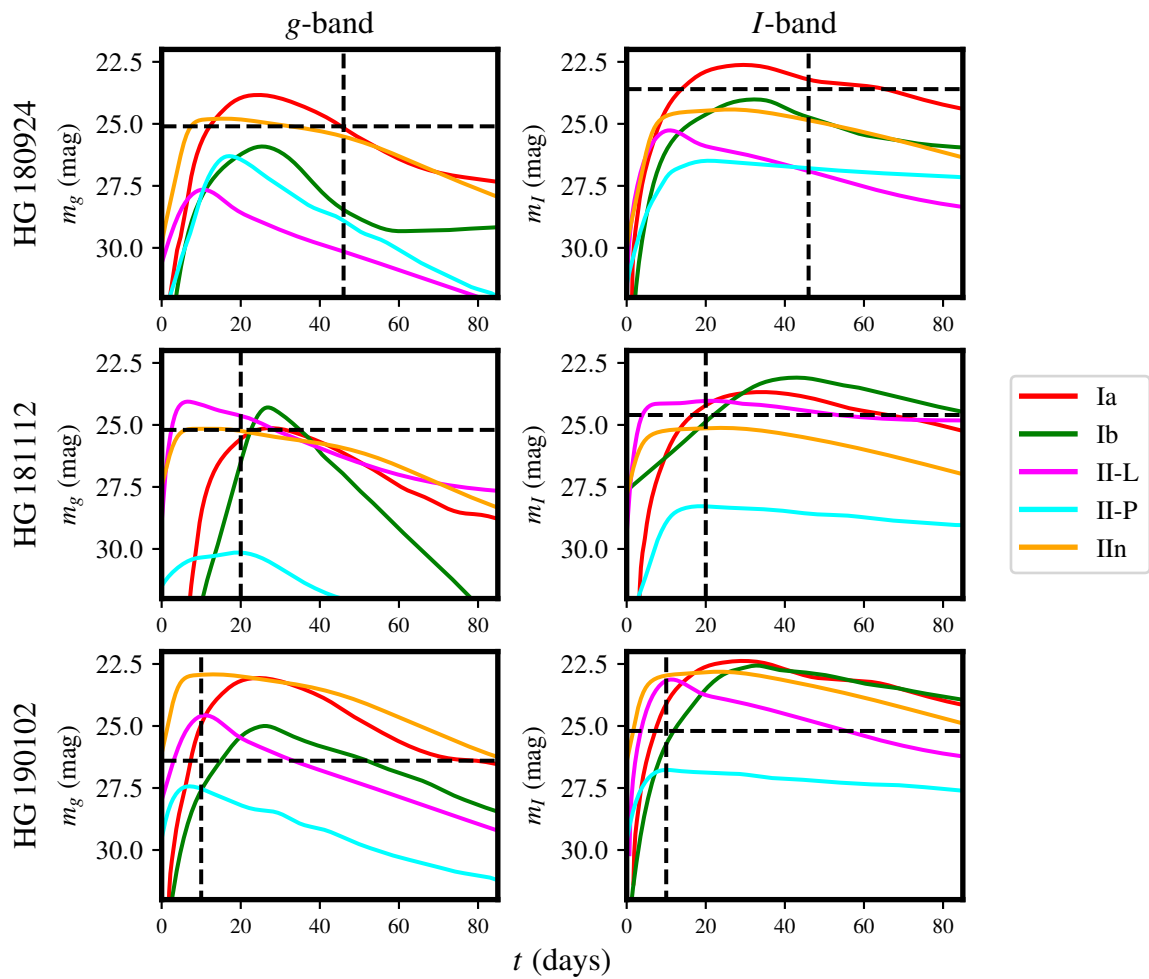[4]https://en.wikipedia.org/wiki/Gumbel_distribution

Figure 4.3: A selection of randomised supernova light curve models (apparent magnitude) from the Monte Carlo analysis sample. Randomised host-galaxy reddening is included in these models, resulting in the different relative brightnesses between rows. The vertical dashed lines demonstrate the epoch of the first VLT observation of each source, and the horizontal dashed line is the detection limit reported in Table 4.1.

sample of Richardson et al, 2014 (145; see Table A.2).

4.4.1.3 Rest-frame rise time

The rise times t_{rise} of Type Ia, Ib and Ic SNe are said to be similar (146), so the same distribution was adopted for all three. Assuming a normal distribution, I adopt $\mu(t_{rise}) = 18.03$ days with $\sigma(t_{rise}) = 0.24$ from Ganeshalingam et al, 2011 (147). The rise times of Type II supernovae are somewhat under-constrained by comparison, as the early-time light curves are often under-observed (148). This is somewhat understandable, since the time at which a supernova is most likely to be detected is at its peak. However, it does make judgements about the brightness we should observe at a particular epoch difficult. Using values quoted in Gonzalez-Gaitan et al, 2015 (148), we take $\mu(t_{rise}) = 7.5$ days, and, in an attempt to capture the wide observed range (148), a standard deviation of 3.5 days.

4.4.1.4 Host galaxy reddening

For the host galaxy, the CCM89 (149) extinction law is used, as this allows us to set the parameter R_V. The extinction distribution given by Holwerda et al, 2014 (140) is adopted. This takes the form $N = N_0 \exp\left(\frac{-A(V)}{\tau}\right)$. With no a priori knowledge of the inclination of

our host galaxies[5], we take the values of $\tau = 0.67$, which corresponds to Holwerda et al's distribution prior to correction for inclination (140). Using the relationship $R_V = \frac{A(V)}{E(B-V)}$ (117), and setting $R_V = 2.3$ as given by Holwerda et al for supernovae (140), we use the distribution of $N = N_0 \exp\left(\frac{-2.3E(B-V)}{0.67}\right)$ to select $E(B-V)_{\text{host}}$. Although this probably *should* correlate with position within the host, there is enough uncertainty in inclination and in the properties of the host galaxy's dust distribution to make this less important.

4.4.1.5   Stretch

The 'stretch' parameter of a Type Ia supernova - that is, the rate of decay in the event's apparent magnitude after peak - is captured in SALT2's x_1 parameter (5, 138). As this influences the supernova's detectability as a function of time, it was deemed necessary to vary this parameter as well. The distribution model used by Scolnic and Kessler, 2016 (143) is adopted here. That work calls this an 'asymmetric Gaussian', in which either side of the mean obeys a normal distribution with a different σ; ie, values greater than μ have standard deviation σ_+ and those less than μ have σ_-. The values adopted here are those given for the SNLS survey (106), the median redshift $z = 0.29$ (143) of which is the nearest of their samples to our FRB host galaxy values. The distribution obeys $\sigma_+ = 0.363$, $\sigma_- = 1.029$, and and $\mu = 0.604$.

Although the stretch, peak magnitude and rise-times of Type Ia supernovae do correlate in reality (5, 141, 150), a key factor in their use-ability as 'standardisable' candles, this is important only to the precision required of supernova cosmology; for the purposes of this work it suffices to draw each parameter from an independent distribution.

4.4.1.6   Position

As transients occurring closer in the sky to the host nucleus would be more difficult to find in the difference image due to extra noise, the position within the galaxy affects detectability. The position of the synthetic transient is selected with the simplifying assumption that the rate of supernovae at a given (sky) position within a galaxy is proportional to the stellar density in that region; and that, in turn, the stellar density is proportional to the g-band surface brightness at that position. Although certainly sufficient for Type Ia SNe, which trace the B-band light distribution of their hosts (151), the first assumption does not hold entirely for core-collapse SNe, which tend to trace star formation rather than the general stellar population (152). However, in the absence of a high-resolution map of star formation for these hosts, the integrated brightness will have to suffice. The position is then chosen from a distribution defined by the image of the galaxy itself; brighter pixels in g are assigned a greater probability of hosting the supernova than dimmer pixels. A sub-pixel position is selected by adding a random number in the range (-0.5, 0.5) to each pixel coordinate.

The exception is for FRB 190608, for which all SNe are inserted at the burst position. Using the light distribution to assign position almost always lands the SN on the galaxy's bright bar-like structure, which makes it impossible for SExtractor to distinguish from the galaxy itself without a subtraction. Because FRB 190608 is very well-localised, its position within the galaxy (on or near the north-western spiral arm) need not be randomised here. This does mean, however, that for this host we are not testing the probability of detecting a SN within the galaxy, but at the burst position.

---

[5]Except, to some degree, with HG 190608, which appears more-or-less face on; but using the pre-correction distribution will bias us away from detectability in that case, so our estimates are more conservative.

FRB	180924		181112		190102		Combined		190608	
Band	g	I	g	I	g	I	g	I	g	I
Limit at burst position (mag)										
FORS2 template	25.1	23.6	25.2	24.6	26.4	25.2	-	-	-	-
X-shooter template	24.7	22.7	25.9	24.0	24.3	-	-	-	22.6	22.5
Probability of non-detection										
Type Ia	34%	12%	44%	34%	78%	88%	12%	4%	95%	69%
Type Ib	94%	54%	91%	91%	99%	99%	85%	49%	98%	77%
Type Ic	94%	49%	88%	80%	98%	98%	82%	39%	97%	81%
Type IIn	40%	41%	34%	47%	39%	65%	6%	13%	82%	70%
Type II-L	69%	48%	78%	79%	63%	76%	34%	29%	90%	79%
Type II-P	89%	73%	75%	89%	74%	90%	50%	59%	96%	86%

Table 4.1: Results of synthetic insertion tests. The probability of non-detection is the probability that, if a supernova of this type did occur in the given host galaxy coincident with the FRB emission, it would not be found. The 'combined' column gives the probability (rounding up to the next percent) that, if a given SN type occurred in all three difference images, it would go undetected. FRB 190608 is not considered in the combined figure because of the difference in method.

4.5 Results and Discussion

4.5.1 Brightness limits

The limits found using the method in § 4.3 are given in Table 4.1. With the exception of HG 181112 in g, the FORS2 - FORS2 subtractions provide a more constraining brightness limit than the FORS2 - X-shooter subtractions. The residuals in the FORS2 - DES difference imaging proved prohibitive to any analysis. This demonstrates that it is favourable to conduct both template and science observations on the same instrument where possible. If this is impractical, the two exposures should at least be of similar depth - as was achieved with X-shooter and FORS2 here. It also helps demonstrate the need for (at least) 8-metre class telescopes in optical FRB follow-up - if the CRAFT sample is typical, then we can expect FRBs to originate from galaxies with redshift up to 0.5 and magnitude up to 23. In the search for optical counterparts to FRBs, observations with less sensitive instruments are likely to be less constraining than these.

4.5.2 Monte Carlo analysis

Results of this analysis are summarised in Table 4.1. A larger sample size would, as always, be preferable. However, time and computational power limited this analysis to 100 per SN type per host galaxy, which at least enables us to place the first truly empirical constraints on an FRB supernova association.

For FRB 180924, taking the stronger figure in I-band, there is an 88% probability that we would have detected a Type Ia supernova had it taken place. The estimate is less constraining for FRB 181112, but still favours detection at 66%. The results for Types Ib and Ic are not very constraining for either FRB 180924 or 181112. For Type IIn SNe, the results mildly favour detection for each host and disfavour it for Type II-L and II-P.

Our initial observations of FRB 190102 took place 10 days after the burst detection, several days before the Type I peak epoch in all cases. This is the reason for the low detection

probability for all Type I SNe in HG 190102. It is hence unlikely that any Type I SN would have been detected by our HG 190102 imaging. However, the fast mean rise time taken from Gonzalez-Gaitan et al (148) often places the 190102 science epoch quite close to peak brightness for Type II SNe. Hence, the probability of detection rises significantly for Type II. Similar to FRBs 180924 and 181112, detection remains unlikely for Types II-L and II-P, but a Type IIn is likely to have been detected in g.

With no template to compare to, only a fraction of supernovae are found in the HG 190608 imaging, with the best figure being 31% (69% non-detection) for Type Ia in I-band. This is found to be unconstraining.

This work finds it unlikely that FRBs 180924 or 181112 occurred simultaneously with Type Ia SNe. We cannot make a similar conclusion about FRB 190102. It is also unlikely, albeit less constraining, that a Type IIn SN accompanied any of the three bursts. The results for Type Ib/c and II-L/P are even less constraining in all individual cases.

Although we cannot rule out that any *one* of FRBs 180924, 181112 or 190102 occurred simultaneously with a host-galaxy supernova, when considered together, it becomes increasingly unlikely that all three did so. There is only a 4% probability that a Type Ia supernova would have gone undetected in all three I-band difference images; the figure for Type IIn in g-band is 6%. Even Type II-L become more constraining when considered like this, with an I-band non-detection probability of 29%. So, although any one of the FRBs considered here could have an SN-like counterpart, it is quite unlikely that all of them occurred simultaneously with Type Ia or Type IIn SNe. It is also improbable that all of them occurred simultaneously with Type II-L SNe.

4.5.3   FRB progenitors and optical counterparts

Despite these findings, this work cannot make any statement about whether these FRBs are caused by supernova shocks at later, fainter, epochs. We also cannot eliminate kilonovae as optical counterparts to FRBs, the faintness of which would put them well below the detection thresholds reported here. Both of these possibilities can only be investigated with even deeper imaging of FRB host galaxies; the more epochs, the better. If there are multiple populations of FRBs, it is possible that supernovae or kilonovae are associated with one but not others.

It also remains entirely possible that FRBs are associated with novel optical transients that are fainter than the limits set here, or too brief to appear in our imaging, or both. Again, deeper imaging is required to investigate the first possibility, and prompt optical follow-up for the second. Now that we are entering an age in which the study of FRB host galaxies is possible, these investigations can be performed.

As discussed in § 2.5, the CRAFT FRB hosts are quite unlike the host of FRB 121102. This host, a dwarf galaxy with low metallicity and high star formation, is considered typical of the hosts of superliminous supernovae (SLSNe; 80). The volumetric rate of SLSNe is significantly lower than that of FRBs (with some assumptions about cosmological distribution; 16, 157); thus, we can eliminate SLSN as counterparts of non-repeating bursts. Although not included in the Monte Carlo analysis here, the higher luminosity of SLSNe would only make them more detectable. However, if SLSN remnants (often believed to be magnetars; 86) are the source of repeating bursts, the rate problem is more surmountable and the FRB need not be coincident in time with the optical component of the SN. Whether the SN can be called an optical 'counterpart' to the FRB in this case is a matter of definition. Worth considering is whether our bursts are emitted from aged repeating magnetars, with a decaying repetition rate and/or decaying energetics resulting in a lack of observed repetitions. In this case, it is not unreasonable to question whether the progenitor objects of our bursts originated at one

Progenitor object/event	Models	Prediction	Status
AGN	Jet-caviton interaction (153) Wandering beam (154)	Association with galactic nucleus.	Ruled out for FRBs 180924, 190608 and 191001 by large nuclear offsets (Table 2.5).
Cosmic strings	String cusp decay (31)	No host galaxy association.	Very unlikely, with all localised FRBs in host galaxies.
Milky Way stars	Stellar flares (155)	Localisation to Galactic flare stars rather than extragalactic sources.	Extremely unlikely; all well-localised FRBs are coincident with galaxies and not with stars.
NS - NS mergers	Magnetic braking (51) Magnetic reconnection (10)	Kilonova counterpart.	Inconclusive.
WD - WD mergers	Magnetic reconnection (9)	Possible SN Ia counterpart.	Counterpart unlikely to accompany all FRBs, based on § 4.5.
SN shocks	NS - SN interaction (53)	SN	Inconclusive.

Table 4.3: Relevant potential FRB progenitor objects, optical counterparts, the models that predict them, and their status based on the CRAFT localisations and this work. Compiled using the FRB Theory Catalogue (156).

point in SLSNe; however, as our hosts are not typical of SLSN hosts, this argument loses some weight.

A summary of relevant progenitor models, and what can be said about them based on this work in conjunction with the CRAFT localisations, is provided in Table 4.3. Independent of this work, the localisations thus far essentially eliminate cosmic string progenitor models (31), which uniquely predict no galactic association (15, 32). FRBs from stellar flares, which were predicted to originate from Galactic stars and accounted for the excess DM with coronal plasma, are similarly ruled out by localisations to host galaxies (155). Due to their apparent separation from the nucleus, a link between several CRAFT FRBs and supermassive black holes and/or AGN becomes similarly unlikely (73).

The white dwarf-white dwarf merger model, which predicts that some FRBs would have Type Ia SN counterparts (9), becomes less likely with each Ia non-detection. Again, it cannot be entirely ruled out at this stage; it has been suggested that the subluminous Type Ia SNe similar to SN 1991bg, which are most likely too faint to be detected here, are caused by WD-WD mergers (158). This presents a possible remaining avenue for association.

5

Conclusions

While fast radio bursts remain enigmatic, and promise to do so for some time, the recent breakthrough by CRAFT and others of localisation to host galaxies allows some light to be shed on their origins.

A photometric analysis of five FRB host galaxies identified by CRAFT, has been undertaken here, and their properties considered in conjunction with CRAFT optical spectroscopic analyses. It becomes increasingly improbable that the host galaxy of FRB 121102, previously the only known FRB host, is typical of fast radio bursts in general - although it may yet be typical of repeating sources. Single fast radio bursts may, based on the CRAFT sample and FRB 190523, typically originate from massive, lightly star-forming galaxies.

This work has also performed a search, by direct subtraction of host galaxy imaging at two epochs, for optical counterparts of three CRAFT-localised fast radio bursts, which are predicted to exist in some FRB progenitor models. No positive identification of an optical counterpart could be made.

To place upper limits on the brightness of any optical transient at the FRB position, synthetic point-sources at a range of brightness were inserted in the science images and searched for in the difference images. In order to quantify further how likely it is that a supernova-like counterpart, should it have occurred, would be missed by the direct subtraction procedure, a Monte Carlo approach was implemented. Light curves of Types Ia, Ib, Ic, IIn, II-L and II-P supernovae were modelled using parameters drawn from distributions based on the astrophysical literature. Point sources, of the brightness predicted by these randomised models for the observation epochs, were inserted in the science images. The percentage of these sources recovered successfully from the difference images is used to estimate the probability of detecting each SN type using direct subtraction.

Although not definitively ruled out, this work finds that it is unlikely that all fast radio bursts are coincident with Type Ia or Type IIn supernova explosions, or other slow optical transients with similar light curves.

A
Supplementary tables and figures

FRB	Right Ascension (J2000)	Declination (J2000)	DM (pc cm^{-3})	z
180924 (2, 73)	$21^h44^m25.255 \pm 0.006 \pm 0.008^s$	$-40°54'00.10 \pm 0.07 \pm 0.09''$	361.42(6)	0.3214(2)
181112 (1, 2)	$21^h49^m23.63 \pm 0.05 \pm 0.24^s$	$-52°58'15.4 \pm 0.3 \pm 1.4''$	589.27(3)	0.4755(2)
190102 (2, 3)	$21^h29^m39.76 \pm 0.06 \pm 0.16^s$	$-79°28'32.50 \pm 0.2 \pm 0.5$"	363.6(3)	0.2913(2)
190608 (2, 3)	$22^h16^m04.74 \pm 0.02 \pm 0.02^s$	$-07°53'53.6 \pm 0.3 \pm 0.3''$	338.7(5)	0.11778
191001 (127)	Redacted from online thesis	Redacted from online thesis	507.4(9)	0.23

Table A.1: CRAFT-localised FRB and host galaxy properties. In the right ascension and declination columns, the first set of uncertainties is statistical, and the second set systematic.
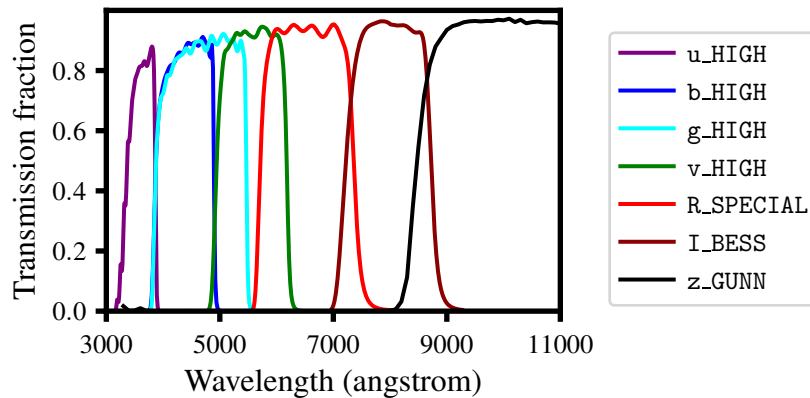

Figure A.1: Transmission curves of the VLT/FORS2 broadband filter set (111, 159), retrieved from the SVO Filter Profile Service (159).
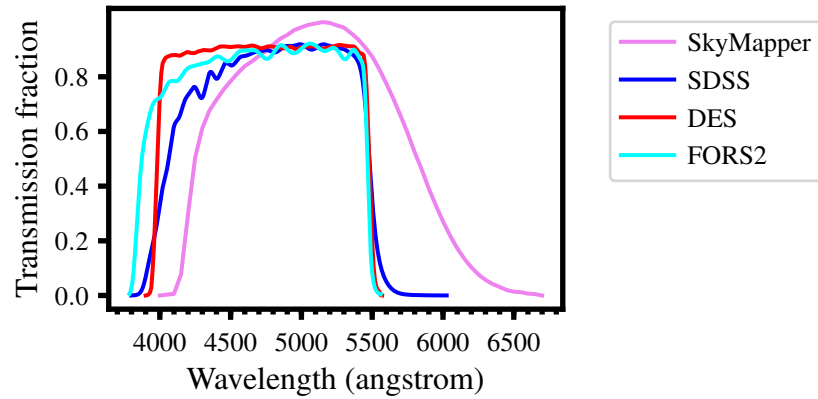
Figure A.2: Transmission curves of all *g*-band filters used for calibration, retrieved from the SVO Filter Profile Service (159).
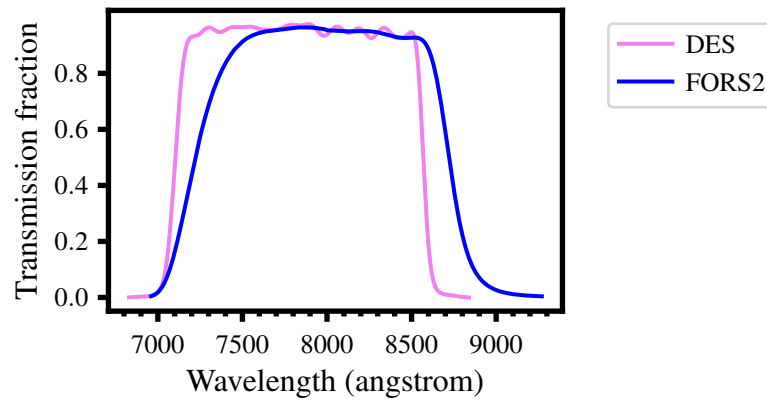

Figure A.3: Transmission curves of *i*-band filters used in this project, retrieved from the SVO Filter Profile Service (159).
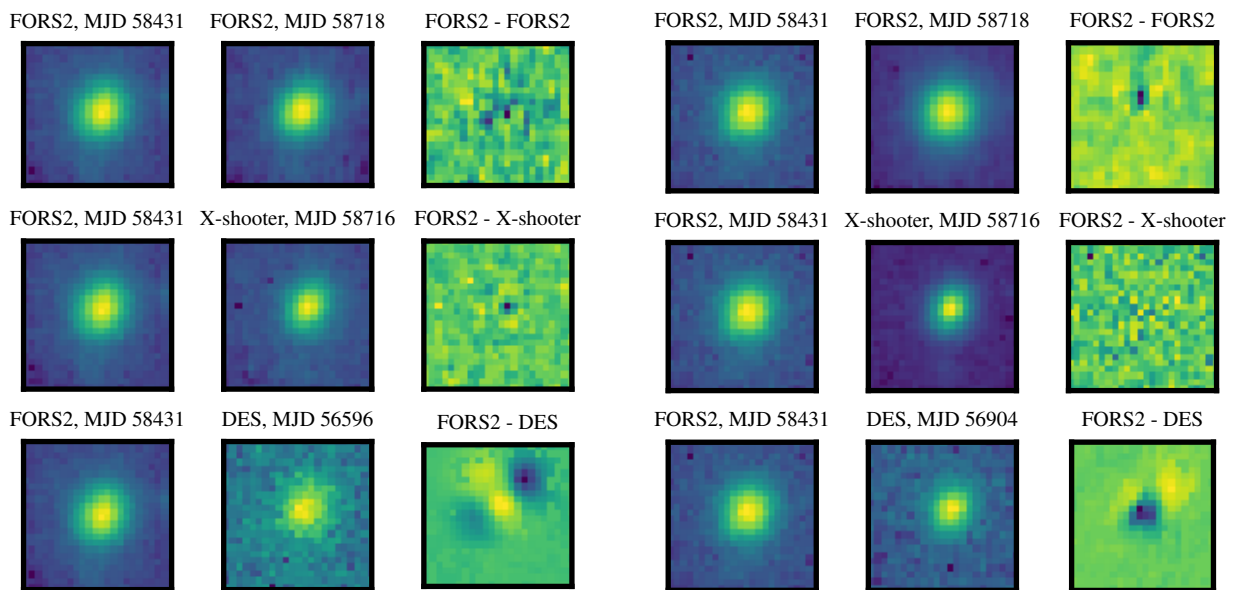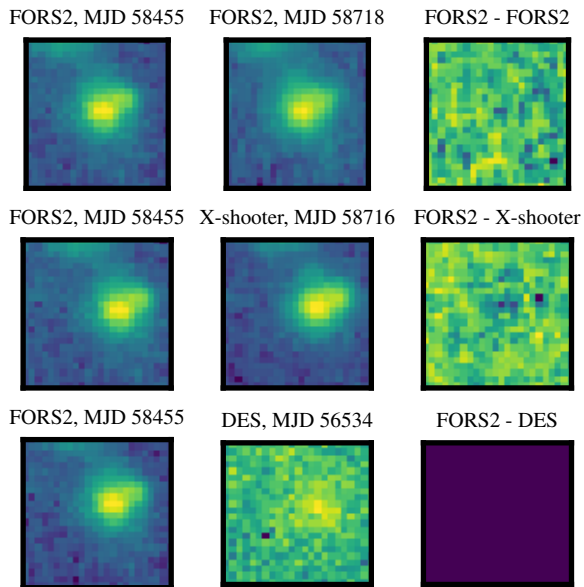

Figure A.4: HG 180924 *g*-band subtractions.

Figure A.5: HG 180924 *I*-band subtractions.

FORS2, MJD 58455　FORS2, MJD 58718　FORS2 - FORS2

FORS2, MJD 58455　X-shooter, MJD 58716　FORS2 - X-shooter

FORS2, MJD 58455　DES, MJD 56534　FORS2 - DES

Figure A.6: HG 181112 *g*-band subtractions.

FORS2, MJD 58455　FORS2, MJD 58718　FORS2 - FORS2

FORS2, MJD 58455　X-shooter, MJD 58716　FORS2 - X-shooter

FORS2, MJD 58455　DES, MJD 56534　FORS2 - DES
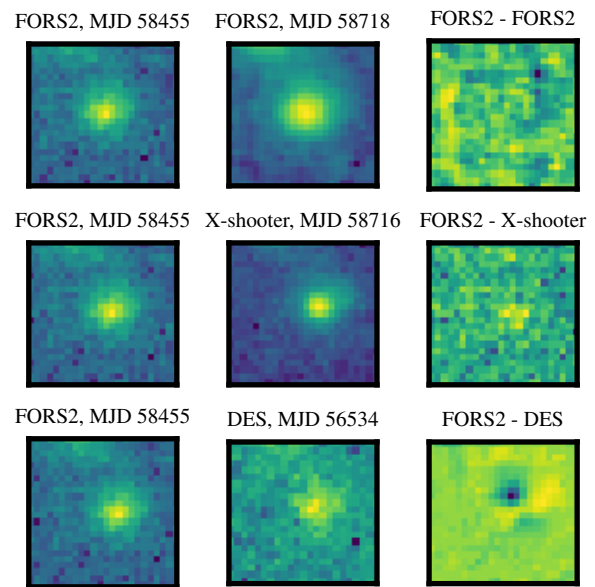
Figure A.7: HG 181112 *I*-band subtractions.

FORS2, MJD 58495　FORS2, MJD 58718　FORS2 - FORS2

FORS2, MJD 58495　X-shooter, MJD 58716　FORS2 - X-shooter
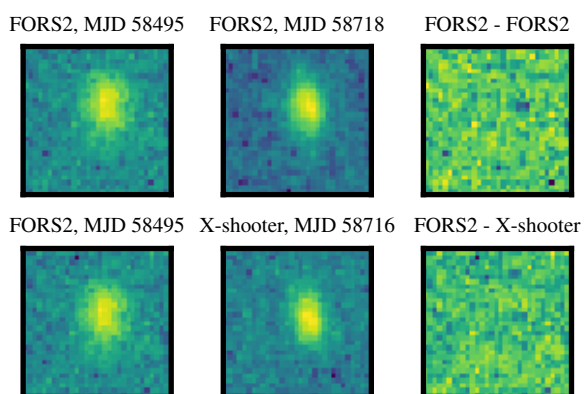
Figure A.8: HG 190102 *g*-band subtractions.

FORS2, MJD 58495　FORS2, MJD 58718　FORS2 - FORS2

FORS2, MJD 58495　X-shooter, MJD 58716　FORS2 - X-shooter
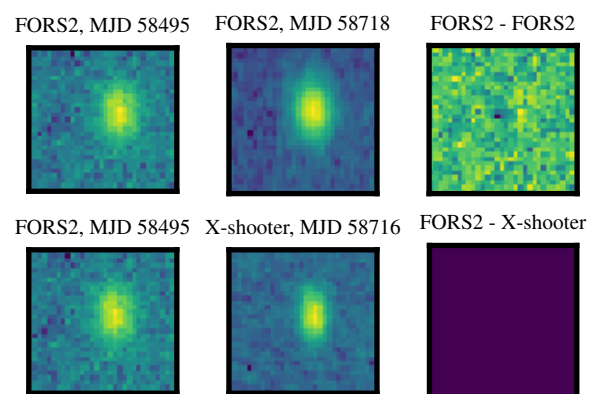
Figure A.9: HG 190102 *I*-band subtractions.

SN Type	$\mu(M_{\text{peak}})$	$\sigma(M_{\text{peak}})$	Reference	Notes
Ia	**−19.09 ± 0.06**	**0.62**	(144)	
	−19.25 ± 0.20	0.50	(145)	Bias-corrected
	−19.26 ± 0.20	0.51	(145)	Volume-limited
Ib	**−17.45 ± 0.33**	**1.12**	(145)	Bias-corrected
	−17.54 ± 0.33	0.94	(145)	Volume-limited
Ic	**−17.66 ± 0.40**	**1.18**	(145)	Bias-corrected
	−17.67 ± 0.40	1.04	(145)	Volume-limited
IIb	**−16.99 ± 0.45**	**0.92**	(145)	Bias-corrected
	−17.03 ± 0.45	0.93	(145)	Volume-limited
II-L	**−17.98 ± 0.34**	**0.86**	(145)	Bias-corrected
	−17.98 ± 0.34	0.90	(145)	Volume-limited
II-P	**−16.75 ± 0.37**	**0.98**	(145)	Bias-corrected
	−16.80 ± 0.37	0.97	(145)	Volume-limited
IIn	**−18.53 ± 0.32**	**1.32**	(145)	Bias-corrected
	−18.62 ± 0.32	1.48	(145)	Volume-limited

Table A.2: A table of supernova peak distributions quoted in the literature. All values are calculated in B-band. Bold values were used to calibrate SNCosmo models (see § 4.4.1.2). μ is the mean of the distribution and σ is the standard deviation.

SNe Type	Rise times (days)	Photometric band	Reference	Notes
Ia	18.03 ± 0.24	B	(147)	Spectroscopically normal sample
	16.63 ± 0.29	B	(147)	High-velocity (HV) sample
	17.3 ± 0.17	B	(160)	
Ib/c	15 to 20		(161)	
II	7.5 ± 0.3	g'	(148)	Sample mean.
	4 to 17	g'	(148)	1σ range.

Table A.3: A table of supernova peak rise times quoted in the literature; used to calibrate SNCosmo models. Rise time is the time elapsed from the explosion to peak luminosity.

B
Glossary of Terms

ADU: Analogue-to-digital unit, the units used for counting flux in astronomical instruments.

ASKAP: Australian Square Kilometre Array Pathfinder, an interferometric radio telescope array in Western Australia (26).

ATCA: Australia Telescope Compact Array.

bias image: A zero-second exposure taken with a closed shutter, intended to capture the read noise of a CCD, together with an ADU offset to avoid negative pixel values.

CCD: Charge-coupled device, an electrical device used in astronomy for capturing images by converting photons into electric charge.

CHIME: Canadian Hydrogen Intensity Mapping Experiment.

CRAFT: Commensal Real-time ASKAP Fast Transients Survey (78)

DES: Dark Energy Survey (81).

dithering: A technique used in astronomical observations in which the pointing of the telescope is shifted slightly between exposures, in order to average out any instrumental effects when the images are stacked.

DM: Dispersion measure, see § 1.1.2.

FITS: Flexible Image Transport System, a data format used for a variety of astronomical purposes, particularly storing imaging data[1].

flat-field image: An image taken at twilight or with a lamp, intended to have a smooth signal across the image. These are used in calibration to account for variation in pixel sensitivity across a CCD.

FORS2: Focal Reducer and Low Dispersion Spectrograph 2[2], an optical instrument on the VLT.

FRB: Fast radio burst. See Chapter 1.

FWHM: Full width at half maximum, a means of measuring the width of a distribution, most usually a normal/Gaussian one.

kilonova: The electromagnetic counterpart of a transient gravitational wave event caused by compact-object mergers, especially neutron stars (50)

---

[1]https://fits.gsfc.nasa.gov/

[2]https://www.eso.org/sci/facilities/paranal/instruments/fors.html

LIGO: Laser Interferometer Gravitational-Wave Observatory.

magnetar: A young, highly-magnetised neutron star.

neutrino: A very low-mass elementary particle, often ejected by supernovae at relativistic speeds.

neutron star: Stellar remnants generated by the core collapse of a massive star, on the order of 10 km across and composed of super-dense matter (45).

pulsar: A variable radio source with a short, and highly regular, period. Pulsars are understood to be magnetised neutron stars.

peryton: A burst of terrestrial radio-frequency interference with some properties similar to an FRB; traced to microwave ovens local to the Parkes radio telescope (29)

PSF: Point-spread function, the function (for a particular image) describing how the light from an unresolved object ('point source') is spread across pixels. Typically modelled as a sum of two-dimensional Gaussians, it is a factor of both instrumental and atmospheric effects.

pulse width (or simply **width**): The temporal duration of an FRB.

read noise: The noise introduced to an image by the electronics during readout of a CCD.

RM: Rotation measure, a measure of the Faraday rotation of a radio pulse; this indicates the strength of any magnetic field it has passed through. See § 1.1.2.

supernova: Extremely bright stellar explosions; see § 1.3.

VLT: Very Large Telescope, a set of four 8.2 m optical telescopes located at Paranal Observatory, Chile.

UTC: Coordinated Universal Time.

WCS: World Coordinate System[3], a standard within FITS which is used to describe the astronomical coordinates of an image.

width (or **pulse width**): The de-dispersed temporal duration of an FRB.

zeropoint: In photometry, this is a property of a given instrument, telescope, and detector system. It is the brightness of an object required to generate one ADU per second in the CCD, and can be expressed either as a flux or in magnitudes. All values used in this thesis are magnitude zeropoints.

---

[3]http://www.atnf.csiro.au/people/mcalabre/WCS/

Bibliography

[1] J. X. Prochaska, J.-P. Macquart, M. McQuinn, S. Simha, R. M. Shannon, C. K. Day, L. Marnoch, S. Ryder, A. Deller, K. W. Bannister, S. Bhandari, R. Bordoloi, J. Bunton, H. Cho, C. Flynn, E. K. Mahony, C. Phillips, H. Qiu, and N. Tejos. *The low density and magnetization of a massive galaxy halo exposed by a fast radio burst*. Science p. eaay0073 (2019). URL http://www.sciencemag.org/lookup/doi/10.1126/science.aay0073.

[2] J.-P. Macquart, J. X. Prochaska, M. McQuinn, K. W. Bannister, S. Bhandari, C. K. Day, A. T. Deller, R. D. Ekers, C. W. James, L. Marnoch, S. Osłowski, C. Phillips, S. D. Ryder, R. M. Shannon, and N. Tejos. *A direct detection of the diffuse missing intergalactic baryons from a set of localised fast radio bursts*. Submitted to Nature (2019).

[3] S. Bhandari, E. M. Sadler, K. W. Bannister, J. X. Prochaska, S. D. Ryder, L. Marnoch, R. M. Shannon, J.-P. Macquart, N. Tejos, and C. Flynn. *ASKAP FRB host galaxies and their progenitors*. Submitted to Astrophysical Journal (2019).

[4] E. Petroff. *Fast radio bursts: recent discoveries and future prospects*. arXiv p. 1709.02189 (2017). URL http://arxiv.org/abs/1709.02189.

[5] K. Maguire. *Type Ia Supernovae*. In *Handbook of Supernovae*, chap. 15, pp. 293–316 (Springer International Publishing, Cham, 2016). URL http://link.springer.com/10.1007/978-3-319-20794-0_36-1.

[6] E. F. Keane. *The future of fast radio burst science*. Nature Astronomy **2**(11), 865 (2018). URL http://dx.doi.org/10.1038/s41550-018-0603-0.

[7] S. Bhandari, E. F. Keane, E. D. Barr, A. Jameson, E. Petroff, S. Johnston, M. Bailes, N. D. Bhat, M. Burgay, S. Burke-Spolaor, M. Caleb, R. P. Eatough, C. Flynn, J. A. Green, F. Jankowski, M. Kramer, V. Venkatraman Krishnan, V. Morello, A. Possenti, B. Stappers, C. Tiburzi, W. van Straten, I. Andreoni, T. Butterley, P. Chandra, J. Cooke, A. Corongiu, D. M. Coward, V. S. Dhillon, R. Dodson, L. K. Hardy, E. J. Howell, P. Jaroenjittichai, A. Klotz, S. P. Littlefair, T. R. Marsh, M. Mickaliger, T. Muxlow, D. Perrodin, T. Pritchard, U. Sawangwit, T. Terai, N. Tominaga, P. Torne, T. Totani, A. Trois, D. Turpin, Y. Niino, R. W. Wilson, A. Albert, M. André, M. Anghinolfi, G. Anton, M. Ardid, J. J. Aubert, T. Avgitas, B. Baret, J. Barrios-Martí, S. Basa, B. Belhorma, V. Bertin, S. Biagi, R. Bormuth, S. Bourret, M. C. Bouwhuis, H. Brânzas, R. Bruijn, J. Brunner, J. Busto, A. Capone, L. Caramete, J. Carr, S. Celli, R. C. El Moursli, T. Chiarusi, M. Circella, J. A. Coelho, A. Coleiro, R. Coniglione, H. Costantini, P. Coyle, A. Creusot, A. F. Díaz, A. Deschamps, G. De Bonis, C. Distefano, I. Di Palma, A. Domi, C. Donzaud, D. Dornic, D. Drouhin, T. Eberl, I. El Bojaddaini, N. El Khayati, D. Elsässer, A. Enzenhöfer, A. Ettahiri, F. Fassi, I. Felis,

L. A. Fusco, P. Gay, V. Giordano, H. Glotin, T. Gregoire, R. Gracia-Ruiz, K. Graf, S. Hallmann, H. van Haren, A. J. Heijboer, Y. Hello, J. J. Hernández-Rey, J. Hößl, J. Hofestädt, C. Hugon, G. Illuminati, C. W. James, M. de Jong, M. Jongen, M. Kadler, O. Kalekin, U. Katz, D. Kießling, A. Kouchner, M. Kreter, I. Kreykenbohm, V. Ku-likovskiy, C. Lachaud, R. Lahmann, D. Lefevre, E. Leonora, S. Loucatos, M. Marcelin, A. Margiotta, A. Marinelli, J. A. Martínez-Mora, R. Mele, K. Melis, T. Michael, P. Migliozzi, A. Moussa, S. Navas, E. Nezri, M. Organokov, G. E. Pavalas, C. Pel-legrino, C. Perrina, P. Piattelli, V. Popa, T. Pradier, L. Quinn, C. Racca, G. Ric-cobene, A. Sánchez-Losa, M. Saldana, I. Salvadori, D. F. Samtleben, M. Sanguineti, P. Sapienza, F. Schüssler, C. Sieger, M. Spurio, T. Stolarczyk, M. Taiuti, Y. Tay-alati, A. Trovato, D. Turpin, C. Tönnis, B. Vallage, V. Van Elewyck, F. Versari, D. Vivolo, A. Vizzocca, J. Wilms, J. D. Zornoza, and J. Zúniga. *The survey for pulsars and extragalactic radio bursts - II. new FRB discoveries and their follow-up*. Monthly Notices of the Royal Astronomical Society **475**(2), 1427 (2018). URL https://academic.oup.com/mnras/article/475/2/1427/4668427.

[8] S. R. Kulkarni. *From gamma-ray bursts to fast radio bursts*. Nature Astronomy **2**(11), 832 (2018). URL https://www.nature.com/articles/s41550-018-0621-y.

[9] K. Kashiyama, K. Ioka, and P. Mészáros. *Cosmological fast radio bursts from binary white dwarf mergers*. The Astrophysical Journal **776**(2), L39 (2013). URL https://iopscience.iop.org/article/10.1088/2041-8205/776/2/L39.

[10] J.-S. Wang, Y.-P. Yang, X.-F. Wu, Z.-G. Dai, and F.-Y. Wang. *Fast Radio Bursts from the Inspiral of Double Neutron Stars*. Astrophysical Journal Letters **822**, L7 (2016). URL https://iopscience.iop.org/article/10.3847/2041-8205/822/1/L7/meta.

[11] N. Tominaga, Y. Niino, T. Totani, N. Yasuda, H. Furusawa, M. Tanaka, S. Bhandari, R. Dodson, E. Keane, T. Morokuma, E. Petroff, and A. Possenti. *Optical follow-up observation of Fast Radio Burst 151230*. Publications of the Astronomical Society of Japan **70**, 103 (2018). URL https://science.sciencemag.org/content/318/5851/777.

[12] P. Hoeflich. *Explosion Physics of Thermonuclear Supernovae and Their Signatures*. In *Handbook of Supernovae*, pp. 1052–1073 (Springer International Publishing, Cham, 2016). URL http://link.springer.com/10.1007/978-3-319-20794-0_56-1.

[13] D. R. Lorimer, M. Bailes, M. A. McLaughlin, D. J. Narkevic, and F. Crawford. *A bright millisecond radio burst of extragalactic origin*. Science **318**(5851), 777 (2007). URL http://dx.doi.org/10.1126/science.1147532.

[14] D. Thornton, B. Stappers, M. Bailes, B. R. Barsdell, S. D. Bates, N. D. R. Bhat, M. Burgay, S. Burke-Spolaor, D. J. Champion, P. Coster, N. D'Amico, A. Jameson, S. Johnston, M. J. Keith, M. Kramer, L. Levin, S. Milia, C. Ng, A. Possenti, and W. van Straten. *A Population of Fast Radio Bursts at Cosmological Distances*. Science, Volume 341, Issue 6141, pp. 53-56 (2013). **341**, 53 (2013). URL https://science.sciencemag.org/content/341/6141/53.

[15] U. L. Pen. *The nature of fast radio bursts*. Nature Astronomy **2**(11), 842 (2018). URL https://www.nature.com/articles/s41550-018-0620-z.

[16] E. Petroff, J. W. T. Hessels, and D. R. Lorimer. *Fast radio bursts*. The Astronomy and Astrophysics Review **27**(1), 4 (2019). URL http://link.springer.com/10.1007/s00159-019-0116-6.

[17] M. Caleb, L. G. Spitler, and B. W. Stappers. *One or several populations of fast radio burst sources?* Nature Astronomy **2**(11), 839 (2018). URL https://www.nature.com/articles/s41550-018-0612-z.

[18] D. Michilli, A. Seymour, J. W. T. Hessels, L. G. Spitler, V. Gajjar, A. M. Archibald, G. C. Bower, S. Chatterjee, J. M. Cordes, K. Gourdji, G. H. Heald, V. M. Kaspi, C. J. Law, C. Sobey, E. A. K. Adams, C. G. Bassa, S. Bogdanov, C. Brinkman, P. Demorest, F. Fernandez, G. Hellbourg, T. J. W. Lazio, R. S. Lynch, N. Maddox, B. Marcote, M. A. McLaughlin, Z. Paragi, S. M. Ransom, P. Scholz, A. P. V. Siemion, S. P. Tendulkar, P. Van Rooy, R. S. Wharton, and D. Whitlow. *An extreme magneto-ionic environment associated with the fast radio burst source FRB 121102*. Nature **553**(7687), 182 (2018). URL http://www.nature.com/articles/nature25149.

[19] E. Platts, A. Weltman, A. Walters, S. Tendulkar, J. Gordin, and S. Kandhai. *A living theory catalogue for fast radio bursts*. Physics Reports (2019). URL https://www.sciencedirect.com/science/article/pii/S037015731930242X.

[20] S. Chatterjee, C. J. Law, R. S. Wharton, S. Burke-Spolaor, J. W. T. Hessels, G. C. Bower, J. M. Cordes, S. P. Tendulkar, C. G. Bassa, P. Demorest, B. J. Butler, A. Seymour, P. Scholz, M. W. Abruzzo, S. Bogdanov, V. M. Kaspi, A. Keimpema, T. J. W. Lazio, B. Marcote, M. A. McLaughlin, Z. Paragi, S. M. Ransom, M. Rupen, L. G. Spitler, and H. J. van Langevelde. *The direct localization of a fast radio burst and its host*. Nature, Volume 541, Issue 7635, pp. 58-61 (2017). **541**, 58 (2017). URL https://www.nature.com/articles/nature20797.

[21] L. G. Spitler, J. M. Cordes, J. W. Hessels, D. R. Lorimer, M. A. McLaughlin, S. Chatterjee, F. Crawford, J. S. Deneva, V. M. Kaspi, R. S. Wharton, B. Allen, S. Bogdanov, A. Brazier, F. Camilo, P. C. Freire, F. A. Jenet, C. Karako-Argaman, B. Knispel, P. Lazarus, K. J. Lee, J. Van Leeuwen, R. Lynch, S. M. Ransom, P. Scholz, X. Siemens, I. H. Stairs, K. Stovall, J. K. Swiggum, A. Venkataraman, W. W. Zhu, C. Aulbert, and H. Fehrmann. *Fast radio burst discovered in the Arecibo pulsar ALFA survey*. Astrophysical Journal **790**(2), 101 (2014). URL https://iopscience.iop.org/article/10.1088/0004-637X/790/2/101/meta.

[22] L. G. Spitler, P. Scholz, J. W. T. Hessels, S. Bogdanov, A. Brazier, F. Camilo, S. Chatterjee, J. M. Cordes, F. Crawford, J. Deneva, R. D. Ferdman, P. C. C. Freire, V. M. Kaspi, P. Lazarus, R. Lynch, E. C. Madsen, M. A. McLaughlin, C. Patel, S. M. Ransom, A. Seymour, I. H. Stairs, B. W. Stappers, J. van Leeuwen, and W. W. Zhu. *A Repeating Fast Radio Burst*. Nature, Volume 531, Issue 7593, pp. 202-205 (2016). **531**, 202 (2016). URL https://www.nature.com/articles/nature17168.

[23] N. Oppermann, H.-R. Yu, and U.-L. Pen. *On the non-Poissonian repetition pattern of FRB121102*. Monthly Notices of the Royal Astronomical Society **475**(4), 5109 (2018). URL https://academic.oup.com/mnras/article/475/4/5109/4791594.

[24] The CHIME/FRB Collaboration, M. Amiri, K. Bandura, M. Bhardwaj, P. Boubel, M. M. Boyce, P. J. Boyle, C. Brar, M. Burhanpurkar, T. Cassanelli, P. Chawla, J. F.

Cliche, D. Cubranic, M. Deng, N. Denman, M. Dobbs, M. Fandino, E. Fonseca, B. M. Gaensler, A. J. Gilbert, A. Gill, U. Giri, D. C. Good, M. Halpern, D. S. Hanna, A. S. Hill, G. Hinshaw, C. Höfer, A. Josephy, V. M. Kaspi, T. L. Landecker, D. A. Lang, H. H. Lin, K. W. Masui, R. Mckinven, J. Mena-Parra, M. Merryfield, D. Michilli, N. Milutinovic, C. Moatti, A. Naidu, L. B. Newburgh, C. Ng, C. Patel, U. L. Pen, T. Pinsonneault-Marotte, Z. Pleunis, M. Rafiei-Ravandi, M. Rahman, S. M. Ransom, A. Renard, P. Scholz, J. R. Shaw, S. R. Siegel, K. M. Smith, I. H. Stairs, S. P. Tendulkar, I. Tretyakov, K. Vanderlinde, and P. Yadav. *A second source of repeating fast radio bursts*. Nature **566**(7743), 235 (2019). URL http://www.nature.com/articles/s41586-018-0864-x.

[25] The CHIME/FRB Collaboration, B. C. Andersen, K. Bandura, M. Bhardwaj, P. Boubel, M. M. Boyce, P. J. Boyle, C. Brar, T. Cassanelli, P. Chawla, D. Cubranic, M. Deng, M. Dobbs, M. Fandino, E. Fonseca, B. M. Gaensler, A. J. Gilbert, U. Giri, D. C. Good, M. Halpern, C. Höfer, A. S. Hill, G. Hinshaw, A. Josephy, V. M. Kaspi, R. Kothes, T. L. Landecker, D. A. Lang, D. Z. Li, H. H. Lin, K. W. Masui, J. Mena-Parra, M. Merryfield, R. Mckinven, D. Michilli, N. Milutinovic, A. Naidu, L. B. Newburgh, C. Ng, C. Patel, U. Pen, T. Pinsonneault-Marotte, Z. Pleunis, M. Rafiei-Ravandi, M. Rahman, S. M. Ransom, A. Renard, P. Scholz, S. R. Siegel, S. Singh, K. M. Smith, I. H. Stairs, S. P. Tendulkar, I. Tretyakov, K. Vanderlinde, P. Yadav, and A. V. Zwaniga. *CHIME/FRB Detection of Eight New Repeating Fast Radio Burst Sources*. arXiv p. 1908.03507 (2019). URL http://arxiv.org/abs/1908.03507.

[26] S. Johnston, M. Bailes, N. Bartel, C. Baugh, M. Bietenholz, C. Blake, R. Braun, J. Brown, S. Chatterjee, J. Darling, A. Deller, R. Dodson, P. G. Edwards, R. Ekers, S. Ellingsen, I. Feain, B. M. Gaensler, M. Haverkorn, G. Hobbs, A. Hopkins, C. Jackson, C. James, G. Joncas, V. Kaspi, V. Kilborn, B. Koribalski, R. Kothes, T. L. Landecker, E. Lenc, J. Lovell, J.-P. Macquart, R. Manchester, D. Matthews, N. M. McClure-Griffiths, R. Norris, U.-L. Pen, C. Phillips, C. Power, R. Protheroe, E. Sadler, B. Schmidt, I. Stairs, L. Staveley-Smith, J. Stil, R. Taylor, S. Tingay, A. Tzioumis, M. Walker, J. Wall, and M. Wolleben. *Science with the Australian Square Kilometre Array Pathfinder*. Publications of the Astronomical Society of Australia **24**(4), 174 (2007). URL https://www.cambridge.org/core/product/identifier/S1323358000003696/type/journal_article.

[27] P. Kumar, R. M. Shannon, S. Osłowski, H. Qiu, S. Bhandari, W. Farah, C. Flynn, M. Kerr, D. R. Lorimer, J. P. Macquart, C. Ng, C. J. Phillips, D. C. Price, and R. Spiewak. *Faint repetitions from a bright Fast Radio Burst source*. arXiv p. 1908.10026 (2019). URL http://arxiv.org/abs/1908.10026.

[28] E. F. Keane, S. Johnston, S. Bhandari, E. Barr, N. D. Bhat, M. Burgay, M. Caleb, C. Flynn, A. Jameson, M. Kramer, E. Petroff, A. Possenti, W. Van Straten, M. Bailes, S. Burke-Spolaor, R. P. Eatough, B. W. Stappers, T. Totani, M. Honma, H. Furusawa, T. Hattori, T. Morokuma, Y. Niino, H. Sugai, T. Terai, N. Tominaga, S. Yamasaki, N. Yasuda, R. Allen, J. Cooke, J. Jencson, M. M. Kasliwal, D. L. Kaplan, S. J. Tingay, A. Williams, R. Wayth, P. Chandra, D. Perrodin, M. Berezina, M. Mickaliger, and C. Bassa. *The host galaxy of a fast radio burst*. Nature **530**(7591), 453 (2016). URL http://www.nature.com/articles/nature17140.

[29] E. Petroff, E. F. Keane, E. D. Barr, J. E. Reynolds, J. Sarkissian, P. G. Edwards, J. Stevens, C. Brem, A. Jameson, S. Burke-Spolaor, S. Johnston, N. D. R. Bhat, P. Chandra, S. Kudale, and S. Bhandari. *Identifying the source of perytons at the Parkes radio telescope*. Monthly Notices of the Royal Astronomical Society, Volume 451, Issue 4, p.3933-3940 **451**, 3933 (2015). URL https://academic.oup.com/mnras/article/451/4/3933/1119649.

[30] L. Van Waerbeke and A. Zhitnitsky. *Fast radio bursts and the axion quark nugget dark matter model*. Physical Review D **99**(4), 043535 (2019). URL https://journals.aps.org/prd/abstract/10.1103/PhysRevD.99.043535.

[31] R. Brandenberger, B. Cyr, and A. V. Iyer. *Fast Radio Bursts from the Decay of Cosmic String Cusps*. arXiv p. 1707.02397 (2017). URL http://arxiv.org/abs/1707.02397.

[32] T. Vachaspati. *Cosmic Sparks from Superconducting Strings*. Physical Review Letters **101**(14), 141301 (2008). URL https://journals.aps.org/prl/abstract/10.1103/PhysRevLett.101.141301.

[33] A. Barrau, C. Rovelli, and F. Vidotto. *Fast Radio Bursts and White Hole Signals*. Physical Review D, Volume 90, Issue 12, id.127503 **90**(12) (2014). URL https://journals.aps.org/prd/abstract/10.1103/PhysRevD.90.127503.

[34] J. Tarrant, G. Beck, and S. Colafranesco. *Probing quantum gravity at low energies*. arXiv p. 1902.02550 (2019). URL https://arxiv.org/abs/1902.02550.

[35] C. Thompson. *Giant Primeval Magnetic Dipoles*. The Astrophysical Journal **844**(1), 65 (2017). URL https://iopscience.iop.org/article/10.3847/1538-4357/aa7684/meta.

[36] A. Caputo, L. Sberna, M. Frías, D. Blas, P. Pani, L. Shao, and W. Yan. *Constraints on millicharged dark matter and axionlike particles from timing of radio waves*. Physical Review D **100**(6), 063515 (2019). URL https://link.aps.org/doi/10.1103/PhysRevD.100.063515.

[37] I. Nikitin. *RDM-stars as sources of fast radio bursts*. arXiv p. 1812.11801 (2018). URL http://arxiv.org/abs/1812.11801.

[38] J. Luan and P. Goldreich. *Physical constraints on fast radio bursts*. Astrophysical Journal Letters **785**(2) (2014). URL https://iopscience.iop.org/article/10.1088/2041-8205/785/2/L26.

[39] M. Lingam and A. Loeb. *Fast Radio Bursts from Extragalactic Light Sails*. The Astrophysical Journal **837**(2), L23 (2017). URL https://iopscience.iop.org/article/10.3847/2041-8213/aa633e/meta.

[40] A. Yalinewich, M. Rahman, A. Obertas, and P. C. Breysse. *Fast Radio Bursts from Terraformation*. arXiv p. 1903.12186 (2019). URL http://arxiv.org/abs/1903.12186.

[41] D. Scott and A. Frolop. *A new kind of radio transient: ERBs*. Journal of Incoherent Astronomy p. 1903.12412 (2019). URL http://arxiv.org/abs/1903.12412.

[42] A. Hewish, S. J. Bell, J. D. H. Pilkington, P. F. Scott, and R. A. Collins. *Observation of a Rapidly Pulsating Radio Source*. Nature **217**(5130), 709 (1968). URL http://www.nature.com/articles/217709a0.

[43] N. Wex. *Neutron Stars as Probes for General Relativity and Gravitational Waves*. In *Handbook of Supernovae*, chap. 54, pp. 1447–1470 (Springer International Publishing, Cham, 2016). URL http://link.springer.com/10.1007/978-3-319-20794-0_72-1.

[44] D. B. Melrose. *Coherent emission mechanisms in astrophysical plasmas*. Reviews of Modern Plasma Physics **1**(1) (2017).

[45] J. Piekarewicz. *Neutron Star Matter Equation of State*. In *Handbook of Supernovae*, chap. 39, pp. 1075–1095 (Springer International Publishing, Cham, 2016). URL http://link.springer.com/10.1007/978-3-319-20794-0_54-1.

[46] B. Marcote and Z. Paragi. *Localizations of Fast Radio Bursts on milliarcsecond scales*. arXiv p. 1901.08541 (2019). URL http://arxiv.org/abs/1901.08541.

[47] E. K. Mahony, R. D. Ekers, J.-P. Macquart, E. M. Sadler, K. W. Bannister, S. Bhandari, C. Flynn, B. S. Koribalski, J. X. Prochaska, S. D. Ryder, R. M. Shannon, N. Tejos, M. T. Whiting, and O. I. Wong. *A Search for the Host Galaxy of FRB 171020*. The Astrophysical Journal **867**(1), L10 (2018). URL https://iopscience.iop.org/article/10.3847/2041-8213/aae7cb/meta.

[48] M. Caleb, B. W. Stappers, K. Rajwade, and C. Flynn. *Are all fast radio bursts repeating sources?* Monthly Notices of the Royal Astronomical Society **484**(4), 5500 (2019). URL https://academic.oup.com/mnras/article/484/4/5500/5315796.

[49] D. R. Lorimer. *A decade of fast radio bursts*. Nature Astronomy **2**(11), 860 (2018). URL https://www.nature.com/articles/s41550-018-0607-9.

[50] O. G. Benvenuto and M. C. Bersten. *Close Binary Stellar Evolution and Supernovae*. In *Handbook of Supernovae*, chap. 26, pp. 1–22 (Springer International Publishing, Cham, 2017). URL http://link.springer.com/10.1007/978-3-319-20794-0_124-1.

[51] T. Totani. *Cosmological Fast Radio Bursts from Binary Neutron Star Mergers*. Publications of the Astronomical Society of Japan **65**(5), L12 (2013). URL https://academic.oup.com/pasj/article-lookup/doi/10.1093/pasj/65.5.L12.

[52] S. Yamasaki, T. Totani, and K. Kiuchi. *Repeating and non-repeating fast radio bursts from binary neutron star mergers*. Publications of the Astronomical Society of Japan **70**(3) (2018). URL https://academic.oup.com/pasj/article/doi/10.1093/pasj/psy029/4960005.

[53] A. E. Egorov and K. A. Postnov. *On the possible observational manifestation of the impact of a supernova shock on the neutron star magnetosphere*. Astronomy Letters **35**(4), 241 (2009). URL https://link.springer.com/article/10.1134%2FS1063773709040033.

[54] LIGO Scientific Collaboration and Virgo Collaboration. *GW170817: Observation of Gravitational Waves from a Binary Neutron Star Inspiral*. Physical Review Letters **119**(16) (2017). URL https://journals.aps.org/prl/abstract/10.1103/PhysRevLett.119.161101.

[55] T. Dahlen, L. G. Strolger, A. G. Riess, S. Mattila, E. Kankare, and B. Mobasher. *The extended Hubble Space Telescope supernova survey: The rate of core collapse supernovae to z ∼ 1* (2012). URL https://iopscience.iop.org/article/10.1088/0004-637X/757/1/70.

[56] P. D. Gupta and N. Saini. *Collapsing supra-massive magnetars: FRBs, the repeating FRB121102 and GRBs*. Journal of Astrophysics and Astronomy **39**(1) (2018). URL https://link.springer.com/article/10.1007%2Fs12036-017-9499-9.

[57] T. Dahlen, L. Strolger, A. G. Riess, B. Mobasher, R. Chary, C. J. Conselice, H. C. Ferguson, A. S. Fruchter, M. Giavalisco, M. Livio, P. Madau, N. Panagia, and J. L. Tonry. *High-Redshift Supernova Rates*. The Astrophysical Journal **613**(1), 189 (2004). URL https://iopscience.iop.org/article/10.1086/422899.

[58] V. Ravi, R. M. Shannon, M. Bailes, K. Bannister, S. Bhandari, N. D. R. Bhat, S. Burke-Spolaor, M. Caleb, C. Flynn, A. Jameson, S. Johnston, E. F. Keane, M. Kerr, C. Tiburzi, A. V. Tuntsov, and H. K. Vedantham. *The magnetic field and turbulence of the cosmic web measured using a brilliant fast radio burst*. Science **354**(6317), 1249 (2016). URL https://science.sciencemag.org/content/354/6317/1249.

[59] J. X. Prochaska and Y. Zheng. *Probing Galactic Halos with Fast Radio Bursts*. Monthly Notices of the Royal Astronomical Society (2019). URL https://academic.oup.com/mnras/article/485/1/648/5300129.

[60] E. Y. Nugaev, G. I. Rubtsov, and Y. V. Zhezher. *Probing Milky Way's hot gas halo density distribution using the dispersion measure of pulsars*. Astronomy Letters **42**(3), 173 (2016). URL https://link.springer.com/article/10.1134%2FS1063773716030063.

[61] J.-P. Macquart. *Probing the Universe's baryons with fast radio bursts*. Nature Astronomy **2**(11), 836 (2018). URL https://www.nature.com/articles/s41550-018-0625-7.

[62] L. K. Hardy, V. S. Dhillon, L. G. Spitler, S. P. Littlefair, R. P. Ashley, A. De Cia, M. J. Green, P. Jaroenjittichai, E. F. Keane, P. Kerry, M. Kramer, D. Malesani, T. R. Marsh, S. G. Parsons, A. Possenti, S. Rattanasoon, and D. I. Sahman. *A search for optical bursts from the repeating fast radio burst FRB 121102*. Monthly Notices of the Royal Astronomical Society **472**(3), 2800 (2017). URL https://academic.oup.com/mnras/article/472/3/2800/4091441.

[63] P. Scholz, L. G. Spitler, J. W. T. Hessels, S. Chatterjee, J. M. Cordes, V. M. Kaspi, R. S. Wharton, C. G. Bassa, S. Bogdanov, F. Camilo, F. Crawford, J. Deneva, J. v. Leeuwen, R. Lynch, E. C. Madsen, M. A. McLaughlin, M. Mickaliger, E. Parent, C. Patel, S. M. Ransom, A. Seymour, I. H. Stairs, B. W. Stappers, and S. P. Tendulkar. *The Repeating Fast Radio Burst FRB 121102: Multi-wavelength Observations and Additional Bursts*. The Astrophysical Journal **833**(2), 177 (2016). URL https://iopscience.iop.org/article/10.3847/1538-4357/833/2/177/meta.

[64] P. Scholz, S. Bogdanov, J. W. T. Hessels, R. S. Lynch, L. G. Spitler, C. G. Bassa, G. C. Bower, S. Burke-Spolaor, B. J. Butler, S. Chatterjee, J. M. Cordes, K. Gourdji, V. M. Kaspi, C. J. Law, B. Marcote, M. A. McLaughlin, D. Michilli, Z. Paragi, S. M. Ransom, A. Seymour, S. P. Tendulkar, and R. S. Wharton. *Simultaneous X-Ray, Gamma-Ray, and Radio Observations of the Repeating Fast Radio Burst FRB 121102*. The Astrophysical Journal **846**(1), 80 (2017). URL https://iopscience.iop.org/article/10.3847/1538-4357/aa8456/meta.

[65] J. M. Cordes and I. Wasserman. *Supergiant pulses from extragalactic neutron stars*. Monthly Notices of the Royal Astronomical Society **457**(1), 232 (2016). URL https://academic.oup.com/mnras/article-lookup/doi/10.1093/mnras/stv2948.

[66] M. Lyutikov and D. R. Lorimer. *How Else Can We Detect Fast Radio Bursts?* The Astrophysical Journal **824**(2), L18 (2016). URL https://iopscience.iop.org/article/10.3847/2041-8205/824/2/L18/meta.

[67] S. Burke-Spolaor. *Multiple messengers of fast radio bursts*. Nature Astronomy **2**(11), 845 (2018). URL https://www.nature.com/articles/s41550-018-0630-x.

[68] LIGO Scientific Collaboration and Virgo Collaboration. *Multi-messenger Observations of a Binary Neutron Star Merger*. The Astrophysical Journal Letters **848**(2), L12 (2017). URL https://iopscience.iop.org/article/10.3847/2041-8213/aa91c9/meta.

[69] S.-X. Yi, H. Gao, and B. Zhang. *Multi-wavelength Afterglows of Fast Radio Bursts*. The Astrophysical Journal **792**(1), L21 (2014). URL https://iopscience.iop.org/article/10.1088/2041-8205/792/1/L21/meta.

[70] I. Andreoni, J. Cooke, S. Webb, A. Rest, T. A. Pritchard, M. Caleb, S.-W. Chang, W. Farah, A. Lien, A. Möller, M. E. Ravasio, T. M. C. Abbott, S. Bhandari, A. Cucchiara, C. M. Flynn, F. Jankowski, E. F. Keane, T. J. Moriya, C. Onken, A. Parthasarathy, D. C. Price, E. Petroff, S. Ryder, and C. Wolf. *Probing the extragalactic fast transient sky at minute timescales with DECam*. arXiv p. 1903.11083 (2019). URL http://arxiv.org/abs/1903.11083.

[71] Y.-P. Yang, B. Zhang, and J.-Y. Wei. *How Bright Are Fast Optical Bursts Associated With Fast Radio Bursts?* The Astrophysical Journal **878**(2), 89 (2019). URL https://iopscience.iop.org/article/10.3847/1538-4357/ab1fe2.

[72] E. Petroff, M. Bailes, E. D. Barr, B. R. Barsdell, N. D. R. Bhat, F. Bian, S. Burke-Spolaor, M. Caleb, D. Champion, P. Chandra, G. Da Costa, C. Delvaux, C. Flynn, N. Gehrels, J. Greiner, A. Jameson, S. Johnston, M. M. Kasliwal, E. F. Keane, S. Keller, J. Kocz, M. Kramer, G. Leloudas, D. Malesani, J. S. Mulchaey, C. Ng, E. O. Ofek, D. A. Perley, A. Possenti, B. P. Schmidt, Y. Shen, B. Stappers, P. Tisserand, W. van Straten, and C. Wolf. *A real-time fast radio burst: polarization detection and multiwavelength follow-up*. Monthly Notices of the Royal Astronomical Society **447**(1), 246 (2015). URL https://www.aanda.org/articles/aa/abs/2016/09/aa29172-16/aa29172-16.html.

[73] K. W. Bannister, A. T. Deller, C. Phillips, J.-P. Macquart, J. X. Prochaska, N. Tejos, S. D. Ryder, E. M. Sadler, R. M. Shannon, S. Simha, C. K. Day, M. McQuinn, F. O. North-Hickey, S. Bhandari, W. R. Arcus, V. N. Bennert, J. Burchett, M. Bouwhuis, R. Dodson, R. D. Ekers, W. Farah, C. Flynn, C. W. James, M. Kerr, E. Lenc, E. K. Mahony, J. O'Meara, S. Osłowski, H. Qiu, T. Treu, V. U, T. J. Bateman, D. C.-J. Bock, R. J. Bolton, A. Brown, J. D. Bunton, A. P. Chippendale, F. R. Cooray, T. Cornwell, N. Gupta, D. B. Hayman, M. Kesteven, B. S. Koribalski, A. MacLeod, N. M. McClure-Griffiths, S. Neuhold, R. P. Norris, M. A. Pilawa, R.-Y. Qiao, J. Reynolds, D. N. Roxby, T. W. Shimwell, M. A. Voronkov, and C. D. Wilson. *A single fast radio burst localized to a massive galaxy at cosmological distance*. Science **365**(6453), 565 (2019). URL https://science.sciencemag.org/content/365/6453/565.

[74] The CHIME/FRB Collaboration, M. Amiri, K. Bandura, M. Bhardwaj, P. Boubel, M. M. Boyce, P. J. Boyle, C. Brar, M. Burhanpurkar, P. Chawla, J. F. Cliche, D. Cubranic, M. Deng, N. Denman, M. Dobbs, M. Fandino, E. Fonseca, B. M.

Gaensler, A. J. Gilbert, U. Giri, D. C. Good, M. Halpern, D. Hanna, A. S. Hill, G. Hinshaw, C. Höfer, A. Josephy, V. M. Kaspi, T. L. Landecker, D. A. Lang, K. W. Masui, R. Mckinven, J. Mena-Parra, M. Merryfield, N. Milutinovic, C. Moatti, A. Naidu, L. B. Newburgh, C. Ng, C. Patel, U.-L. Pen, T. Pinsonneault-Marotte, Z. Pleunis, M. Rafiei-Ravandi, S. M. Ransom, A. Renard, P. Scholz, J. R. Shaw, S. R. Siegel, K. M. Smith, I. H. Stairs, S. P. Tendulkar, I. Tretyakov, K. Vanderlinde, and P. Yadav. *Observations of fast radio bursts at frequencies down to 400 megahertz*. Nature **566**(7743), 230 (2019). URL http://www.nature.com/articles/s41586-018-0867-7.

[75] P. K. G. Williams and E. Berger. *No precise localization for FRB 150418: claimed radio transient is AGN variability*. The Astrophysical Journal **821**(2), L22 (2016). URL https://iopscience.iop.org/article/10.3847/2041-8205/821/2/L22/meta.

[76] M. Giroletti, B. Marcote, M. A. Garrett, Z. Paragi, J. Yang, K. Hada, T. W. B. Muxlow, and C. C. Cheung. *FRB 150418: clues to its nature from European VLBI Network and e-MERLIN observations*. Astronomy & Astrophysics **593**, L16 (2016). URL http://www.aanda.org/10.1051/0004-6361/201629172.

[77] B. Marcote, Z. Paragi, J. W. T. Hessels, A. Keimpema, H. J. v. Langevelde, Y. Huang, C. G. Bassa, S. Bogdanov, G. C. Bower, S. Burke-Spolaor, B. J. Butler, R. M. Campbell, S. Chatterjee, J. M. Cordes, P. Demorest, M. A. Garrett, T. Ghosh, V. M. Kaspi, C. J. Law, T. J. W. Lazio, M. A. McLaughlin, S. M. Ransom, C. J. Salter, P. Scholz, A. Seymour, A. Siemion, L. G. Spitler, S. P. Tendulkar, and R. S. Wharton. *The Repeating Fast Radio Burst FRB 121102 as Seen on Milliarcsecond Angular Scales*. The Astrophysical Journal **834**(2), L8 (2017). URL https://iopscience.iop.org/article/10.3847/2041-8213/834/2/L8.

[78] J.-P. Macquart, M. Bailes, N. D. R. Bhat, G. C. Bower, J. D. Bunton, S. Chatterjee, T. Colegate, J. M. Cordes, L. D'Addario, A. Deller, R. Dodson, R. Fender, K. Haines, P. Hall, C. Harris, A. Hotan, S. Johnston, D. L. Jones, M. Keith, J. Y. Koay, T. J. W. Lazio, W. Majid, T. Murphy, R. Navarro, C. Phillips, P. Quinn, R. A. Preston, B. Stansby, I. Stairs, B. Stappers, L. Staveley-Smith, S. Tingay, D. Thompson, W. van Straten, K. Wagstaff, M. Warren, R. Wayth, and L. Wen. *The Commensal Real-time ASKAP Fast Transients (CRAFT) survey*. Publications of the Astronomical Society of Australia, Volume 27, Issue 3, pp. 272-282. **27**, 272 (2010). URL https://www.cambridge.org/core/journals/publications-of-the-astronomical-society-of-australia/article/commensal-realtime-askap-fasttransients-craft-survey/55ADB71037F1B83434C5D97B837CB359.

[79] V. Ravi, M. Catha, L. D. Addario, S. G. Djorgovski, G. Hallinan, R. Hobbs, J. Kocz, S. R. Kulkarni, J. Shi, H. K. Vedantham, S. Weinreb, and D. P. Woody. *A fast radio burst localized to a massive galaxy*. Nature p. 1 (2019). URL http://www.nature.com/articles/s41586-019-1389-7.

[80] S. P. Tendulkar, C. G. Bassa, J. M. Cordes, G. C. Bower, C. J. Law, S. Chatterjee, E. A. K. Adams, S. Bogdanov, S. Burke-Spolaor, B. J. Butler, P. Demorest, J. W. T. Hessels, V. M. Kaspi, T. J. W. Lazio, N. Maddox, B. Marcote, M. A. McLaughlin, Z. Paragi, S. M. Ransom, P. Scholz, A. Seymour, L. G. Spitler, H. J. van Langevelde, and R. S. Wharton. *The Host Galaxy and Redshift of the Repeating Fast Radio Burst FRB 121102*. The Astrophysical Journal **834**(2), L7 (2017). URL https://iopscience.iop.org/article/10.3847/2041-8213/834/2/L7/meta.

[81] T. M. C. Abbott, F. B. Abdalla, S. Allam, A. Amara, J. Annis, J. Asorey, S. Avila, O. Ballester, M. Banerji, W. Barkhouse, L. Baruah, M. Baumer, K. Bechtol, M. . R. Becker, A. Benoit-Lévy, G. M. Bernstein, E. Bertin, J. Blazek, S. Bocquet, D. Brooks, D. Brout, E. Buckley-Geer, D. L. Burke, V. Busti, R. Campisano, L. Cardiel-Sas, A. C. a. Rosell, M. C. Kind, J. Carretero, F. J. Castander, R. Cawthon, C. Chang, X. Chen, C. Conselice, G. Costa, M. Crocce, C. E. Cunha, C. B. D'Andrea, L. N. da Costa, R. Das, G. Daues, T. M. Davis, C. Davis, J. De Vicente, D. L. DePoy, J. DeRose, S. Desai, H. T. Diehl, J. P. Dietrich, S. Dodelson, P. Doel, A. Drlica-Wagner, T. F. Eifler, A. E. Elliott, A. E. Evrard, A. Farahi, A. F. Neto, E. Fernandez, D. A. Finley, M. Fitzpatrick, B. Flaugher, R. J. Foley, P. Fosalba, D. N. Friedel, J. Frieman, J. García-Bellido, E. G. Tanaga, D. W. Gerdes, T. Giannantonio, M. S. S. Gill, K. Glazebrook, D. A. Goldstein, M. Gower, D. Gruen, R. A. Gruendl, J. Gschwend, R. R. Gupta, G. Gutierrez, S. Hamilton, W. G. Hartley, S. R. Hinton, J. M. Hislop, D. Hollowood, K. Honscheid, B. Hoyle, D. Huterer, B. Jain, D. J. James, T. Jeltema, M. W. G. Johnson, M. D. Johnson, S. Juneau, T. Kacprzak, S. Kent, G. Khullar, M. Klein, A. Kovacs, A. M. G. Koziol, E. Krause, and A. Kremin. *The Dark Energy Survey Data Release 1*. The Astrophysical Journal Supplement Series **239**(2), 25 (2018). URL https://iopscience.iop.org/article/10.3847/1538-4365/aae9f0/meta.

[82] A. Gal-Yam. *Observational and Physical Classification of Supernovae*. In *Handbook of Supernovae*, chap. 12, pp. 195–237 (Springer International Publishing, Cham, 2016). URL http://link.springer.com/10.1007/978-3-319-20794-0_35-1.

[83] E. Pian and P. A. Mazzali. *Hydrogen-Poor Core-Collapse Supernovae*. In *Handbook of Supernovae*, chap. 14, pp. 239–276 (Springer International Publishing, Cham, 2016). URL http://link.springer.com/10.1007/978-3-319-20794-0_40-1.

[84] A. Pastorello, M. Turatto, S. Benetti, E. Cappellaro, I. J. Danziger, P. A. Mazzali, F. Patat, A. V. Filippenko, D. J. Schlegel, and T. Matheson. *The type IIn supernova 1995G: Interaction with the circumstellar medium*. Monthly Notices of the Royal Astronomical Society **333**(1), 27 (2002). URL https://academic.oup.com/mnras/article/333/1/27/1187467.

[85] I. Arcavi. *Hydrogen-Rich Core-Collapse Supernovae*. In *Handbook of Supernovae*, chap. 13, pp. 239–277 (Springer International Publishing, Cham, 2016). URL http://link.springer.com/10.1007/978-3-319-20794-0_39-1.

[86] A. Gal-Yam. *The Most Luminous Supernovae*. Annual Review of Astronomy and Astrophysics **57**(1), 305 (2019). URL https://www.annualreviews.org/doi/full/10.1146/annurev-astro-081817-051819.

[87] B. D. Metzger, G. Martínez-Pinedo, S. Darbha, E. Quataert, A. Arcones, D. Kasen, R. Thomas, P. Nugent, I. V. Panov, and N. T. Zinner. *Electromagnetic counterparts of compact object mergers powered by the radioactive decay of r-process nuclei*. Monthly Notices of the Royal Astronomical Society **406**(4), 2650 (2010). URL https://academic.oup.com/mnras/article-lookup/doi/10.1111/j.1365-2966.2010.16864.x.

[88] M. R. Drout, A. L. Piro, B. J. Shappee, C. D. Kilpatrick, J. D. Simon, C. Contreras, D. A. Coulter, R. J. Foley, M. R. Siebert, N. Morrell, K. Boutsia, F. Di Mille, T. W.-S. Holoien, D. Kasen, J. A. Kollmeier, B. F. Madore, A. J. Monson, A. Murguia-Berthier, Y.-C. Pan, J. X. Prochaska, E. Ramirez-Ruiz, A. Rest, C. Adams, K. Alatalo,

E. Bañados, J. Baughman, T. C. Beers, R. A. Bernstein, T. Bitsakis, A. Campillay, T. T. Hansen, C. R. Higgs, A. P. Ji, G. Maravelias, J. L. Marshall, C. M. Bidin, J. L. Prieto, K. C. Rasmussen, C. Rojas-Bravo, A. L. Strom, N. Ulloa, J. Vargas-González, Z. Wan, and D. D. Whitten. *Light curves of the neutron star merger GW170817/SSS17a: Implications for r-process nucleosynthesis.* Science **358**(6370), 1570 (2017). URL https://science.sciencemag.org/content/358/6370/1570.long.

[89] N. Guessoum, H. Zitouni, and R. Mochkovitch. *Detecting the imprint of a kilonova or supernova in short GRB afterglows.* Astronomy & Astrophysics **620**, A131 (2018). URL https://www.aanda.org/articles/aa/abs/2018/12/aa32940-18/aa32940-18.html.

[90] I. Appenzeller, K. Fricke, W. Fürtig, W. Gässler, R. Häfner, R. Harke, H.-J. Hess, W. Hummel, P. Jürgens, R.-P. Kudritzki, K.-H. Mantel, W. Meisl, B. Muschielok, H. Nicklas, G. Rupprecht, W. Seifert, O. Stahl, T. Szeifert, and K. Tarantik. *Successful commissioning of FORS1 - the first optical instrument on the VLT.* The Messenger **94**, 1 (1998). URL https://ui.adsabs.harvard.edu/abs/1998Msngr..94....1A.

[91] J. Vernet, H. Dekker, S. D'Odorico, L. Kaper, P. Kjaergaard, F. Hammer, S. Randich, F. Zerbi, P. J. Groot, J. Hjorth, I. Guinouard, R. Navarro, T. Adolfse, P. W. Albers, J.-P. Amans, J. J. Andersen, M. I. Andersen, P. Binetruy, P. Bristow, R. Castillo, F. Chemla, L. Christensen, P. Conconi, R. Conzelmann, J. Dam, V. De Caprio, A. De Ugarte Postigo, B. Delabre, P. Di Marcantonio, M. Downing, E. Elswijk, G. Finger, G. Fischer, H. Flores, P. François, P. Goldoni, L. Guglielmi, R. Haigron, H. Hanenburg, I. Hendriks, M. Horrobin, D. Horville, N. C. Jessen, F. Kerber, L. Kern, M. Kiekebusch, P. Kleszcz, J. Klougart, J. Kragt, H. H. Larsen, J.-L. Lizon, C. Lucuix, V. Mainieri, R. Manuputy, C. Martayan, E. Mason, R. Mazzoleni, N. Michaelsen, A. Modigliani, S. Moehler, P. Møller, A. Norup Sørensen, P. Nørregaard, C. Péroux, F. Patat, E. Pena, J. Pragt, C. Reinero, F. Rigal, M. Riva, R. Roelfsema, F. Royer, G. Sacco, P. Santin, T. Schoenmaker, P. Spano, E. Sweers, R. Ter Horst, M. Tintori, N. Tromp, P. van Dael, H. van der Vliet, L. Venema, M. Vidali, J. Vinther, P. Vola, R. Winters, D. Wistisen, G. Wulterkens, and A. Zacchei. *X-shooter, the new wide band intermediate resolution spectrograph at the ESO Very Large Telescope.* Astronomy & Astrophysics **536**, A105 (2011). URL http://www.aanda.org/10.1051/0004-6361/201117752.

[92] C. Martayan, A. Mehner, G. Beccari, E. Peña, W. Hummel, A. Smette, A. Modigliani, J. Vernet, H. Dekker, N. Neumayer, V. Mainieri, S. Moehler, R. Castillo, and M. Riquelme. *The X-shooter Imaging Mode.* The Messenger **156**, 21 (2014). URL https://ui.adsabs.harvard.edu/abs/2014Msngr.156...21M/abstract.

[93] R. J. Hanisch, A. Farris, E. W. Greisen, W. D. Pence, B. M. Schlesinger, P. J. Teuben, R. W. Thompson, and A. Warnock. *Definition of the Flexible Image Transport System (FITS).* Astronomy & Astrophysics **376**(1), 359 (2001). URL http://www.aanda.org/10.1051/0004-6361:20010923.

[94] T. P. Robitaille, E. J. Tollerud, P. Greenfield, M. Droettboom, E. Bray, T. Aldcroft, M. Davis, A. Ginsburg, A. M. Price-Whelan, W. E. Kerzendorf, A. Conley, N. Crighton, K. Barbary, D. Muna, H. Ferguson, F. Grollier, M. M. Parikh, P. H. Nair, H. M. Günther, C. Deil, J. Woillez, S. Conseil, R. Kramer, J. E. Turner, L. Singer, R. Fox, B. A. Weaver, V. Zabalza, Z. I. Edwards, K. Azalee Bostroem, D. J. Burke, A. R. Casey,

S. M. Crawford, N. Dencheva, J. Ely, T. Jenness, K. Labrie, P. L. Lim, F. Pierfederici, A. Pontzen, A. Ptak, B. Refsdal, M. Servillat, and O. Streicher. *Astropy: A community Python package for astronomy*. Astronomy and Astrophysics **558**(A33), 9 (2013). URL https://www.aanda.org/articles/aa/abs/2013/10/aa22068-13/aa22068-13.html.

[95] A. M. Price-Whelan, B. M. Sipőcz, H. M. Günther, P. L. Lim, S. M. Crawford, S. Conseil, D. L. Shupe, M. W. Craig, N. Dencheva, A. Ginsburg, J. T. VanderPlas, L. D. Bradley, D. Pérez-Suárez, M. de Val-Borro, T. L. Aldcroft, K. L. Cruz, T. P. Robitaille, E. J. Tollerud, C. Ardelean, T. Babej, Y. P. Bach, M. Bachetti, A. V. Bakanov, S. P. Bamford, G. Barentsen, P. Barmby, A. Baumbach, K. L. Berry, F. Biscani, M. Boquien, K. A. Bostroem, L. G. Bouma, G. B. Brammer, E. M. Bray, H. Breytenbach, H. Buddelmeijer, D. J. Burke, G. Calderone, J. L. C. Rodríguez, M. Cara, J. V. M. Cardoso, S. Cheedella, Y. Copin, L. Corrales, D. Crichton, D. D'Avella, C. Deil, E. Depagne, J. P. Dietrich, A. Donath, M. Droettboom, N. Earl, T. Erben, S. Fabbro, L. A. Ferreira, T. Finethy, R. T. Fox, L. H. Garrison, S. L. J. Gibbons, D. A. Goldstein, R. Gommers, J. P. Greco, P. Greenfield, A. M. Groener, F. Grollier, A. Hagen, P. Hirst, D. Homeier, A. J. Horton, G. Hosseinzadeh, L. Hu, J. S. Hunkeler, Z. Ivezić, A. Jain, T. Jenness, G. Kanarek, S. Kendrew, N. S. Kern, W. E. Kerzendorf, A. Khvalko, J. King, D. Kirkby, A. M. Kulkarni, A. Kumar, A. Lee, D. Lenz, S. P. Littlefair, Z. Ma, D. M. Macleod, M. Mastropietro, C. McCully, S. Montagnac, B. M. Morris, M. Mueller, S. J. Mumford, D. Muna, N. A. Murphy, S. Nelson, G. H. Nguyen, J. P. Ninan, M. Nöthe, S. Ogaz, S. Oh, J. K. Parejko, N. Parley, S. Pascual, R. Patil, A. A. Patil, A. L. Plunkett, J. X. Prochaska, T. Rastogi, V. R. Janga, J. Sabater, P. Sakurikar, M. Seifert, L. E. Sherbert, H. Sherwood-Taylor, A. Y. Shih, J. Sick, M. T. Silbiger, S. Singanamalla, L. P. Singer, P. H. Sladen, K. A. Sooley, S. Sornarajah, O. Streicher, P. Teuben, S. W. Thomas, G. R. Tremblay, J. E. H. Turner, V. Terrón, M. H. v. Kerkwijk, A. de la Vega, L. L. Watkins, B. A. Weaver, J. B. Whitmore, J. Woillez, and V. Zabalza. *The Astropy Project: Building an Open-science Project and Status of the v2.0 Core Package*. The Astronomical Journal **156**(3), 19 (2018). URL https://iopscience.iop.org/article/10.3847/1538-3881/aabc4f.

[96] W. Freudling, M. Romaniello, D. M. Bramich, P. Ballester, V. Forchi, C. E. Garcia-Dablo, S. Moehler, and M. J. Neeser. *Automated data reduction workflows for astronomy*. Astronomy & Astrophysics **559**, 96 (2013). URL https://www.aanda.org/articles/aa/abs/2013/11/aa22494-13/aa22494-13.html.

[97] M. Craig, S. Crawford, M. Seifert, T. Robitaille, B. Sipocz, J. Walawender, Z. Vinícius, J. P. Ninan, M. Droettboom, J. Youn, E. Tollerud, E. Bray, walkerna22, V. R. Janga, stottsco, H. M. Günther, E. Rol, Y. P. Bach, L. Bradley, C. Deil, A. Price-Whelan, K. Barbary, A. Horton, W. Schoenell, Nathan, F. Gasdia, S. Nelson, and O. Streicher. *astropy/ccdproc: v1.3.0.post1*. Zenodo (2017). URL https://zenodo.org/record/1043589.

[98] E. Bertin. *SWarp: Resampling and Co-adding FITS Images Together* (2010). URL http://ascl.net/1010.068.

[99] J. C. Jacob, D. S. Katz, G. B. Berriman, J. Good, A. C. Laity, E. Deelman, C. Kesselman, G. Singh, M.-H. Su, T. A. Prince, and R. Williams. *Montage: An Astronomical Image Mosaicking Toolkit* (2010). URL http://ascl.net/1010.036.

[100] D. Lang, D. W. Hogg, K. Mierle, M. Blanton, and S. Roweis. *Astrometry.net: Blind astrometric calibration of arbitrary astronomical images*. The Astronomical Journal **139**(5), 1782 (2010). URL https://iopscience.iop.org/article/10.1088/0004-6256/139/5/1782.

[101] L. Lindegren, J. Hernández, A. Bombrun, S. Klioner, U. Bastian, M. Ramos-Lerate, A. de Torres, H. Steidelmüller, C. Stephenson, D. Hobbs, U. Lammers, M. Biermann, R. Geyer, T. Hilger, D. Michalik, U. Stampa, P. McMillan, J. Castañeda, M. Clotet, G. Comoretto, M. Davidson, C. Fabricius, G. Gracia, N. Hambly, A. Hutton, A. Mora, J. Portell, F. van Leeuwen, U. Abbas, A. Abreu, M. Altmann, A. Andrei, E. Anglada, L. Balaguer-Núñez, C. Barache, U. Becciani, S. Bertone, L. Bianchi, S. Bouquillon, G. Bourda, T. Brüsemeister, B. Bucciarelli, D. Busonero, R. Buzzi, R. Cancelliere, T. Carlucci, P. Charlot, N. Cheek, M. Crosta, C. Crowley, J. de Bruijne, F. de Felice, R. Drimmel, P. Esquej, A. Fienga, E. Fraile, M. Gai, N. Garralda, J. González-Vidal, R. Guerra, M. Hauser, W. Hofmann, B. Holl, S. Jordan, M. Lattanzi, H. Lenhardt, S. Liao, E. Licata, T. Lister, W. Löffler, J. Marchant, J.-M. Martin-Fleitas, R. Messineo, F. Mignard, R. Morbidelli, E. Poggio, A. Riva, N. Rowell, E. Salguero, M. Sarasso, E. Sciacca, H. Siddiqui, R. Smart, A. Spagna, I. Steele, F. Taris, J. Torra, A. van Elteren, W. van Reeven, and A. Vecchiato. *Gaia Data Release 2: The astrometric solution*. Astronomy & Astrophysics **616**, A2 (2018). URL https://www.aanda.org/10.1051/0004-6361/201832727.

[102] L. Bradley, B. Sipocz, T. Robitaille, E. Tollerud, Z. Vinícius, C. Deil, K. Barbary, H. M. Günther, M. Cara, I. Busko, S. Conseil, M. Droettboom, A. Bostroem, E. M. Bray, L. A. Bratholm, T. Wilson, M. Craig, G. Barentsen, S. Pascual, A. Donath, J. Greco, G. Perren, P. L. Lim, and W. Kerzendorf. *astropy/photutils: v0.6*. Zenodo (2019). URL https://zenodo.org/record/2533376.

[103] E. Bertin and S. Arnouts. *SExtractor: Software for source extraction*. Astronomy and Astrophysics Supplement Series **117**(2), 393 (1996). URL http://aas.aanda.org/10.1051/aas:1996164.

[104] A. Dolphin and Andrew. *DOLPHOT: Stellar photometry* (2016). URL http://ascl.net/1608.013.

[105] B. W. Holwerda. *Source Extractor for Dummies v5*. arXiv pp. astro–ph/0512139 (2005). URL http://mensa.ast.uct.ac.za/~holwerda/SE/Manual.html.

[106] J. Guy, M. Sullivan, A. Conley, N. Regnault, P. Astier, C. Balland, S. Basa, R. G. Carlberg, D. Fouchez, D. Hardin, I. M. Hook, D. A. Howell, R. Pain, N. Palanque-Delabrouille, K. M. Perrett, C. J. Pritchet, J. Rich, V. Ruhlmann-Kleider, D. Balam, S. Baumont, R. S. Ellis, S. Fabbro, H. K. Fakhouri, N. Fourmanoit, S. González-Gaitán, M. L. Graham, E. Hsiao, T. Kronborg, C. Lidman, A. M. Mourao, S. Perlmutter, P. Ripoche, N. Suzuki, and E. S. Walker. *The Supernova Legacy Survey 3-year sample: Type Ia supernovae photometric distances and cosmological constraints*. Astronomy & Astrophysics **523**, A7 (2010). URL http://www.aanda.org/10.1051/0004-6361/201014468.

[107] R. P. Norris, A. M. Hopkins, J. Afonso, S. Brown, J. J. Condon, L. Dunne, I. Feain, R. Hollow, M. Jarvis, M. Johnston-Hollitt, E. Lenc, E. Middelberg, P. Padovani,

I. Prandoni, L. Rudnick, N. Seymour, G. Umana, H. Andernach, D. M. Alexander, P. N. Appleton, D. Bacon, J. Banfield, W. Becker, M. J. I. Brown, P. Ciliegi, C. Jackson, S. Eales, A. C. Edge, B. M. Gaensler, G. Giovannini, C. A. Hales, P. Hancock, M. T. Huynh, E. Ibar, R. J. Ivison, R. Kennicutt, A. E. Kimball, A. M. Koekemoer, B. S. Koribalski, A. R. López-Sánchez, M. Y. Mao, T. Murphy, H. Messias, K. A. Pimbblet, A. Raccanelli, K. E. Randall, T. H. Reiprich, I. G. Roseboom, H. Röttgering, D. J. Saikia, R. G. Sharp, O. B. Slee, I. Smail, M. A. Thompson, J. S. Urquhart, J. V. Wall, and G.-B. Zhao. *EMU: Evolutionary Map of the Universe*. Publications of the Astronomical Society of Australia **28**(3), 215 (2011). URL https://www.cambridge. org/core/journals/publications-of-the-astronomical-society-of-australia/article/ emu-evolutionary-map-of-the-universe/38E4A2706715B1217EFAFE264A1D39DC.

[108] E. C. Kool, S. Ryder, E. Kankare, S. Mattila, T. Reynolds, R. M. McDermid, M. A. Pérez-Torres, R. Herrero-Illana, M. Schirmer, A. Efstathiou, F. E. Bauer, J. Kotilainen, P. Väisänen, C. Baldwin, C. Romero-Cañizales, and A. Alberdi. *First results from GeMS/GSAOI for project SUNBIRD: Supernovae UNmasked By Infra-Red Detection*. Monthly Notices of the Royal Astronomical Society **473**(4), 5641 (2018). URL https: //academic.oup.com/mnras/article/473/4/5641/4259573.

[109] C. Wolf, C. A. Onken, L. C. Luvaul, B. P. Schmidt, M. S. Bessell, S.-W. Chang, G. S. Da Costa, D. Mackey, T. Martin-Jones, S. J. Murphy, T. Preston, R. A. Scalzo, L. Shao, J. Smillie, P. Tisserand, M. C. White, and F. Yuan. *SkyMapper Southern Survey: First Data Release (DR1)*. Publications of the Astronomical Society of Australia **35**, e010 (2018). URL https://www. cambridge.org/core/journals/publications-of-the-astronomical-society-of-australia/ article/skymapper-southern-survey-first-data-release-dr1/ 3ED272F4F20E663CCF313F9C15659437.

[110] C. Izzo, L. de Bilbao, and J. M. Larsen. *The Very Large Telescope: FORS Pipeline User Manual*. Tech. rep., European Southern Observatory (2018). URL http://www. eso.org/public/teles-instr/vlt.html.

[111] J. Anderson, S. Mieske, and A. Kaufer. *Very Large Telescope - FORS2 User Manual*. Tech. rep., Paranal Science Operations (2018). URL http://www.eso.org/sci/facilities/ paranal/instruments/fors/doc/VLT-MAN-ESO-13100-1543_P03.pdf.

[112] D. S. Aguado, R. Ahumada, A. Almeida, S. F. Anderson, B. H. Andrews, B. Anguiano, E. A. Ortíz, A. Aragón-Salamanca, M. Argudo-Fernández, M. Aubert, V. Avila-Reese, C. Badenes, S. Barboza Rembold, K. Barger, J. Barrera-Ballesteros, D. Bates, J. Bautista, R. L. Beaton, T. C. Beers, F. Belfiore, M. Bernardi, M. Bershady, F. Beutler, J. Bird, D. Bizyaev, G. A. Blanc, M. R. Blanton, M. Blomqvist, A. S. Bolton, M. Boquien, J. Borissova, J. Bovy, W. Nielsen Brandt, J. Brinkmann, J. R. Brownstein, K. Bundy, A. Burgasser, N. Byler, M. Cano Diaz, M. Cappellari, R. Carrera, B. Cervantes Sodi, Y. Chen, B. Cherinka, P. Doohyun Choi, H. Chung, D. Coffey, J. M. Comerford, J. Comparat, K. Covey, G. da Silva Ilha, L. da Costa, Y. Sophia Dai, G. Damke, J. Darling, R. Davies, K. Dawson, V. de Sainte Agathe, A. Deconto Machado, A. Del Moro, N. De Lee, A. M. Diamond-Stanic, H. Domínguez Sánchez, J. Donor, N. Drory, H. du Mas des Bourboux, C. Duckworth, T. Dwelly, G. Ebelke, E. Emsellem, S. Escoffier, J. G. Fernández-Trincado, D. Feuillet, J.-L. Fischer, S. W. Fleming, A. Fraser-McKelvie, G. Freischlad, P. M. Frinchaboy, H. Fu, L. Galbany,

R. Garcia-Dias, D. A. García-Hernández, L. Alberto Garma Oehmichen, M. Antonio Geimba Maia, H. Gil-Marín, K. Grabowski, M. Gu, H. Guo, J. Ha, E. Harrington, S. Hasselquist, C. R. Hayes, F. Hearty, H. Hernandez Toledo, H. Hicks, D. W. Hogg, K. Holley-Bockelmann, J. A. Holtzman, B.-C. Hsieh, J. A. S. Hunt, H. Seong Hwang, H. J. Ibarra-Medel, C. Eduardo Jimenez Angel, J. Johnson, A. Jones, H. Jönsson, K. Kinemuchi, J. Kollmeier, C. Krawczyk, K. Kreckel, S. Kruk, I. Lacerna, T.-W. Lan, R. R. Lane, D. R. Law, Y.-B. Lee, C. Li, J. Lian, L. Lin, Y.-T. Lin, C. Lintott, D. Long, P. Longa-Peña, J. Ted Mackereth, A. de la Macorra, S. R. Majewski, O. Malanushenko, A. Manchado, C. Maraston, V. Mariappan, M. Marinelli, R. Marques-Chaves, T. Masseron, K. L. Masters, R. M. McDermid, N. Medina Peña, S. Meneses-Goytia, A. Merloni, M. Merrifield, S. Meszaros, D. Minniti, R. Minsley, D. Muna, A. D. Myers, P. Nair, J. Correa do Nascimento, J. A. Newman, C. Nitschelm, M. D. Olmstead, A. Oravetz, D. Oravetz, R. A. Ortega Minakata, Z. Pace, N. Padilla, P. A. Palicio, K. Pan, H.-A. Pan, T. Parikh, J. Parker, S. Peirani, S. Penny, W. J. Percival, I. Perez-Fournon, T. Peterken, M. H. Pinsonneault, A. Prakash, M. J. Raddick, A. Raichoor, R. A. Riffel, R. Riffel, H.-W. Rix, A. C. Robin, A. Roman-Lopes, B. Rose, A. J. Ross, G. Rossi, K. Rowlands, K. H. R. Rubin, S. F. Sánchez, J. R. Sánchez-Gallego, C. Sayres, A. Schaefer, R. P. Schiavon, J. S. Schimoia, E. Schlafly, D. Schlegel, D. P. Schneider, M. Schultheis, H.-J. Seo, S. J. Shamsi, Z. Shao, S. Shen, S. Shetty, G. Simonian, R. J. Smethurst, J. Sobeck, B. J. Souter, A. Spindler, D. V. Stark, K. G. Stassun, M. Steinmetz, T. Storchi-Bergmann, G. S. Stringfellow, G. Suárez, J. Sun, M. Taghizadeh-Popp, M. S. Talbot, J. Tayar, A. R. Thakar, D. Thomas, P. Tissera, R. Tojeiro, N. W. Troup, E. Unda-Sanzana, O. Valenzuela, M. Vargas-Magaña, J. Antonio Vázquez-Mata, D. Wake, B. Alan Weaver, A.-M. Weijmans, K. B. Westfall, V. Wild, J. Wilson, E. Woods, R. Yan, M. Yang, O. Zamora, G. Zasowski, K. Zhang, Z. Zheng, Z. Zheng, G. Zhu, J. C. Zinn, and H. Zou. *The Fifteenth Data Release of the Sloan Digital Sky Surveys: First Release of MaNGA-derived Quantities, Data Visualization Tools, and Stellar Library*. The Astrophysical Journal Supplement Series **240**(2), 23 (2019). URL https://iopscience.iop.org/article/10.3847/1538-4365/aaf651.

[113] E. Bertin. *Automated Morphometry with SExtractor and PSFEx*. Astronomical Data Analysis Software and Systems XX **442**, 435 (2011). URL http://aspbooks.org/custom/publications/paper/442-0435.html.

[114] J. S. Mathis. *Interstellar Dust and Extinction*. Annual Review of Astronomy and Astrophysics **28**(1), 37 (1990). URL http://www.annualreviews.org/doi/10.1146/annurev.aa.28.090190.000345.

[115] E. F. Schlafly and D. P. Finkbeiner. *Measuring reddening with Sloan Digital Sky Survey stellar spectra and recalibrating SFD*. Astrophysical Journal **737**(2) (2011). URL https://iopscience.iop.org/article/10.1088/0004-637X/737/2/103.

[116] D. J. Schlegel, D. P. Finkbeiner, and M. Davis. *Maps of Dust Infrared Emission for Use in Estimation of Reddening and Cosmic Microwave Background Radiation Foregrounds*. The Astrophysical Journal **500**(2), 525 (1998). URL https://iopscience.iop.org/article/10.1086/305772.

[117] E. L. Fitzpatrick. *Correcting for the Effects of Interstellar Extinction*. Publications of the Astronomical Society of the Pacific **111**(755), 63 (1999). URL http://iopscience.iop.org/article/10.1086/316293.

[118] R. G. Kron. *Photometry of a complete sample of faint galaxies*. The Astrophysical Journal Supplement Series **43**, 305 (1980). URL https://ui.adsabs.harvard.edu/abs/1980ApJS...43..305K/abstract.

[119] E. Wright. *A Cosmology Calculator for the World Wide Web*. Publications of the Astronomical Society of the Pacific **118**(850), 1711 (2006). URL http://iopscience.iop.org/article/10.1086/510102.

[120] R. J. Cool, J. Moustakas, M. R. Blanton, S. M. Burles, A. L. Coil, D. J. Eisenstein, K. C. Wong, G. Zhu, J. Aird, R. A. Bernstein, A. S. Bolton, D. W. Hogg, and A. J. Mendez. *The prism multi-object survey (Primus). II. Data reduction and redshift fitting*. Astrophysical Journal **767**(2), 118 (2013). URL https://iopscience.iop.org/article/10.1088/0004-637X/741/1/8.

[121] A. L. Coil, M. R. Blanton, S. M. Burles, R. J. Cool, D. J. Eisenstein, J. Moustakas, K. C. Wong, G. Zhu, J. Aird, R. A. Bernstein, A. S. Bolton, and D. W. Hogg. *The prism multi-object survey (PRIMUS). I. Survey overview and characteristics*. Astrophysical Journal **741**(1), 8 (2011). URL https://iopscience.iop.org/article/10.1088/0004-637X/767/2/118.

[122] C. G. Bassa, S. P. Tendulkar, E. A. K. Adams, N. Maddox, S. Bogdanov, G. C. Bower, S. Burke-Spolaor, B. J. Butler, S. Chatterjee, J. M. Cordes, J. W. T. Hessels, V. M. Kaspi, C. J. Law, B. Marcote, Z. Paragi, S. M. Ransom, P. Scholz, L. G. Spitler, and H. J. v. Langevelde. *FRB 121102 Is Coincident with a Star-forming Region in Its Host Galaxy*. The Astrophysical Journal **843**(1), L8 (2017). URL https://iopscience.iop.org/article/10.3847/2041-8213/aa7a0c/meta.

[123] J. A. Baldwin, M. M. Phillips, and R. Terlevich. *Classification parameters for the emission-line spectra of extragalactic objects*. Publications of the Astronomical Society of the Pacific **93**, 5 (1981). URL http://iopscience.iop.org/article/10.1086/130766.

[124] D. C. Martin, T. K. Wyder, D. Schiminovich, T. A. Barlow, K. Forster, P. G. Friedman, P. Morrissey, S. G. Neff, M. Seibert, T. Small, B. Y. Welsh, L. Bianchi, J. Donas, T. M. Heckman, Y. Lee, B. F. Madore, B. Milliard, R. M. Rich, A. S. Szalay, and S. K. Yi. *The UV-Optical Galaxy Color-Magnitude Diagram. III. Constraints on Evolution from the Blue to the Red Sequence*. The Astrophysical Journal Supplement Series **173**(2), 342 (2007). URL https://iopscience.iop.org/article/10.1086/516639.

[125] I. Strateva, Z. Ivezić, G. R. Knapp, V. K. Narayanan, M. A. Strauss, J. E. Gunn, R. H. Lupton, D. Schlegel, N. A. Bahcall, J. Brinkmann, R. J. Brunner, T. Budavári, I. Csabai, F. J. Castander, M. Doi, M. Fukugita, Z. Győry, M. Hamabe, G. Hennessy, T. Ichikawa, P. Z. Kunszt, D. Q. Lamb, T. A. McKay, S. Okamura, J. Racusin, M. Sekiguchi, D. P. Schneider, K. Shimasaku, and D. York. *Color Separation of Galaxy Types in the Sloan Digital Sky Survey Imaging Data*. The Astronomical Journal **122**(4), 1861 (2001). URL https://iopscience.iop.org/article/10.1086/323301.

[126] E. F. Bell, C. Wolf, K. Meisenheimer, H. Rix, A. Borch, S. Dye, M. Kleinheinrich, L. Wisotzki, and D. H. McIntosh. *Nearly 5000 Distant Early-Type Galaxies in COMBO-17: A Red Sequence and Its Evolution since z ∼ 1*. The Astrophysical Journal **608**(2), 752 (2004). URL https://iopscience.iop.org/article/10.1086/420778.

[127] P. Kumar and J. X. Prochaska. *Private communication* (2019).

[128] B. Zackay, E. O. Ofek, and A. Gal-Yam. *Proper Image Subtraction—Optimal Transient Detection, Photometry, and Hypothesis Testing*. The Astrophysical Journal **830**(1), 27 (2016). URL https://iopscience.iop.org/article/10.3847/0004-637X/830/1/27/meta.

[129] C. Alard, R. Lupton, C. Alard, and R. Lupton. *ISIS: A method for optimal image subtraction*. Astrophysics Source Code Library p. ascl:9909.003 (1999). URL http://www.ascl.net/9909.003.

[130] E. O. Ofek and E. O. *MATLAB package for astronomy and astrophysics* (2014). URL http://ascl.net/1407.005.

[131] A. Becker and Andrew. *HOTPANTS: High Order Transform of PSF ANd Template Subtraction* (2015). URL http://ascl.net/1504.004.

[132] C. Alard. *Image subtraction using a space-varying kernel*. Astronomy and Astrophysics Supplement Series **144**(2), 363 (2000). URL http://aas.aanda.org/10.1051/aas:2000214.

[133] C. Alard and R. H. Lupton. *A Method for Optimal Image Subtraction*. The Astrophysical Journal **503**(1), 325 (1998). URL https://iopscience.iop.org/article/10.1086/305984.

[134] E. Bertin. *SkyMaker: astronomical image simulations made easy*. Memorie della Societa Astronomica Italiana **80**, 422 (2009). URL https://ui.adsabs.harvard.edu/abs/2009MmSAI..80..422B/abstract.

[135] K. Barbary. *sncosmo v0.4.2*. Zenodo (2014). URL https://zenodo.org/record/11938.

[136] J. D. R. Pierel, S. Rodney, A. Avelino, F. Bianco, A. V. Filippenko, R. J. Foley, A. Friedman, M. Hicken, R. Hounsell, S. W. Jha, R. Kessler, R. P. Kirshner, K. Mandel, G. Narayan, D. Scolnic, and L. Strolger. *Extending Supernova Spectral Templates for Next-generation Space Telescope Observations*. Publications of the Astronomical Society of the Pacific **130**(993), 114504 (2018). URL https://iopscience.iop.org/article/10.1088/1538-3873/aadb7a.

[137] P. J. Brown, G. Hosseinzadeh, S. W. Jha, D. Sand, E. Vieira, X. Wang, M. Dai, K. G. Dettman, J. Mould, S. Uddin, L. Wang, I. Arcavi, J. Bento, C. R. Burns, T. Diamond, D. Hiramatsu, D. A. Howell, E. Y. Hsiao, G. H. Marion, C. McCully, P. A. Milne, D. Mirzaqulov, A. J. Ruiter, S. Valenti, and D. Xiang. *Red and Reddened: Ultraviolet through Near-infrared Observations of Type Ia Supernova 2017erp*. The Astrophysical Journal **877**(2), 152 (2019). URL https://iopscience.iop.org/article/10.3847/1538-4357/ab1a3f.

[138] J. Guy, P. Astier, S. Baumont, D. Hardin, R. Pain, N. Regnault, S. Basa, R. G. Carlberg, A. Conley, S. Fabbro, D. Fouchez, I. M. Hook, D. A. Howell, K. Perrett, C. J. Pritchet, J. Rich, M. Sullivan, P. Antilogus, E. Aubourg, G. Bazin, J. Bronder, M. Filiol, N. Palanque-Delabrouille, P. Ripoche, and V. Ruhlmann-Kleider. *SALT2: using distant supernovae to improve the use of type Ia supernovae as distance indicators*. Astronomy & Astrophysics **466**(1), 11 (2007). URL http://www.aanda.org/10.1051/0004-6361:20066930.

[139] F.-W. Zhang, Y.-Z. Fan, L. Shao, and D.-M. Wei. *Cosmological time dilation in durations of SWIFT long gamma-ray bursts*. The Astrophysical Journal **778**(1), L11 (2013). URL https://iopscience.iop.org/article/10.1088/2041-8205/778/1/L11.

[140] B. W. Holwerda, A. Reynolds, M. Smith, and R. C. Kraan-Korteweg. *SN Ia host galaxy properties and the dust extinction distribution*. Monthly Notices of the Royal Astronomical Society **446**(4), 3768 (2015). URL https://ui.adsabs.harvard.edu/abs/2015MNRAS.446.3768H/abstract.

[141] H. Lampeitl, M. Smith, R. C. Nichol, B. Bassett, D. Cinabro, B. Dilday, R. J. Foley, J. A. Frieman, P. M. Garnavich, A. Goobar, M. Im, S. W. Jha, J. Marriner, R. Miquel, J. Nordin, L. Östman, A. G. Riess, M. Sako, D. P. Schneider, J. Sollerman, and M. Stritzinger. *The effect of host galaxies on Type Ia supernovae in the SDSS-II supernova survey*. Astrophysical Journal **722**(1), 566 (2010). URL https://iopscience.iop.org/article/10.1088/0004-637X/722/1/566.

[142] R. Hounsell, D. Scolnic, R. J. Foley, R. Kessler, V. Miranda, A. Avelino, R. C. Bohlin, A. V. Filippenko, J. Frieman, S. W. Jha, P. L. Kelly, R. P. Kirshner, K. Mandel, A. Rest, A. G. Riess, S. A. Rodney, and L. Strolger. *Simulations of the WFIRST Supernova Survey and Forecasts of Cosmological Constraints*. The Astrophysical Journal **867**(1), 23 (2018). URL https://iopscience.iop.org/article/10.3847/1538-4357/aac08b.

[143] D. Scolnic and R. Kessler. *Measuring Type Ia supernova populations of stretch and color and predicting distance biases*. The Astrophysical Journal **822**(2), L35 (2016). URL https://iopscience.iop.org/article/10.3847/2041-8205/822/2/L35.

[144] C. Ashall, P. Mazzali, M. Sasdelli, and S. J. Prentice. *Luminosity distributions of Type Ia supernovae*. Monthly Notices of the Royal Astronomical Society **460**(4), 3529 (2016). URL https://academic.oup.com/mnras/article/460/4/3529/2609107.

[145] D. Richardson, R. L. Jenkins III, J. Wright, and L. Maddox. *Absolute-magnitude distributions of supernovae*. The Astronomical Journal **147**(5), 118 (2014). URL https://iopscience.iop.org/article/10.1088/0004-6256/147/5/118.

[146] D. Richardson, D. Branch, D. Casebeer, J. Millard, R. C. Thomas, and E. Baron. *A Comparative Study of the Absolute Magnitude Distributions of Supernovae*. The Astronomical Journal **123**(2), 745 (2002). URL https://iopscience.iop.org/article/10.1086/338318.

[147] M. Ganeshalingam, W. Li, and A. V. Filippenko. *The rise-time distribution of nearby Type Ia supernovae*. Monthly Notices of the Royal Astronomical Society **416**(4), 2607 (2011). URL https://academic.oup.com/mnras/article-lookup/doi/10.1111/j.1365-2966.2011.19213.x.

[148] S. Gonzalez-Gaitan, N. Tominaga, J. Molina, L. Galbany, F. Bufano, J. P. Anderson, C. Gutierrez, F. Forster, G. Pignata, M. Bersten, D. A. Howell, M. Sullivan, R. Carlberg, T. de Jaeger, M. Hamuy, P. V. Baklanov, and S. I. Blinnikov. *The rise-time of Type II supernovae*. Monthly Notices of the Royal Astronomical Society **451**(2), 2212 (2015). URL https://academic.oup.com/mnras/article-lookup/doi/10.1093/mnras/stv1097.

[149] J. A. Cardelli, G. C. Clayton, and J. S. Mathis. *The relationship between infrared, optical, and ultraviolet extinction*. The Astrophysical Journal **345**, 245 (1989). URL https://ui.adsabs.harvard.edu/abs/1989ApJ...345..245C/abstract.

[150] M. M. Phillips and C. R. Burns. *The Peak Luminosity–Decline Rate Relationship for Type Ia Supernovae*. In *Handbook of Supernovae*, pp. 1–19 (Springer International Publishing, Cham, 2016). URL http://link.springer.com/10.1007/978-3-319-20794-0_100-1.

[151] J. P. Anderson, P. A. James, F. Förster, S. González-Gaitán, S. M. Habergham, M. Hamuy, and J. D. Lyman. *On the environments of Type Ia supernovae within host galaxies*. Monthly Notices of the Royal Astronomical Society **448**(1), 732 (2015). URL https://academic.oup.com/mnras/article/448/1/732/1748724.

[152] J. P. Anderson and P. A. James. *Comparisons of the radial distributions of core-collapse supernovae with those of young and old stellar populations*. Monthly Notices of the Royal Astronomical Society **399**(2), 559 (2009). URL https://academic.oup.com/mnras/article/399/2/559/1059013.

[153] G. E. Romero, M. V. Del Valle, and F. L. Vieyro. *Mechanism for fast radio bursts*. Physical Review D **93**(2) (2016). URL https://journals.aps.org/prd/abstract/10.1103/PhysRevD.93.023001.

[154] J. I. Katz. *FRB as products of accretion disc funnels*. Monthly Notices of the Royal Astronomical Society: Letters **471**(1), L92 (2017). URL https://academic.oup.com/mnrasl/article/471/1/L92/3979013.

[155] A. Loeb, Y. Shvartzvald, and D. Maoz. *Fast radio bursts may originate from nearby flaring stars*. Monthly Notices of the Royal Astronomical Society: Letters **439**(1) (2014). URL https://academic.oup.com/mnrasl/article/439/1/L46/1029141.

[156] E. Petroff, E. D. Barr, A. Jameson, E. F. Keane, M. Bailes, M. Kramer, V. Morello, D. Tabbara, and W. Van Straten. *FRBCAT: The fast radio burst catalogue*. Publications of the Astronomical Society of Australia **33** (2016). URL https://www.cambridge.org/core/journals/publications-of-the-astronomical-society-of-australia/article/frbcat-the-fast-radio-burst-catalogue/09A20B3E45ACD2B130BCBE4577117FEA.

[157] S. Prajs, M. Sullivan, M. Smith, A. Levan, N. V. Karpenka, T. D. P. Edwards, C. R. Walker, W. M. Wolf, C. Balland, R. Carlberg, D. A. Howell, C. Lidman, R. Pain, C. Pritchet, and V. Ruhlmann-Kleider. *The volumetric rate of superluminous supernovae at z ∼ 1*. Monthly Notices of the Royal Astronomical Society **464**(3), 3568 (2017). URL https://academic.oup.com/mnras/article/464/3/3568/2514563.

[158] S. Taubenberger. *The Extremes of Thermonuclear Supernovae*. In *Handbook of Supernovae*, pp. 317–373 (Springer International Publishing, 2017).

[159] C. Rodrigo, E. Solano, and A. Bayo. *SVO Filter Profile Service Version 1.0*. Tech. rep., International Virtual Observatory Alliance (2012). URL http://ui.adsabs.harvard.edu/abs/2012ivoa.rept.1015R/abstract.

[160] B. T. Hayden, P. M. Garnavich, R. Kessler, J. A. Frieman, S. W. Jha, B. Bassett, D. Cinabro, B. Dilday, D. Kasen, J. Marriner, R. C. Nichol, A. G. Riess, M. Sako, D. P. Schneider, M. Smith, and J. Sollerman. *The rise and fall of Type Ia supernova light curves in the SDSS-II Supernova Survey*. The Astrophysical Journal **712**(1), 350 (2010). URL https://iopscience.iop.org/article/10.1088/0004-637X/712/1/350.

[161] F. Taddia, J. Sollerman, G. Leloudas, M. D. Stritzinger, S. Valenti, L. Galbany, R. Kessler, D. P. Schneider, and J. C. Wheeler. *Early-time light curves of Type Ib/c supernovae from the SDSS-II Supernova Survey*. Astronomy & Astrophysics **574**, A60 (2015). URL http://www.aanda.org/10.1051/0004-6361/201423915.